NOAA Technical Report NWS 49

Linear Statistical Short-Term Climate Predictive Skill in the Northern Hemisphere

Camp Springs, Md.
September 1993

U.S. DEPARTMENT OF COMMERCE
National Oceanic and Atmospheric Administration
National Weather Service

NOAA Technical Report NWS 49

Linear Statistical Short-Term Climate Predictive Skill in the Northern Hemisphere

Anthony G. Barnston
Climate Analysis Center
National Meteorological Center
National Weather Service

Camp Springs, Md.
September 1993

U.S. DEPARTMENT OF COMMERCE
Ronald H. Brown, Secretary
National Oceanic and Atmospheric Administration
D. James Baker, Under Secretary
National Weather Service
Dr. Elbert W. Friday, Jr., Assistant Administrator

CONTENTS

Abstract

In this study the sources and strengths of statistical short-term climate predictability for local surface climate (temperature and precipitation) and 700 mb geopotential height in the Northern Hemisphere are explored at lead times of up to one year. Canonical correlation analysis (CCA) is the linear statistical methodology employed. Predictor and predictand averaging periods of 1 and 3 months are used, with four consecutive predictor periods followed by a lead time and then a single predictand period. Predictor fields are quasi-global sea surface temperature (SST), Northern Hemisphere (NH) 700 mb height, and prior values of the predictand field itself. Cross-validation is used to obtain, to first order, uninflated skill estimates.

Results reveal mainly modest statistical predictive skill except for certain fields, locations and times of the year when predictability is far above chance expectation and good enough to be economically useful. Global SST is the most skill-producing predictor field, perhaps because (1) the lower boundary condition is a more consistent influence on climate on 1 to 3 month time scales than the atmosphere's internal dynamics, or (2) SST is the only field in this study that provides tropical information directly. Prediction is generally more skillful on the 3 month than 1 month time scale. The skill of the forecasts is often insensitive to the forecast lead time; i.e, inserting three, or sometimes six or more, months between the predictor and predictand periods causes little skill decrease from that of one month or less. This has favorable implications for long-lead forecasting.

Much of the higher skill occurs in association with fluctuations of ENSO and is found in mid-winter through mid-spring in specific pockets of the Pacific and North American regions. Predictive skill for precipitation is also found in the same context, but is lower than that for 700 mb height or temperature.

Warm season predictability, slightly lower than that of winter-spring, has its origins in ocean-atmosphere associations not clearly documented in earlier work. Generalized positive (negative) 700 mb and surface temperature anomalies in middle to late summer (but fall in southern Europe), generally at subtropical latitudes throughout much of the Northern Hemisphere (but with some mid-latitude continental protrusions), occur following episodes of uniformly positive (negative) SST anomalies in the tropical oceans throughout the world in the preceding winter through late spring. The occurrence of a mature warm (cold) ENSO extreme the previous winter may contribute to such a worldwide SST condition in the intervening spring season. In the U.S. the effect is a general (monopole) anomalous warmth (coolness) from mid-July through August across much of the country.

This report is also being presented as a journal article (Barnston 1994) containing less detail but including field significance evaluations of the forecast skill fields.

1. Introduction

a. Motivation and Background

In this study a multivariate linear statistical model is used to describe predictive relationships between evolving large scale patterns in Northern Hemisphere (NH) 700 mb circulation and near-global sea surface temperature (SST) fields (predictors), and subsequent patterns in the NH 700 mb circulation and United States and European surface temperature and/or precipitation. A lead interval of varying length is placed between a series of consecutive predictor periods and a single predictand period. An objective evaluation of the strength of such relationships is a primary motivation underlying the work, given that the Climate Analysis Center (CAC) of NOAA is responsible for issuing long-range forecasts and is seeking opportunities to increase their skill and their lead time.

Statistical analyses provide empirical knowledge that can lead to more skillful forecasts even in the absence of explicit physical understanding. However, the information may also provide guidance toward identification of the physical processes contributing to or limiting the predictability. The choice to use an empirical approach reflects the fact that both simple and complex general circulation models (GCMs), either with prescribed boundary conditions or with actual oceanic coupling, do not yet adequately reproduce the processes of the real atmosphere at the lead times and averaging periods of concern here (Shukla 1985, Livezey 1990, Brankovic et al. 1990, Milton 1990). Limitations in numerical approaches may be due, first, to inherent limits in predictability using initial conditions to integrate through instantaneous atmospheric states (Lorenz 1982, Chen 1989). Secondly, limitations may exist because of our currently inadequate knowledge of how to predict the lower frequency components of the total variability (whose inherent predictability limits are more favorable [Van den Dool and Saha 1990]), either through better use of boundary conditions or through the equations of the atmosphere's and oceans's internal dynamics. We hope and assume that eventually, with advances in physical understanding, dynamical prediction approaches will outperform statistical ones.

Prediction of United States time-averaged surface climate has received considerable attention over the last two decades. Using the GCM approach, work has been done by Blackmon et al. (1983), Shukla and Wallace (1983), Lau (1985), Chervin (1986), among many others. Among empirically oriented studies, several approaches have been used. First, the potentially predictable portion of the total variability of a given predictand has been empirically estimated using ratios of predictand variability at different frequencies (Madden 1976, Madden and Shea 1978, Trenberth 1984, Shea and Madden 1990). Direct attempts at forecasting and verification have been made using analog approaches (Barnett and Preisendorfer 1978, Livezey and Barnston 1988, Barnston and Livezey 1989, Toth 1989) and linear statistical approaches with either several preselected predictor elements or

whole predictor fields (Barnett 1981, Harnack 1979, Harnack 1982, Harnack and Lanzante 1984, Dixon and Harnack 1986, Barnett and Preisendorfer 1987, among others).

Despite gains in empirical knowledge resulting from the above studies, our present empirical knowledge is considerably less than it could be given the sample sizes and quality of the available NH upper atmospheric gridded data from the late 1940s and dense coverage of quasi-global SST from the mid-1950s. Most past studies have not availed themselves of an abundant set of potential predictors (i.e. full fields) nor have they used methods that are designed to simultaneously relate sets of predictors to sets of predictands. Some of them did not evaluate predictive skill properly (e.g. hindcasting was done rather than cross-validation). The study of Barnett and Preisendorfer (1987) was an exception, but did not evaluate predictability over the entire seasonal cycle or for a predictand field covering most of the NH.

The decision to use quasi-global SST and NH 700 mb height as predictor fields is based on the findings of other studies as well as data availability. The SST field has been shown to have influence on extratropical climate, as for example, through the El Nino/Southern Oscillation (ENSO) for tropical Pacific SST (Opsteegh and Van den Dool 1980, Hoskins and Karoly 1981) and, more weakly, through regional response patterns for extratropical SST (Namias 1982, Lanzante 1984, Iwaska et al. 1987, among others) and even local effects (Van den Dool 1984, Van den Dool and Nap 1985). The 700 mb height field may have predictive value in addition to that supplied by the SST field, both through low frequency internal dynamics and perhaps indirectly through communication of lower boundary effects that are incompletely represented by the SST data themselves. The 700 mb height field is limited to the extratropical NH because of the lack of global data availability prior to the late 1970's. While quasi-global sea level pressure (SLP) data are available back through the 1950's and earlier (Barnett et al. 1984) and might provide additional predictive skill, these data are often of questionable reliability in the tropics (Murphree and Van den Dool 1988, Barnston and Ropelewski 1992) and over elevated land where reduction to sea level is needed. This data quality problem may be alleviated following the ongoing long-term multi-institutional project to reanalyze several decades of data using a consistent data assimilation scheme (Kinter and Shukla 1989, Kalnay and Jenne 1991). The tropics represent a critically important predictor area; coverage there is cautiously limited to the more reliable SST data for this work.

Although prediction of United States and European surface temperature and United States precipitation is the ultimate goal of this research, prediction of NH 700 mb height is also of concern. This is the case because of the importance of the hemisphere-wide circulation anomalies to an understanding of large scale atmospheric processes and their often close correspondence to the surface climate (Klein 1983, Klein and Yang 1986, Klein et al. 1989). Indeed, the locations of pockets of relatively high predictive skill for 700 mb height in this study,

it turns out, correspond approximately to regions having good surface climate predictability. Thus, skillful predictions of 700 mb height here may contribute to subsequent Northern Hemispheric surface climate prediction studies in regions outside the United States and Europe.

b. Use of Multivariate Predictor-Predictand Linkages

A primary reason for our underachievement in empirical knowledge, we suspect, has been the regional or otherwise incomplete character of many studies--either in terms of the predictor fields used, the predictand fields, or both. While the collection of such studies may provide information for most of the globe, the differing choices of predictors, predictands, period of record, averaging period and methodology make it difficult to combine many of the individual results.

Many of the signals that are active over short-term climate time scales have comparably large spatial extents, as evidenced in teleconnection patterns (Namias 1981, Wallace and Gutzler 1981, Esbensen 1984) and rotated principal component patterns (Horel 1981, Barnston and Livezey 1987, Kushnir and Wallace 1989). The climate at a given location is often determined by the combined effects of several systematic relationships. Most of these relationships are of large spatial scale, such that the location in question is part of a broad region that is affected similarly.

When multiple regression analysis is used to predict a single location, the spatial pattern of the predictand field is not utilized in defining the relationship with the predictor(s). Identification of predictand patterns as wholes can enhance predictive skill at constituent individual predictand locations. This is the case largely because there is information in the patterns that cannot be captured by noisy measurements at individual points. When the predictand field is considered as a whole, the portion of the variability of each predictand element participating in a large-scale predictand variability pattern associated with the predictor(s) can more easily be identified and separated from the random variability.

The disadvantage of treating the predictand as a multivariate entity is that variability unique to one predictand element is likely to be regarded as noise whether it is truly random or represents a forecastable local scale physical signal. In the second case, treatment on the pattern level may jeopardize individual location forecasts. This would occur when the climate at the location is governed most heavily by local effects such as terrain, water bodies, or any factors modifying anomaly persistence or otherwise reducing conformity to the surrounding large scale anomaly pattern. (See Klein and Walsh (1983) for a methodological experiment relating to this issue.) In this study the pattern-to-pattern strategy is used, predicated on the premise that a number of large scale signals collectively produce the most favorable magnitude and spatial coverage of forecast skill.

The direct effect of local persistence is expected to be weak in forecasts made with nonzero lead time as compared with that found for adjacent predictor-predictand periods.

Following a description of the data and a discussion of the methodology in sections 2 and 3 respectively, results are presented in section 4. A summary, discussion and concluding remarks are given in section 5.

2. Data

In this study the data sets, spanning the 1955-1991 period, include (1) quasi-global SST, (2) NH 700 mb height, (3) United States and European surface temperature, and (4) United States surface precipitation. The SST field is used only as a predictor; the other fields are used as either a predictor or predictand. While monthly means are the basis for the SST, European surface temperature, and U.S. climate division precipitation data, the other data begin as daily values from which half-monthly means are formed. The half-monthly time scale is chosen in order to be able more finely to resolve changes in predictive skill as a function of forecast lead time as well as phase of the annual cycle, and also to use the forecasts as an input for the 1 month official CAC forecasts which are issued on a half-monthly basis. The predictor and predictand averaging periods used in this study are one or three months.

Monthly mean SST data come from the COADS (Slutz et al. 1985) through 1979, from in situ (i.e., ship) data from 1980 to 1981 and from blended ship/satellite data thereafter (Reynolds 1988). The study period of 1955-1991 is constrained by the onset of relatively good tropical Pacific SST data in the middle 1950s (Halpert and Ropelewski 1989). While the data are available in 2^{o} by 2^{o} squares, means for 10^{o} by 10^{o} squares were developed for this study. Because the mean within a 10^{o} by 10^{o} square was determined by any report within this relatively larger area, the occurrences of boxes with missing data is greatly reduced. While some unrepresentativeness due to sparse data within one square is expected in high gradient mid-latitude regions, this problem is minor in the more critical tropical Pacific where missing data in the 1950s is an occasional problem. In the few instances in which there were no reports in the large squares, both temporal and spatial anomaly interpolations were carried out to estimate the missing value. Squares with more than 2 percent missings were excluded unless they were located in the tropical Pacific belt. Six such squares in the tropics were admitted, the highest missing percentage being 6.5 percent for the square centered at 0^{o}N, 130^{o}W; four of the five other squares are located in the equatorial Pacific at the Date Line and westward.

To adapt the monthly mean SST data to half-monthly time increments used here, a weighted average of two adjacent monthly mean values was formed (e.g. the SST for the second half of January was estimated using 0.75 times the January monthly mean plus 0.25 times the February monthly mean). Figure 1a shows the

center locations of the 235 SST squares used.

Daily NH 700 mb height data were obtained from the National Meteorological Center (NMC) on an approximately equal area 358-point grid from 20°N northward (Fig. 1b). Missing data were virtually nonexistent (<0.1 percent); the few missed days were omitted from the half-monthly averages.

Daily maximum and minimum United States surface temperatures and daily total precipitation at 59 stations (chosen on the basis of data quality) were obtained from the National Climatic Data Center in Asheville, North Carolina for the 1955-1972 period, and from NMC for the 1973-1991 period. Half monthly temperature means were derived from the daily average [(maximum + minimum)/2] temperatures, and half monthly precipitation totals were formed from the daily values. Missing data occurred in less than 0.5 percent of the study period at all stations, and less than 0.1 percent at most stations. Missing days were omitted in the computation of half monthly means. The network of predictand stations is shown in Fig. 1c. Monthly total climate division precipitation data (NOAA 1983) were also used. Presentation of the European surface temperature station network is deferred to section 4e.

3. Analysis Method

a. Choice of Predictor Fields

For forecasts of U.S. or European surface temperature, the previous U.S or European temperature field is normally used as a predictor in addition to SST and 700 mb height. When the predictand is precipitation or 700 mb height, only the preceding SST and 700 mb height fields are used as predictors. This decision is based on studies by Huang and Van den Dool (1993), among others, in which effectively no linear relationship is found between the heights and preceding surface temperature, or precipitation and the preceding precipitation or temperature. The predictor fields are introduced in a temporal sequence consisting of four consecutive periods (temporally "stacked" predictors) prior to forecast time. Thus, there is a total of 2608 predictor elements for U.S. or European surface temperature forecasts (4 X [235+358+59]) and 2372 elements for precipitation or 700 mb height forecasts. As will be discussed in section 3c(1), the relative overall weighting of the predictor fields is adjusted according to their approximate relative contributions to forecast skill.

b. Choices of Multivariate Linear Statistical Methodologies

Predicting patterns over areas on monthly to seasonal time scales requires a methodology that is capable of defining pattern-to-pattern (multivariate) relationships, given sets of predictor and predictand elements. Three linear such methodologies that have come into prevalent use are canonical correl-

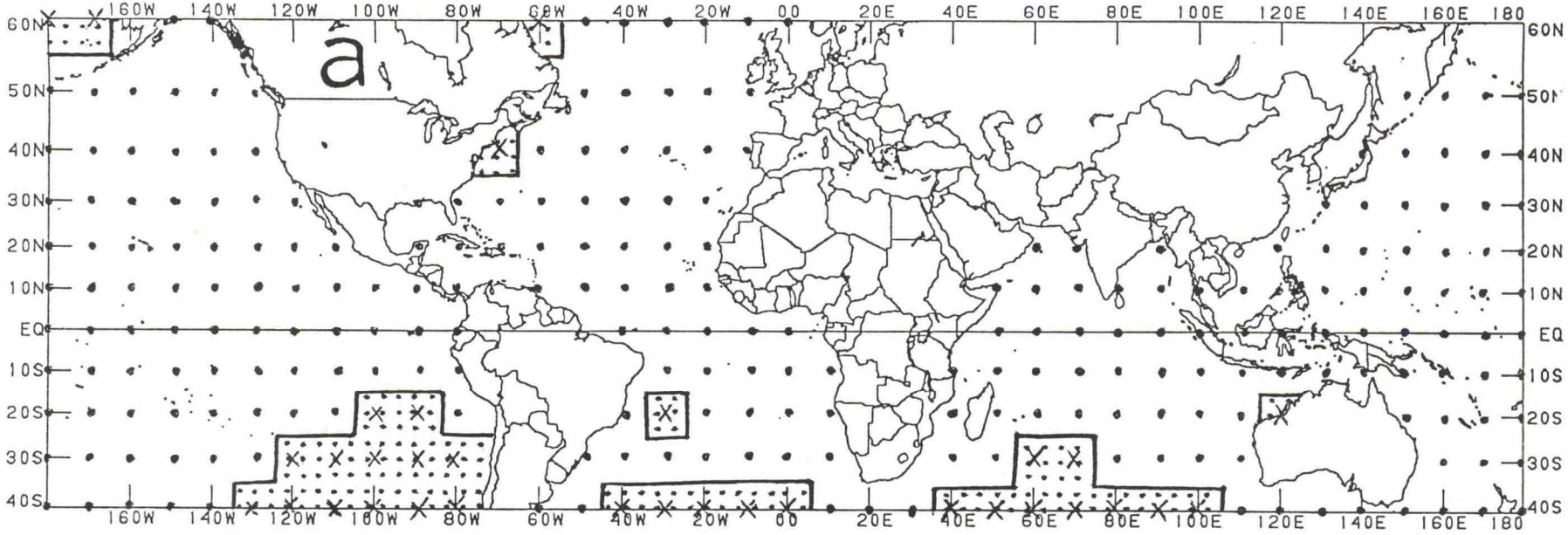

1. Part (a): The quasi-global SST grid, composed of 235 10 X 10 degree boxes. The boxes with an "X" are not used due to data problems. Part (b): The 358-point Northern Hemisphere 700 mb grid. Circled grid points have had an early 1950's bias adjustment (see Appendix A of Barnston and Livezey 1987) and points with an "X" are not used due to data problems. Part (c): The United States surface temperature/ precipitation predictand stations.

b

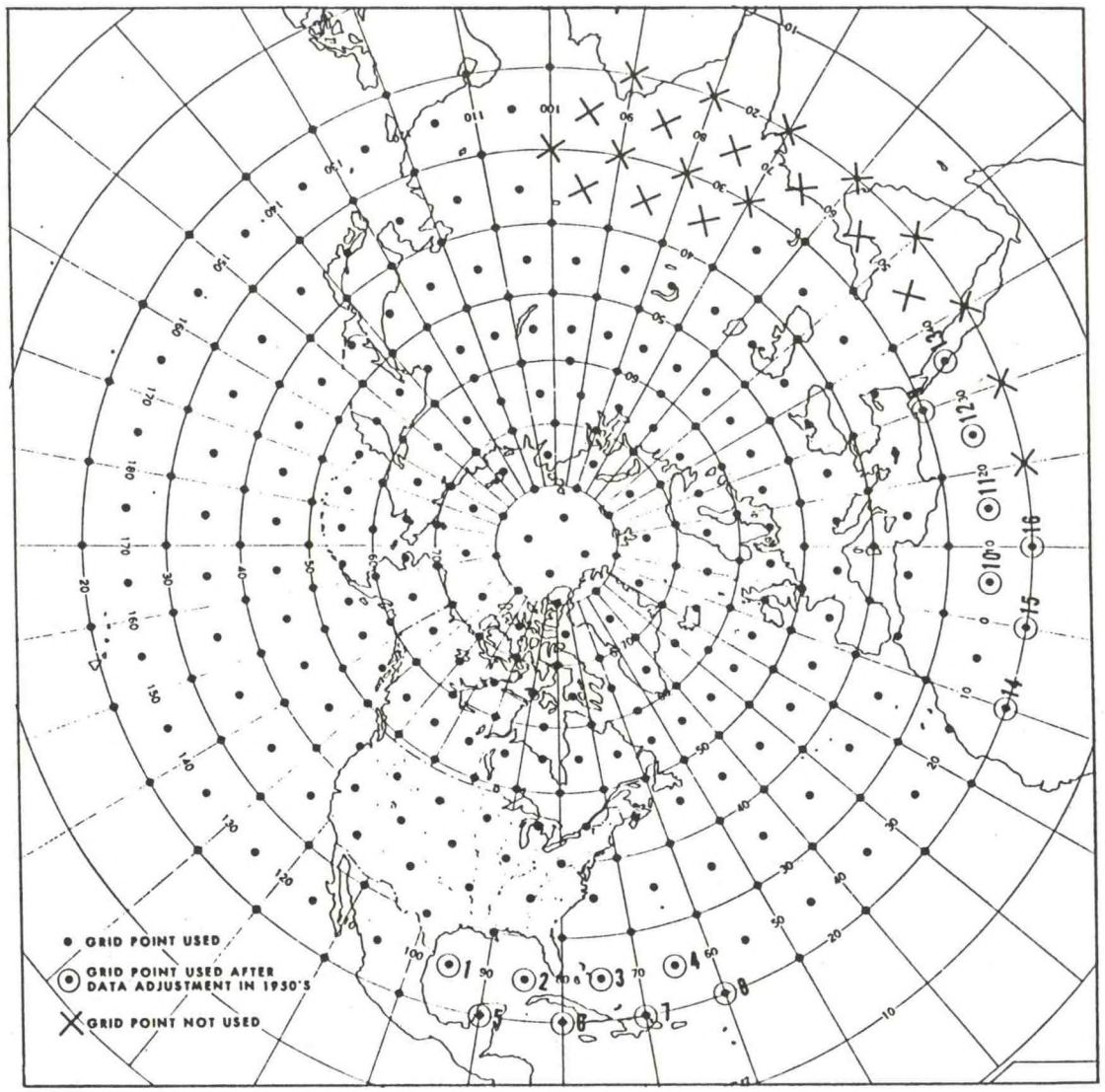
GRID POINT USED
GRID POINT USED AFTER DATA ADJUSTMENT IN 1930'S
GRID POINT NOT USED

c

ation analysis (CCA), singular value decomposition (SVD), and principal oscillation pattern (POP) analysis. Both CCA and SVD calculate linear combinations of a set of predictors that maximize relationships (using a least squared error criterion) to similarly calculated linear combinations of a set of predictands. Multiple predictor and/or predictand fields can be used together. In POP analysis, pattern periodicities, propagation and damping are modelled through cognizance of the datasets' multivariate autoregressive as well as oscillatory behavior.

CCA is essentially a multiple regression that is extended to relate multicomponent predictors to multicomponent predictands with a specific application of empirical orthogonal function (EOF) analysis. It has been described in the non-meteorological literature (Hotelling 1936, Anderson 1984) as well as in meteorological or geophysical contexts (Glahn 1963, Barnett and Preisendorfer 1987, Nicholls 1987, Graham et al. 1987a,1987b), and is currently used for ENSO predictions at CAC (Barnston and Ropelewski 1992). CCA is most suitable when (1) substantial predictability involves predictor elements having low case-to-case variance (e.g. SST in the tropical Atlantic or western tropical Pacific) and (2) predictor-to-predictand cross-dataset linkage patterns are not necessarily similar to the clusters of coherent variability (e.g. EOFs) within the predictors or predictands (Bretherton et al. 1992, Wallace et al. 1992). If EOF analysis is done as a preprocessing step as in Barnett and Preisendorfer (1987), CCA is then also most appropriate for predictors and predictands whose behavior is governed by only a few relatively broad, general, possibly multifaceted factors (e.g. the ENSO).

SVD (Wallace et al. 1992, Bretherton et al. 1992) involves less filtering and transforming of the raw predictor and predictand input data than CCA. SVD omits a normalization of the input time series which would set all series on an equal footing for entry into a CCA, and also often does not preprocess the input data with an EOF filter. SVD performs favorably when predictor-predictand pattern linkages are more localized, numerous, and varied in strength than those for which CCA (especially if pre-EOFs are used) would be preferred. SVD would also be favored when the predictor and predictand elements participating in each pattern linkage are similar to those found in the individual dataset EOF patterns.

POP analysis (Hasselmann 1988, von Storch et al. 1988, Penland 1989, Xu and von Storch 1990) utilizes the autoregressive and periodic properties of predictor and predictand data sets in deriving predictive relations. It defines the phasing and damping rates of the coherent structures among both data sets. Sharing some characteristics with the more explicit multivariate autoregressive techniques and with cross-spectral analysis, POP analysis would be expected to do best in environments with well defined periodicities, damping and propagations that tie together predictors and predictands. POP analysis is only applicable when the predictor and predictand are the same multi-element field variable in a lead-lag framework. It also has some useful diagnostic aspects not found in CCA and SVD.

In the absence of predictor-predictand characteristics corresponding clearly to one of the sets of suitability criteria given above for the three methodologies, determination of the favored methodology for a given prediction problem would require a series of trials with each. Such exhaustive experimentation was performed in Bretherton et al. (1992), where more detailed criteria for making methodological choices are provided. Based partly on comparative findings in that study as well as on knowledge of the relative breadth and paucity of the number of processes that are thought to significantly affect the NH's 1 to 3 month climate fluctuations, the CCA approach with pre-orthogonalization is used here and believed to be the most suitable of the possible options. The other side of the same coin is that by using CCA, the relatively large scale pattern relationships, which we think typically dominate the climate variability, are emphasized.

c. CCA Procedure and Products

At the heart of CCA, eigenanalysis is used to define the structure of the covariance between predictor and predictand data sets under the constraint of maximization of cross-dataset correlation explained with each successive mode. CCA is distinguished from standard EOF analysis, which calculates an orthogonal coordinate system that maximizes variance explained within a single dataset with each successive mode. In the case of predictor and/or predictand fields containing a relatively short period of record but a large number of elements, many of which have high intercorrelations (e.g. neighboring points of a gridded field), a recommended major preprocessing step is pre-orthogonalization using standard EOF analysis. The CCA procedure used here is essentially identical to that used in Barnett and Preisendorfer (1987), Graham et al. (1987a,b), and Barnston and Ropelewski (1992). The description here is brief; more detail is available in the above references (e.g., the appendix in Barnett and Preisendorfer 1987 or section 3.2 in Graham et al. 1987a).

1) DATA PREPROCESSING

Before beginning the CCA, each predictor and predictand data element is detrended and then standardized so that all elements possess temporal stationarity and are weighted equally to produce a correlation-based CCA. The detrending consists of computation of a single linear regression fit for the time series, followed by substitution of the residual from the regression line for each point and then addition of the overall mean value. The detrending is done to filter out artificial effects such as dataset biases that change over time (there are no known serious such biases in our data sets over the period used here), but might remove some authentic climatic nonstationarities also. Detrending also helps safeguard against artificial skill in cross-validation skill estimations (see section 3e). The standardizations ensure that all locations have equal opportunity to partic-

ipate in the predictive patterns, regardless of their latitude and longitude dependent interannual variances. The last pre-processing step prior to the pre-EOF analysis is final interfield weighting, which adjusts the relative weighting of two (or more) predictor fields, as wholes, relative to one another. If this step were not carried out, the relative weights would be proportional to the relative number of elements (e.g. grid points) in the respective fields. Unless the fields share the same grid this is not necessarily a desired weighting. Based on a series of forecast skill sensitivity tests, the SST elements are usually given double the weight of the 700 mb elements in the present study, resulting in an overall SST/700 mb weighting ratio of 1.31--i.e. (2 X 235) / 358. This reflects the generally greater predictive value of SST than 700 mb height on monthly to seasonal time scales. In order to avoid a posteriori optimization which can result in artificial skill, this relative weighting is fixed for most of the experiments, regardless of season and lead time. Where surface temperature is also included as a predictor of itself at a later time, its natural weight of 59/358 = 0.16 times the weight of the 700 mb height field is found to be favorable, as it generally contributes only a small increment of skill to the predictions.

The predictor and predictand data sets are then pre-orthogonalized with separate EOF analyses. Within the predictor pre-orthogonalization, the predictor fields from four consecutive prior periods (forming a temporal sequence) enter into the process together, producing an extended (in time as well as across predictor fields) EOF analysis. Here the relative weighting of the predictor fields, as wholes, is of critical importance, for it determines to what extent the resulting orthogonal components contain the influence of one field versus another.

The mode truncation point occurs after 6 modes, based partly on Monte Carlo experiments that determine the statistical separability of the eigenvalue curve from that resulting from random input data (Preisendorfer 1988). Additionally, truncation occurs before any mode whose eigenvalue is less than one percent of that of the leading mode. For the predictor data used here, these rules usually result in 6 (rarely 5) retained EOF modes, where the first mode usually accounts for roughly 15 percent of the original variance and the set of 5 or 6 modes accounts for 40 percent. Forecast skill sensitivity tests suggest that this truncation point is appropriate. For the 3 month mean U.S. surface temperature predictand EOFs the first mode often explains 30 (in summer) to 45 (in winter) percent of the original variance and the set of 5 or 6 retained modes 75 (summer) to 92 (winter) percent.

2) THE CCA ITSELF

Following detrending, standardization, interfield weighting and orthogonalization, a correlation matrix between each predictor (predictand) and all predictands (predictors) is formed. Note that only cross-dataset pairings are used; i.e. no predic-

tor-predictor or predictand-predictand correlation coefficients are used (as was in the EOF preprocessing). This is not necessarily a square matrix, but becomes square and symmetric when it is post- or premultiplied by its transpose, each of which operation is carried out for the predictor and predictand CCA solutions, respectively. The predictor and predictand product matrices are then used to obtain CCA eigenvectors and eigenvalues for predictors and predictands, with equal eigenvalues for corresponding mode numbers. An alternate, less tedious procedure is to perform the above step for only one of the two product matrices (e.g. only predictor) and then obtain the remaining set of eigenvectors (e.g. for predictand) from the former (predictor) ones rather than from their own product matrix.

As in standard EOF analysis, the eigenvectors and the original time series (following orthogonalization in the present CCA case) are used to compute an amplitude time series for each mode, which in CCA is done separately for the predictor and the predictand. In the present application the predictor eigenvector belonging to each mode consists of a set of four preferred (in association with the mode's predictand pattern, or eigenvector) temporally staggered ("stacked") spatial patterns (such a set being called a canonical loading pattern). The associated time series, having one element per year, is called a canonical component. The predictand portions of each mode also have their canonical loading patterns and canonical components, except that the former consist of only single spatial patterns in the present study. A schematic illustration of how the pre-orthogonalization and the CCA products are produced is given in Fig. 2. The square roots of the eigenvalues are the correlations between the predictor and predictand canonical component time series associated with the canonical loading patterns for the mode in question. The predictor and predictand canonical loading patterns represent linear combinations of the respective input variables that maximize the cross-dataset correlation accounted for by the mode.

The truncation rules for the CCA itself are the same as those for the pre-orthogonalization. This usually results in 5 or 6 canonical modes, and 4 once in a while. The amount of original predictor and predictand field variance explained by each CCA mode varies considerably with season, lead time, and the particular experiment. For forecasts of 3 month mean U.S. surface temperature using four consecutive 3 month mean predictor periods, for example, the first CCA mode quite uniformly explains 8 to 15 percent of original predictor variance, and the set of 4 to 6 modes about 25 to 40 percent. For the original predictand variance, the first CCA mode explains 5 to 10 percent in cases of poor predictability, and the set of 4 to 6 modes 10 to 15 percent. For the higher predictability cases these figures increase to 10 to 20 percent and 20 to 35 percent, respectively. These percentages of variance represent an average predictability over the predictand domain. They are related to hindcast CCA skill, which includes the artificial skill from noise fitting that is inherent in all regression techniques. A less biased predictability estimate is made using cross-validation (section 3e).

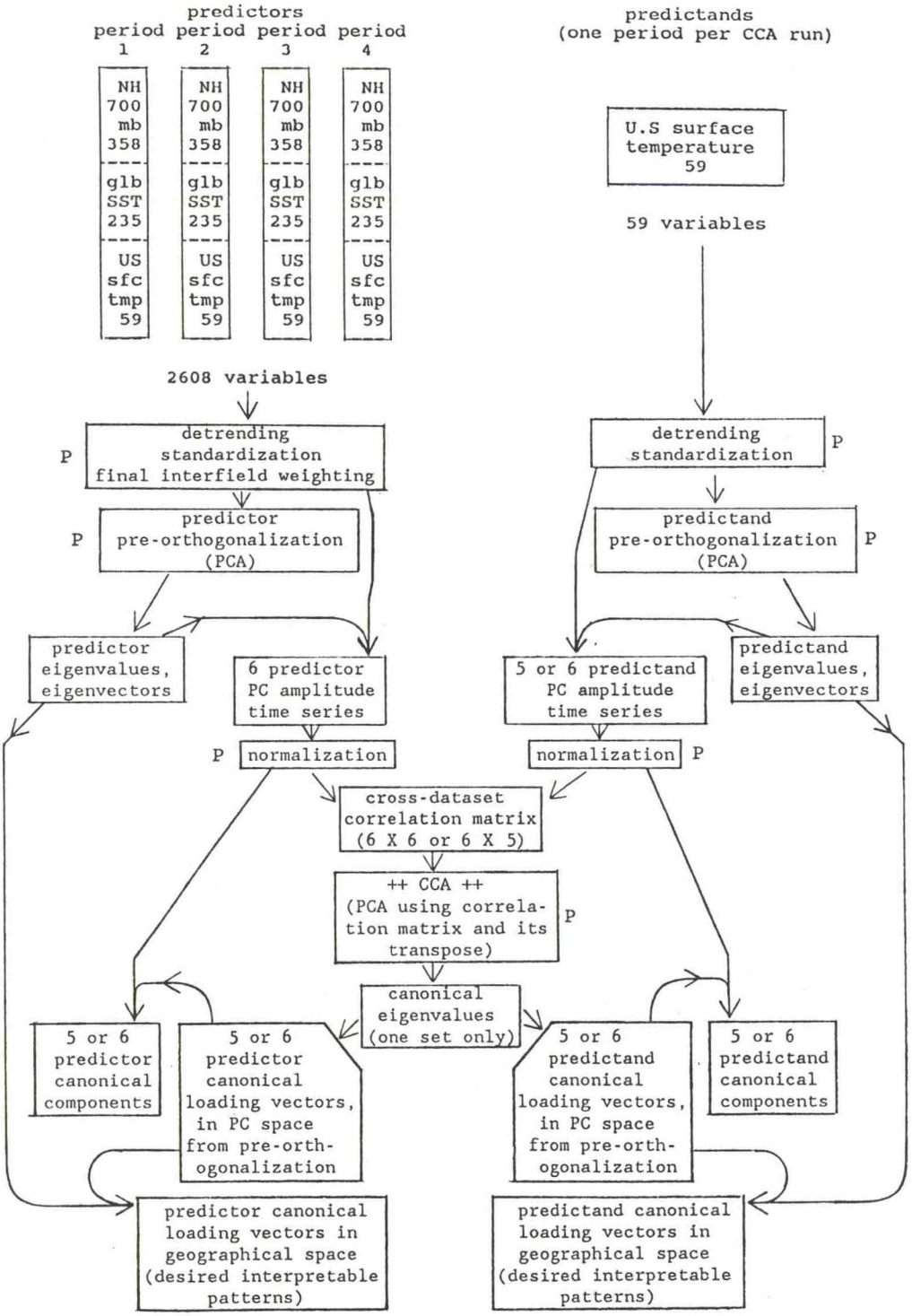

2. Schematic illustration of the production of the CCA products. The left (right) side shows processes involving predictors (predictands) and the middle shows processes involving both. Rectangles with a "P" to the side denote processing steps; all other rectangles denote bodies of data. Matrix calculations are implied when two arrows merge into one. From top to bottom the flow chart shows the raw data and its preprocessing, followed by pre-orthogonalization and normalization, formation of a cross-dataset correlation matrix (which is generally asymmetric and nonsquare), the CCA itself, and the resulting canonical loading vectors, components, and eigenvalues.

d. Lead Time Specification

The lead time, or number of seasons "skipped" between the final (fourth) predictor season and the predictand season, is varied from 0 to 4. When the lead time is one or more seasons, forecasts for the season(s) in between the final predictor season and the predictand season are not made as part of the process, in contrast to, for instance, numerical weather prediction or POP analysis, both of which use time continuity.

Fig. 3 illustrates the lead time structure for forecasts of the winter season (December-January-February)--in this particular case, winter of 1993-94. Each of the five rows represents a different lead time, the top row depicting a zero lead forecast. The four consecutive predictor periods are of the same length as the predictand period, but recede in time as the lead increases for the fixed target period. The configuration shown in Fig. 3 is used analogously for any other possible 3 month target period (Jan-Feb-Mar, Feb-Mar-Apr, ..., Nov-Dec-Jan). For 1 month forecasting the predictor periods are usually also of monthly duration, and the lead time is also reduced to monthly increments. Note that in real time forecasting the diagram would be modified such that the four predictor periods would remain fixed (representing the most recent four periods of available data) and the forecast target period would be one period farther into the future for each successive increase in lead time.

e. Cross-validation

In order to reduce the problem of artificial skill produced from the overfitting of random variability in the data sample, and obtain more realistic estimates of future forecast skill, a cross-validation design is used. In cross-validation, forecast models (whether derived from multiple regression, CCA, analogs, or any statistical technique) are developed using only part of the available data set and then applied to the independent data points held out in reserve for testing. In the most exhaustive version of cross-validation (Michaelsen 1987) that is now commonly used, this exercise is extensively repeated with each of all possible points (or sets of points) held out for forecast testing. This version, which has been used in a number of prediction studies (Barnett and Preisendorfer 1978, Harnack et al. 1985, Dixon and Harnack 1986, Michaelsen 1987, Barnett and Preisendorfer 1987, Livezey and Barnston 1988, Barnston and Livezey 1989, Livezey et al. 1990, Barnston and Ropelewski 1992), is used in the current work. That is, each of the 37 (or 36, depending on season and lead time) years from 1955 (or 1956) to 1991 is held out in turn and CCA is used to develop a prediction model from the remaining 36 (or 35) years. The entire sequence of data preprocessing (detrending, standardization, interfield weighting and pre-orthogonalization) is performed anew for each case, using the remaining years. The predictor data for the withheld year are then projected onto the predictor CCA loading patterns and predictand values are generated and verified against observed

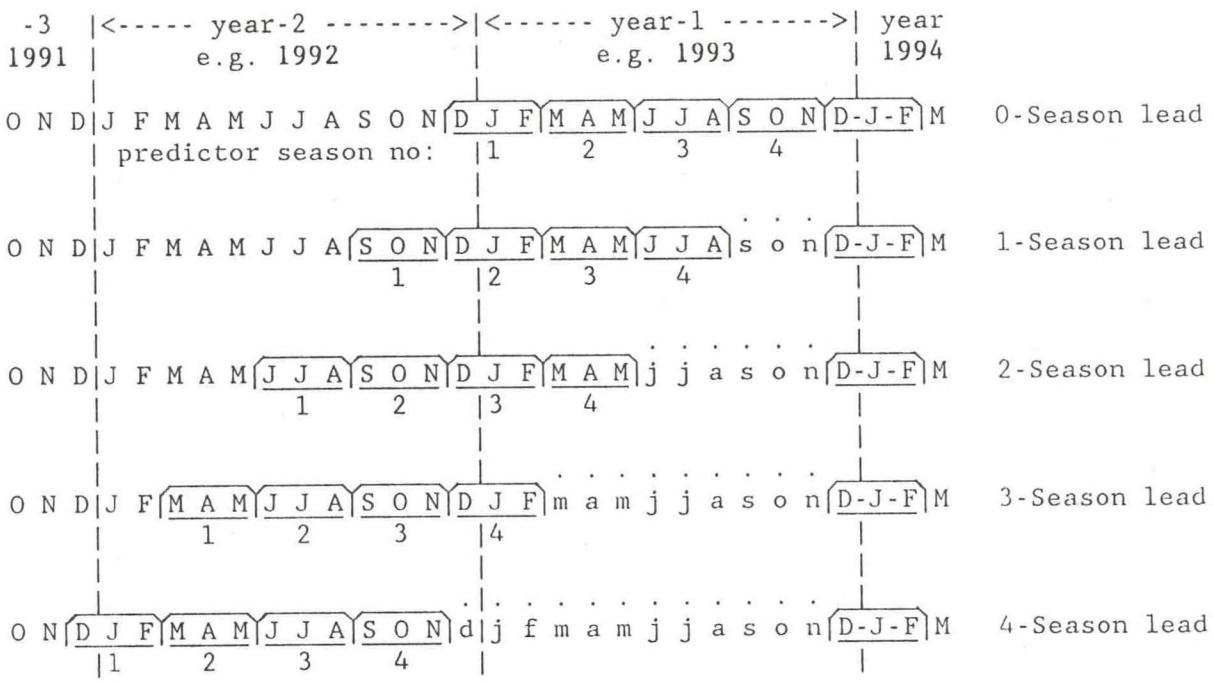

3. Schematic of the timing of the predictor and predictand periods for the five lead times used in the study, for the example of forecasting Dec-Jan-Feb 1993/94. Each row illustrates a progressively larger lead time, with the four predictor periods (numbered beneath the month abbreviations) retreating farther into the past with increasing lead. The lead period is represented by lowercase month abbreviations with dots above them. A similar diagram could be drawn for other target seasons, or for fixed predictor periods and a variable target period as in real-time forecasting using the most recent 12 months of predictor data.

data. The predicted and the observed values for the withheld year are standardized with respect to only the nonwithheld years (Van den Dool 1987). The verification measure used here is the temporal correlation between the series of forecasts and observations. The correlation is not sensitive to the ratio of variances of forecasts and observations. This means that either raw CCA forecasts (which have lower variance than the observations, being designed to minimize squared errors) or standardized (or otherwise inflated) CCA forecasts may be verified with no impact on this particular skill measure.

Further discussion on cross-validation, including its quality of skill estimation, problems, etc. is found in Michaelsen (1987), Graham et al. (1987b), Barnston and Ropelewski (1992), and Barnston and Van den Dool (1993).[1]

f. Persistence as a Control Measure

As a competitor for the temporal correlation between CCA-forecast and observed anomalies, the autocorrelation of the predictand over the lead time in question (i.e., persistence) is computed. If the autocorrelation is computed over all years in the sample, the implied persistence skill has an unfair advantage relative to the cross-validation CCA skill because the former is not computed in a cross-validation mode. To make and verify persistence (including antipersistence) forecasts in a cross-validation framework, the persistence forecasts are formed using a different coefficient as a function of target year, based on the autocorrelation computed from the nontarget years.

4. Results

In this section, results are presented for prediction of the 59-station network of United States surface temperature and precipitation, followed by forecasts of 700 mb height for the Pacific/North American (PNA) region (59 grid points), for the NH as a whole (358 grid points), and then for European temperature.

---

[1]One detail worth mentioning is that when the skill in the non-cross-validated sample (i.e. the full sample, with no years withheld) is near zero, the cross-validated correlation measured skill is likely to be strongly negative (e.g. <-0.5). These degenerate cases (Barnston and Van den Dool 1993) lead to unrepresentatively low mean results over all stations. One remedy for this problem is to set all negative individual scores to zero. The more conservative option used here is to multiply negative results by the ratio of the amplitude of the forecasts to that of the observations. (When degenerate cases occur, the amplitude of the forecast time series is always tiny.) This solution usually weakens negative skill scores of -0.5 to -0.8 to the -0.01 to -0.10 range which is comparable to RMSE cross-validation scores of 1.4 to 1.5 (for standardized data, where 1.41 corresponds to random results) in similar no-skill cases.

In all presentations, attention is given to (1) the seasonal variation of overall skill, (2) the geographical distribution of the skill for seasons having noteworthy overall skill, and (3) the implied scenarios of oceanic and atmospheric events leading to the skillful aspects of the forecasts, based on the canonical loading patterns of the predictors and predictands. When more than one CCA mode contributes substantially to the forecast skill, two or more superposed scenarios of events may be highlighted. For example, one CCA mode may depict a developing ENSO episode while another mode describes an ENSO event peaking during an early predictor period and dissipating toward the end of the 4-period predictor window. It turns out that just the leading CCA mode often represents the predictor-predictand relationship contributing to the majority of the skill.

Extensive repetition of the skill experiments with various detailed spatial and temporal combinations of predictors was not done for two reasons: (1) With 37 years of records, sampling errors would be inevitable (i.e. randomly generated patterns might be interpreted as meaningful), and (2) Because full fields are used as predictors, the characteristics of the predictor loading patterns already provide information that in less comprehensive experimental designs could be found only with much experimental repetition.

a. Prediction of United States Surface Temperature

1) PREDICTION OF 3-MONTH MEANS

The temporal correlation between the CCA cross-validation forecasts and the observations of U.S. surface temperatures averaged over the 59 stations is shown in Fig. 4a for 24 half-month-apart "seasons" for five lead times ranging from 1 month (solid line) to 13 months, for 3 month mean predictor and target periods. The length of the lead time in Fig. 4a is denoted by the size of the dashes. The target period is defined by its final half-month number (e.g. 1 refers to the period from mid-October to mid-January, and 16 is the June-July-August period). Peaks in skill occur in winter and early spring, as well as in middle to late summer. In these forecasts there is no predictor field weighting; i.e., the relative weighting of the SST, 700 mb height, and previous U.S. surface temperature is as naturally prescribed by their numbers of grid points (235, 358, and 59, respectively) and their spatial correlation functions which determine how many less degrees of freedom there are than the numbers of grid points. It is remarkable that increasing the lead time by three months lowers the skill only by relatively small increments up to 10 months. The skill of seasonal cross-validated persistence forecasts (Fig. 4b) lacks the semiannual peaks found in the CCA skill.

Figure 5 shows results using only SST (part a), only 700 mb height (part b) and only U.S. surface temperature (part c). Noteworthy findings here are (1) SST appears to carry the most predictive information (particularly in winter), followed by 700

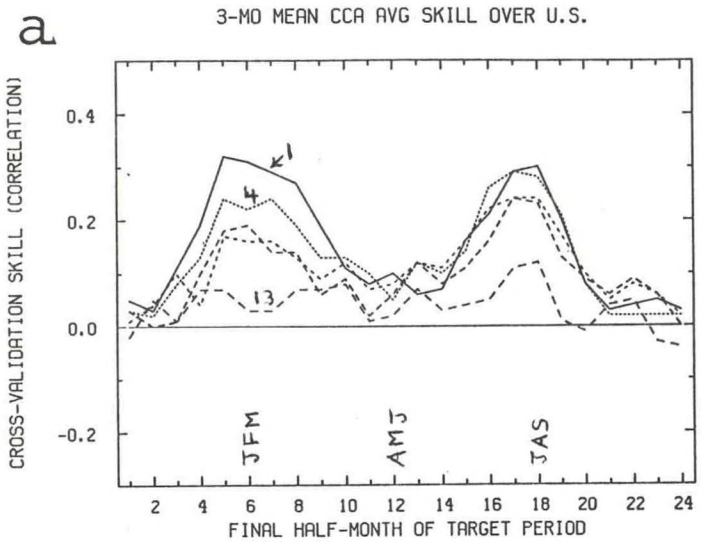

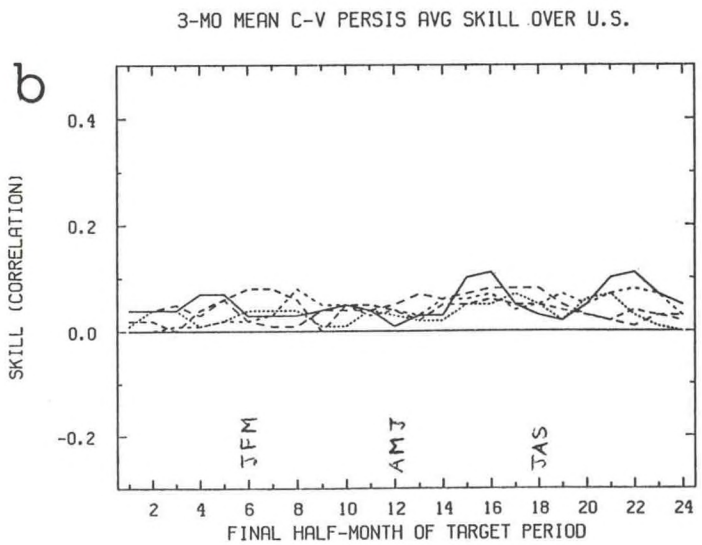

4. Part (a): Seasonal variation of CCA forecast skill averaged over the U.S. for 3-month mean temperature. Each of the four predictor periods is three months in duration. See text for seasonal definition and identification of each of the 5 lead time curves. The three predictor fields assume their natural weights. Part (b): As in part (a) except for persistence forecasts.

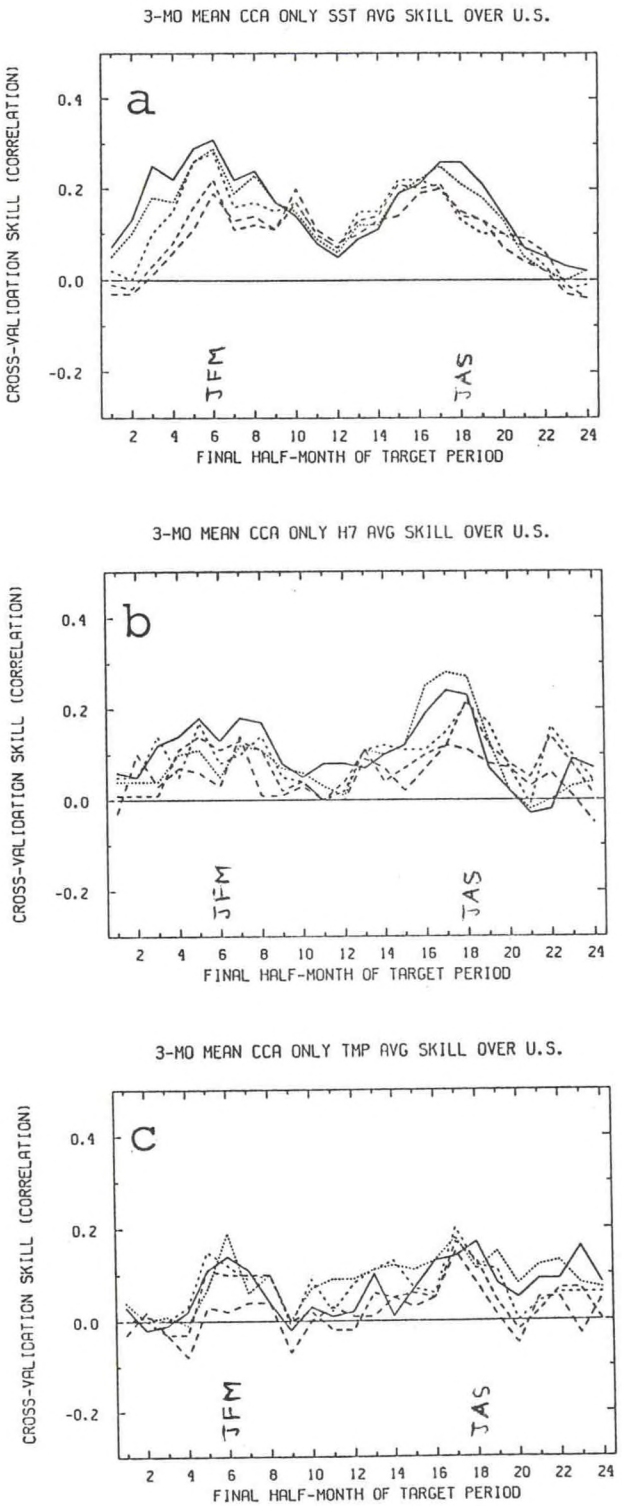

5. Part (a): CCA forecast skill (as in Fig. 4a) except using only SST as a predictor. Part (b): As in part (a) except using 700 mb height as the only predictor field. Part (c): As in part (a) except using U.S. surface temperature itself as the only predictor field. Part (d): As in part (a) except using only tropical (25N-25S) SST predictors. Part (e): As in part (a) except using only extratropical (>25N and >25S) predictors.

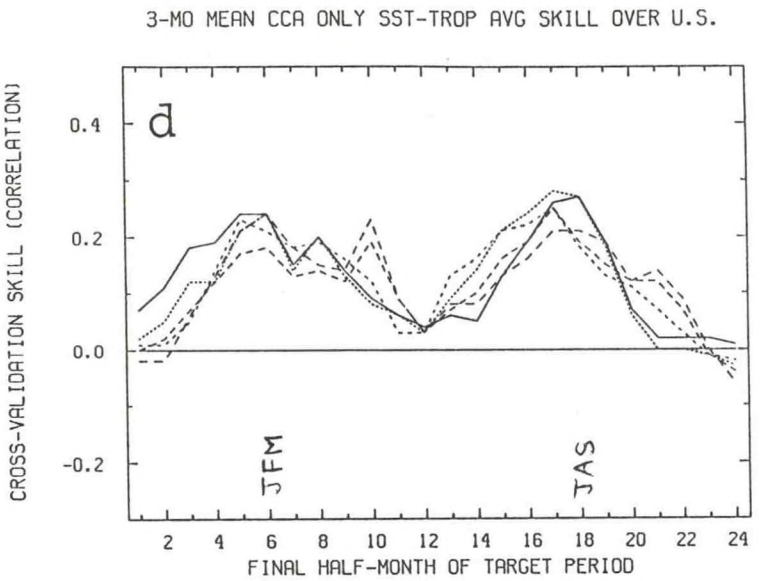
3-MO MEAN CCA ONLY SST-TROP AVG SKILL OVER U.S.
d
CROSS-VALIDATION SKILL (CORRELATION)
0.4
0.2
0.0
-0.2
JFM
JAS
2 4 6 8 10 12 14 16 18 20 22 24
FINAL HALF-MONTH OF TARGET PERIOD

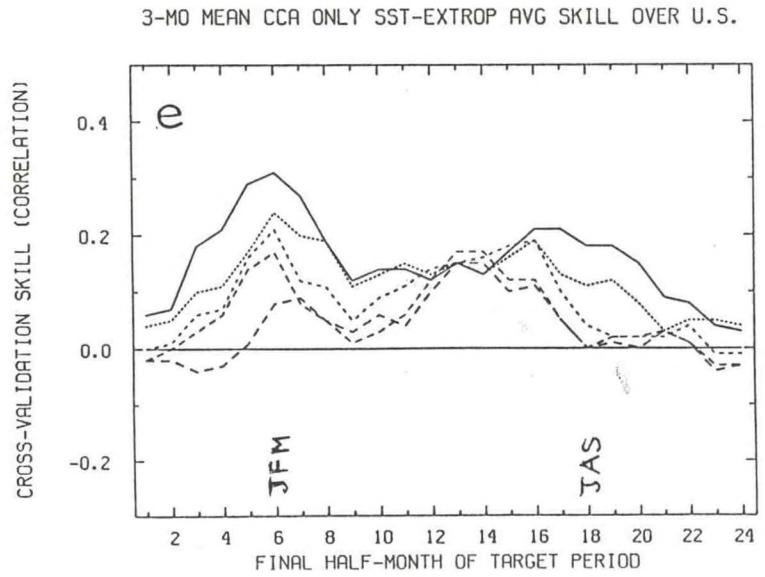
3-MO MEAN CCA ONLY SST-EXTROP AVG SKILL OVER U.S.
e
CROSS-VALIDATION SKILL (CORRELATION)
0.4
0.2
0.0
-0.2
JFM
JAS
2 4 6 8 10 12 14 16 18 20 22 24
FINAL HALF-MONTH OF TARGET PERIOD

mb height and then U.S surface temperature, and (2) there is redundancy among the three fields, as evidenced by the appearance of roughly similar annual profile shapes by each, and the greater amounts of skill produced by each than would be expected for independent contributions. Redundancy between 700 mb height and SST is also suggested by results using combinations of two out of three of the predictor fields (not shown). The SST alone experiment was further examined by using only tropical SST (25N-25S) and only extratropical SST (>25 degrees from equator). The results (Figs. 5d, 5e) reveal that (1) predictive signal is available from both tropics and extratropics, (2) skill tends to drop off much more quickly with increasing lead time using extratropical than tropical SST predictors, and (3) winter skill is available from either portion of the SST domain (at least for short leads), whereas summer skill is more favorable using tropical than extratropical SST predictors. It turns out that much of the winter predictive skill is attributable to ENSO, part of whose SST signature occurs in the north Pacific at a later time than the more basic tropical Pacific part; this explains why short lead winter forecasts based on extratropical SST can be as skillful as those that use tropical SST. Predictive skill using the global SST predictors (Fig. 5a) has the combined benefits of the features noted in Figs. 5d and 5e.

On the basis of the above experiments the three fields were retained as predictors but SST was weighted double its natural weight. The resulting skill profile is shown in Fig. 6, in which a favorable effect is noted as compared with Fig. 4a.

The skill level reflected in Fig. 6 for a given lead time at a particular time of the year is a spatial mean of skills at the 59 U.S. stations. A map of the geographical distribution of skill is associated with each such point in the Fig. 6 plot. Figure 7 presents the distributions of skill for 1 month lead for eight 1.5-month-apart 3 month periods spanning the annual cycle: Jan-Feb-Mar, mid-Feb to mid-May, Apr-May-Jun, etc. During the cold season (parts h, a and b) substantial skill is found in the southern and northern tiers of states, with some skill along the west coast. In the middle and late portions of the warm season (parts d and e) skill appears in the southern, eastern, far western, and changeable portions of the midsection of the country. In the spring (part c), while mean skill is lower, geographical continuity with the preceding and following periods is present with highest skill in the southern and western regions. In fall (parts f and g) what little skill exists is found in the far West, with another local peak in the extreme southern Rockies.

To determine which predictor fields and periods are most responsible for the skill of the set of forecasts made at a given lead at a specific time of the year, the canonical loading patterns are examined both by time and field. The "centers of action" in the loading patterns identify the predictor field's geographic regions giving rise to the skill. We next examine these skill sources for the relatively skillful forecasts of late winter (Jan-Feb-Mar) and late summer (mid-Jun to mid-Sep).

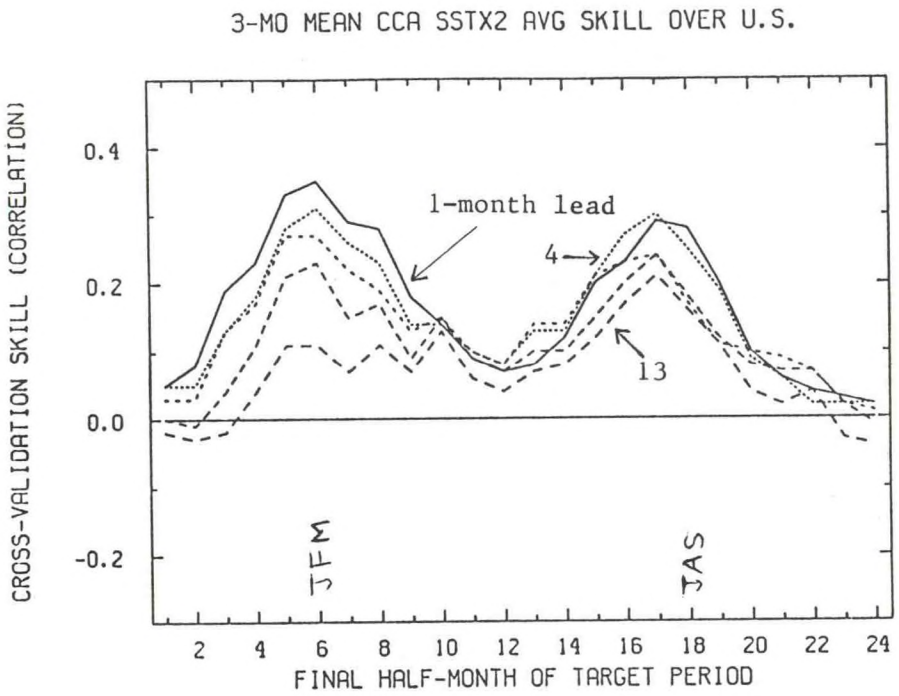

6. CCA forecast skill averaged over the U.S. for 3 month mean temperature (as in Fig. 4a), except the SST field is weighted double its natural value.

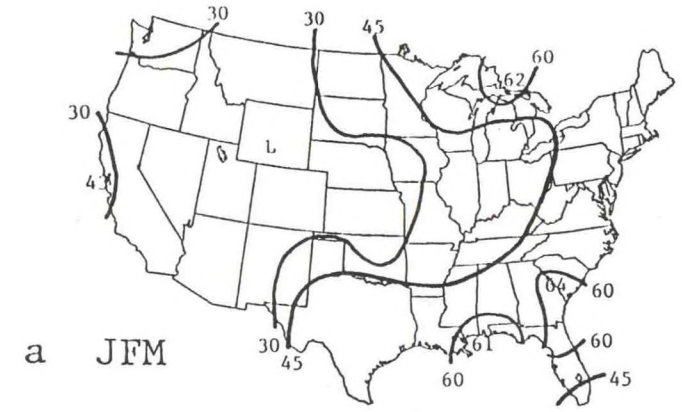

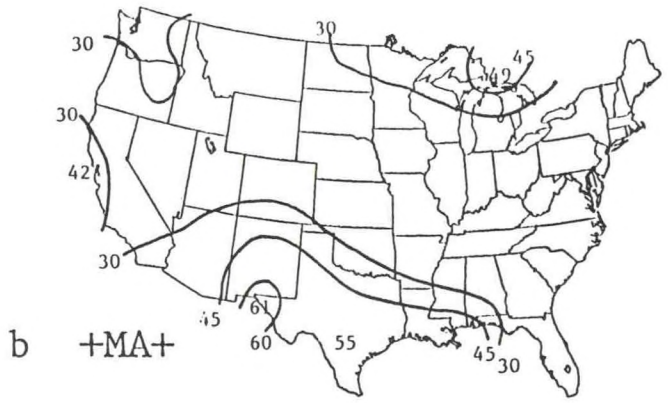

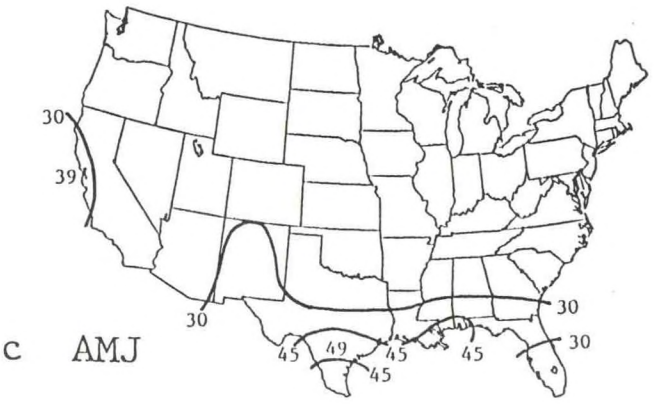

7. Geographical distribution of CCA skill in forecasting 3-month mean U.S. surface temperature at 1-month lead with double-weighted SST predictors for (a) JFM, (b) +MA+, (c) AMJ, (d) +JJ+, (e) JAS, (f) +SO+, (g) OND, and (h) +DJ+, where the "+" denotes the adjacent half of the neighboring month.

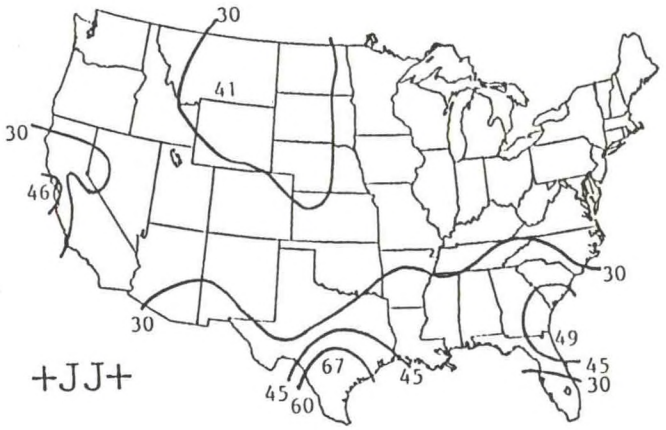
30
41
30
46
30
30
49
67
45
45
45
60
30

d +JJ+

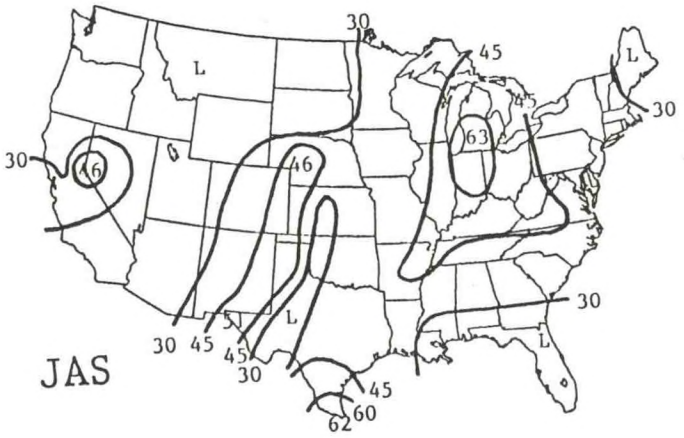
30
45
L
30
63
30
46
46
L
30
45
45
30
45
62
60
L

e JAS


30
41
30

f +SO+

g OND

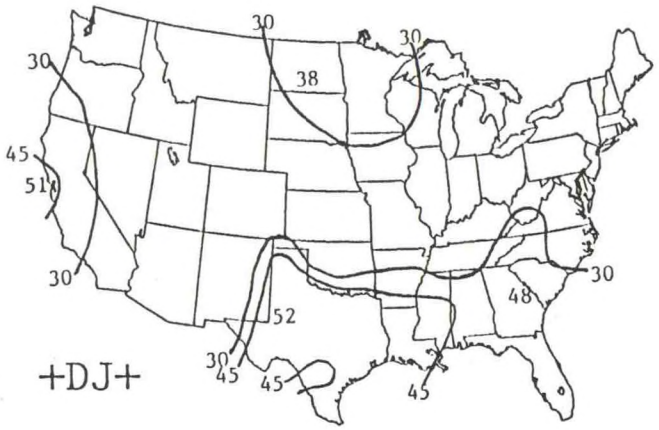

h +DJ+

(a) COLD SEASON 3-MONTH PREDICTABILITY

The skill of Jan-Feb-Mar forecasts made at the end of November (target period 6 at 1 month lead) is 0.31 for the originally weighted SST (Fig. 4a), and 0.35 for the double weighted SST (Fig. 6). Figure 7a shows the geographic distribution of skill for the forecasts using double weighted SST, revealing highest skill in the eastern U.S., especially in the southeastern, Gulf, and Great Lakes regions. Skill also appears in segments of the West Coast, to a lesser degree. The first three canonical modes, explaining 12, 11 and 5 percent respectively of the original predictand variance in a hindcast sense, contribute most systematically to this skill structure.

The SST predictor loading patterns for the four consecutive 3 month predictor seasons for the leading canonical mode are shown in Fig. 8. The times of these patterns include the winter beginning 13 months prior to the predictand period (i.e. Dec-Jan-Feb; part a), spring (part b), summer (part c) and the leading fall (Sep-Oct-Nov; part d). The patterns portray the development of a cold tropical Pacific SST ENSO event beginning the previous spring and strengthening dramatically in the summer and leading fall. The corresponding mode 1 700 mb height loadings (Fig. 9) are weaker and noisier. While development of positive loadings in the North Pacific, suggested from the spring (part b) through fall (part d) panels, would not necessarily be expected to accompany a cold tropical Pacific SST event during the warm half of the year, in the leading fall this center is farther north and becomes part of a negatively phased PNA-like pattern with the added presence of a negative loading center in western Canada. The U.S. surface temperature predictor loadings for mode 1 (not shown) are generally weak and noisy, although they do show consistency (perhaps redundancy) with the 700 mb height loading patterns of Fig. 9.

The principal predictand map, containing the U.S. surface temperature predictand loadings for CCA mode 1, is shown in Fig. 10. This is the Jan-Feb-Mar temperature pattern associated with the mode 1 SST, 700 mb and U.S. surface temperature predictor scenario described above. It is the linear combination of predictand elements most related to the linear combination of the predictor elements. While its shape is somewhat similar to that of the cross-validated skill shown in Fig. 7a, the sign of the loadings over the Gulf states is opposite that in the Great Lakes region. It is the forecasting of this dipole pattern that gives rise to highest skill near the poles of the pattern. The strength of the loadings in Fig. 10 (as also in Figs. 8 and 9) may be stronger than the forecast versus observation correlations in Fig. 7a, because the former are not subjected to cross-validation. The strength of the loadings may also be weaker than the skills, given that the latter are based on the additive contributions of the first four to six CCA modes and not just the first (strongest) one shown in Figs. 8-10. The fact that Figs. 7a and 10 show rough pattern similarity implies that CCA mode 1 is

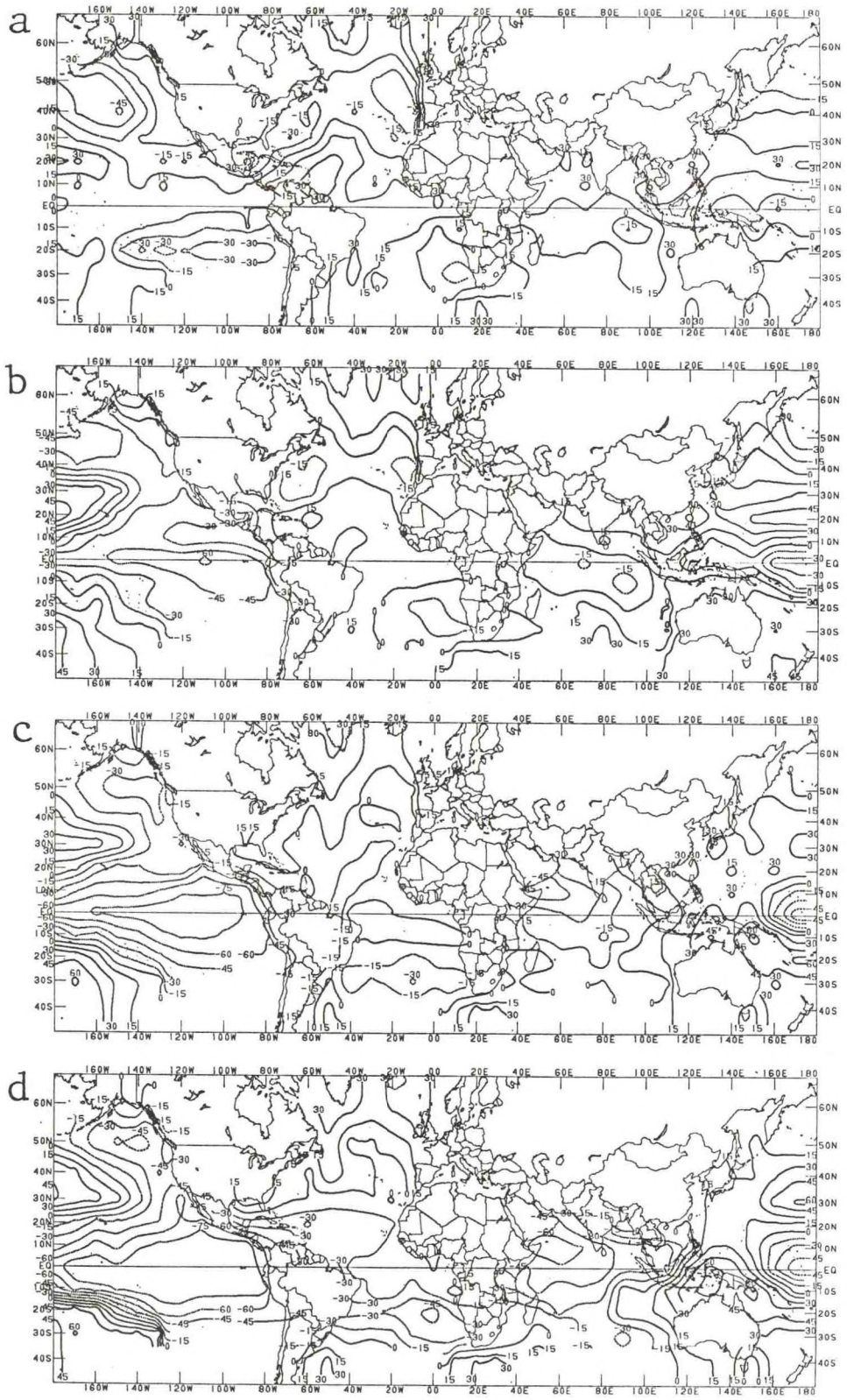

8. SST predictor CCA loadings for mode 1 for prediction of Jan-Feb-Mar U.S. surface temperature at 1 month lead. Parts (a), (b), (c), and (d) show loadings for the first (Dec-Jan-Feb), second (Mar-Apr-May), third (Jun-Jul-Aug) and fourth (Sep-Oct-Nov) predictor periods, respectively.

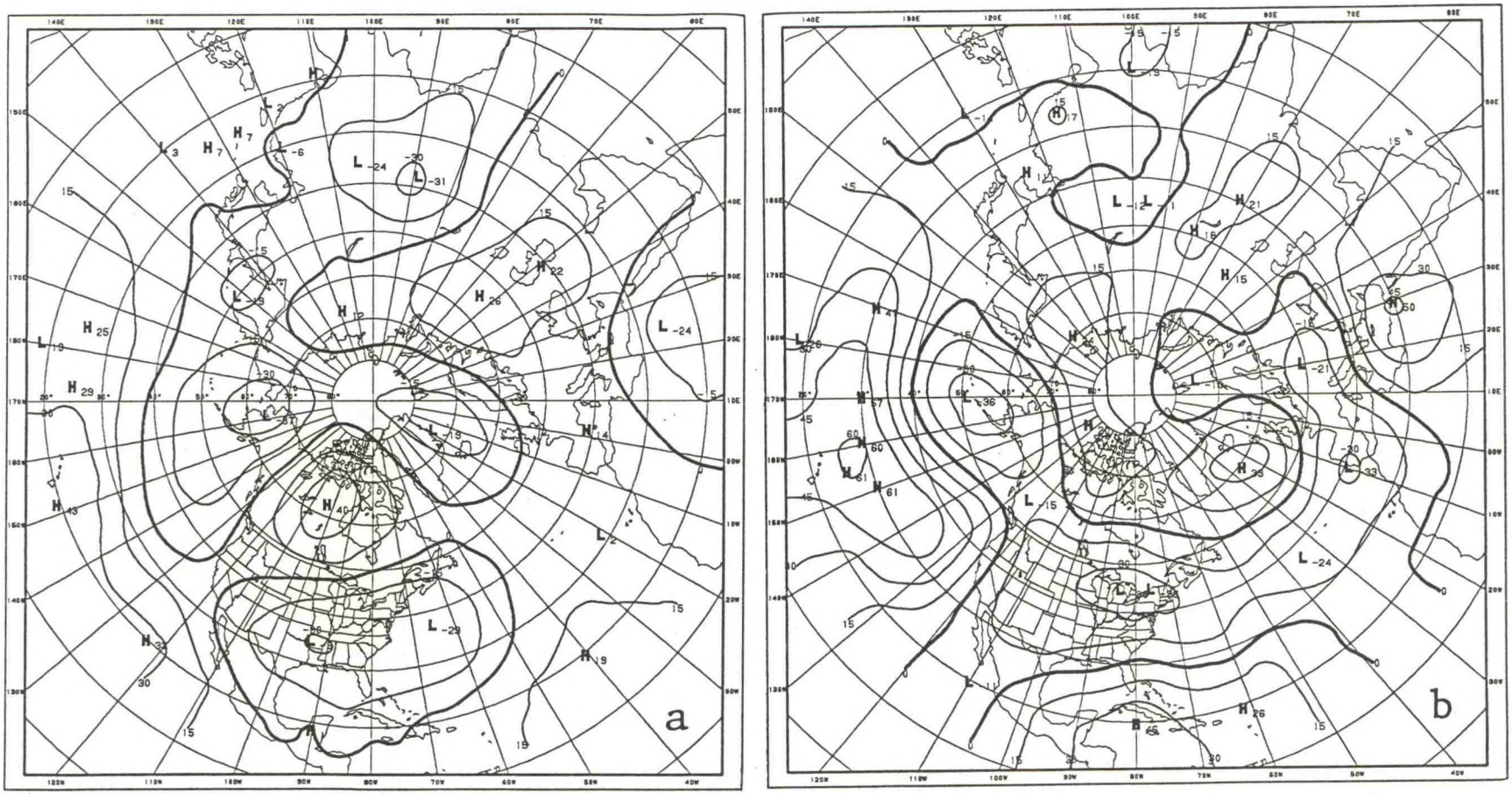

9. As in Fig. 8, except for 700 mb predictor loadings for forecasts of Jan-Feb-Mar U.S. surface temperature.

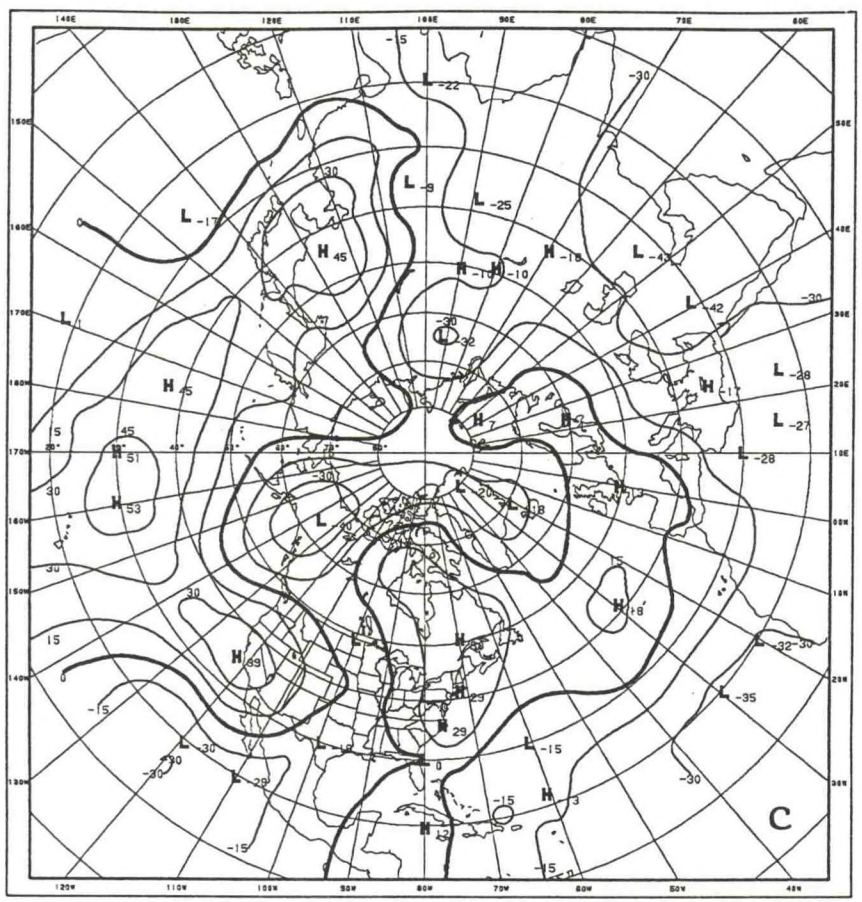
c

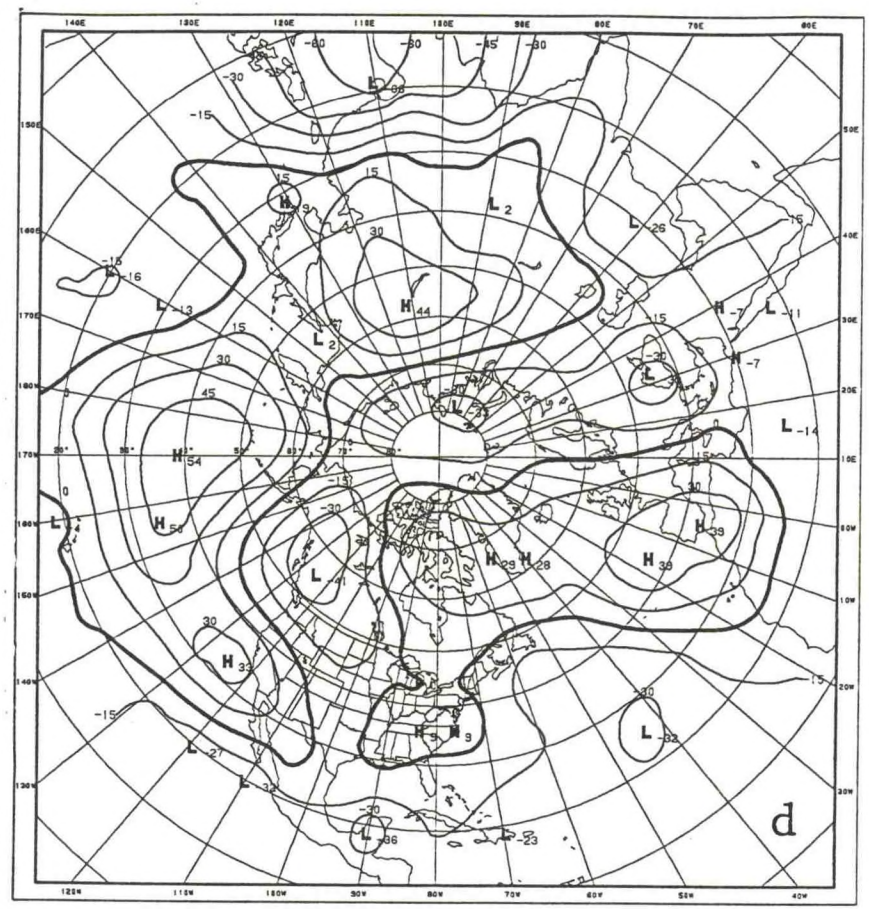
d

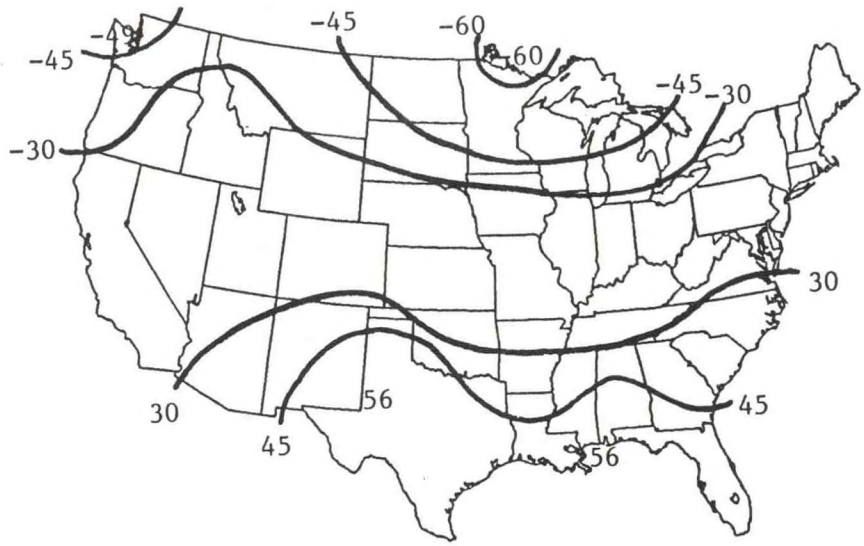

10. The principal predictand loading pattern for mode 1 for the prediction of Jan-Feb-Mar U.S. surface temperature at 1 month lead.

dominant in shaping the spatial skill distribution as well as the pattern of the forecasts. In this case it points to the importance of ENSO events in determining the Jan-Feb-Mar U.S. surface temperature. CCA mode 1 describes how the Jan-Feb-Mar temperature responds to a spring/summer onset and fall/winter maturation of a cold (warm) ENSO episode: The southern states tend to have positive (negative) temperature anomalies and the northern Plains and Great Lakes negative (positive) anomalies when (1) the SST anomaly in the central and eastern tropical Pacific becomes increasingly negative (positive) beginning the previous spring, (2) the SST anomaly near Indonesia becomes increasingly positive (negative) beginning the previous summer, and (3) the SST anomaly well south of the Aleutian Islands becomes somewhat positive (negative) beginning the previous summer. These relationships are all in broad agreement with other descriptions of simultaneous ENSO related climate effects (e.g. Van Loon and Madden 1981, Ropelewski and Halpert 1986). (The statements are equally applicable to warm or cold ENSO events. This is based on the linearity of CCA, in which the displayed polarity of the loadings is arbitrary as long as polarity opposites and matches are respected.) While the role of 700 mb height predictors may sometimes be substantial, this does not appear to be the case during much of the predictor period for mode 1.

The canonical component time series associated with the mode 1 predictor scenario, shown in Fig. 11, confirms that ENSO is being described by this mode. The "W" and "C" symbols denote warm and cold ENSO years as identified by Ropelewski and Halpert (1987,1989) (labeled by the year leading into the mature ENSO winter, which is when the predictors show their ENSO-discriminating behavior).

CCA mode 2 is weaker than mode 1. Its predictor loading patterns for the prior summer (3rd predictor period), which are strongest among the 4 periods, for SST and 700 mb height are shown in Figs. 12a and 12b, respectively. The principal predictand loading map, shown in Fig. 12c, suggests that this mode contributes to the cross-validated skill (Fig. 7a) in the central and south portions of the eastern U.S. While the tropical Pacific SST does not play a key role here, the tropical Atlantic and Indian Ocean SST does. The scenario implied in Fig. 12 is that the middle Atlantic and southeastern states tend to receive below (above) normal Jan-Feb-Mar temperatures (Fig. 12c) when (1) the SST anomaly in the eastern Indian Ocean and tropical Atlantic is negative (positive) the previous spring (not shown) and summer (Fig. 12a) and (2) there is a weak but recognizable Subtropical/Zonal (SZ) 700 mb height pattern (Barnston and Livezey 1987) with mostly negative (positive) anomalies in the subtropical latitudes (except in North America) in the prior summer (Fig. 12b). The canonical component times series associated with this mode (not shown) shows a quasi-decadal cycle with some major higher frequency oscillations superimposed. The origin of this mode is unknown.

CCA mode 3 describes the aftereffects of a mature ENSO event from the previous winter and spring. Figures 13 and 14 show the

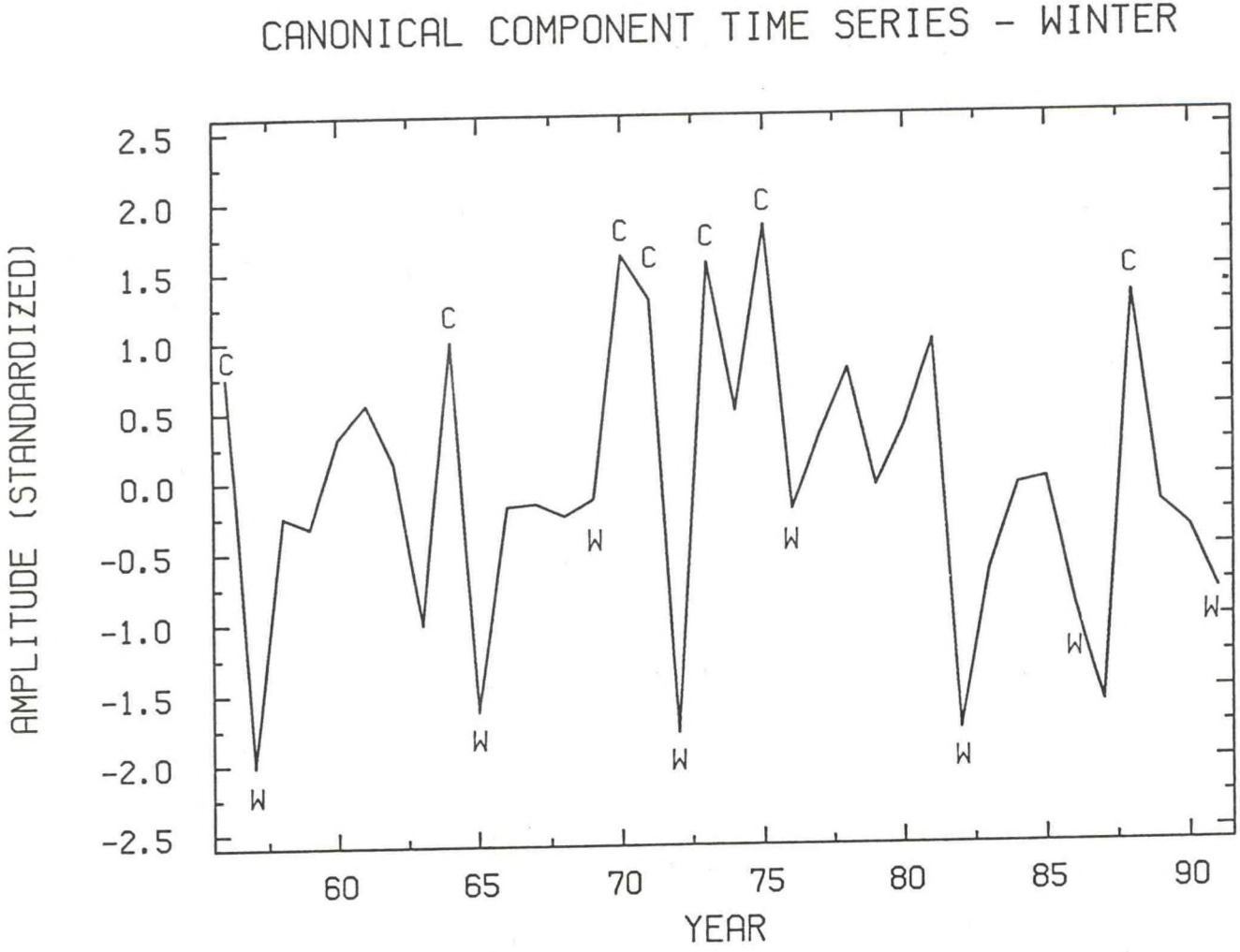

11. The canonical component predictor time series for mode 1 for the prediction of Jan-Feb-Mar U.S. surface temperature.

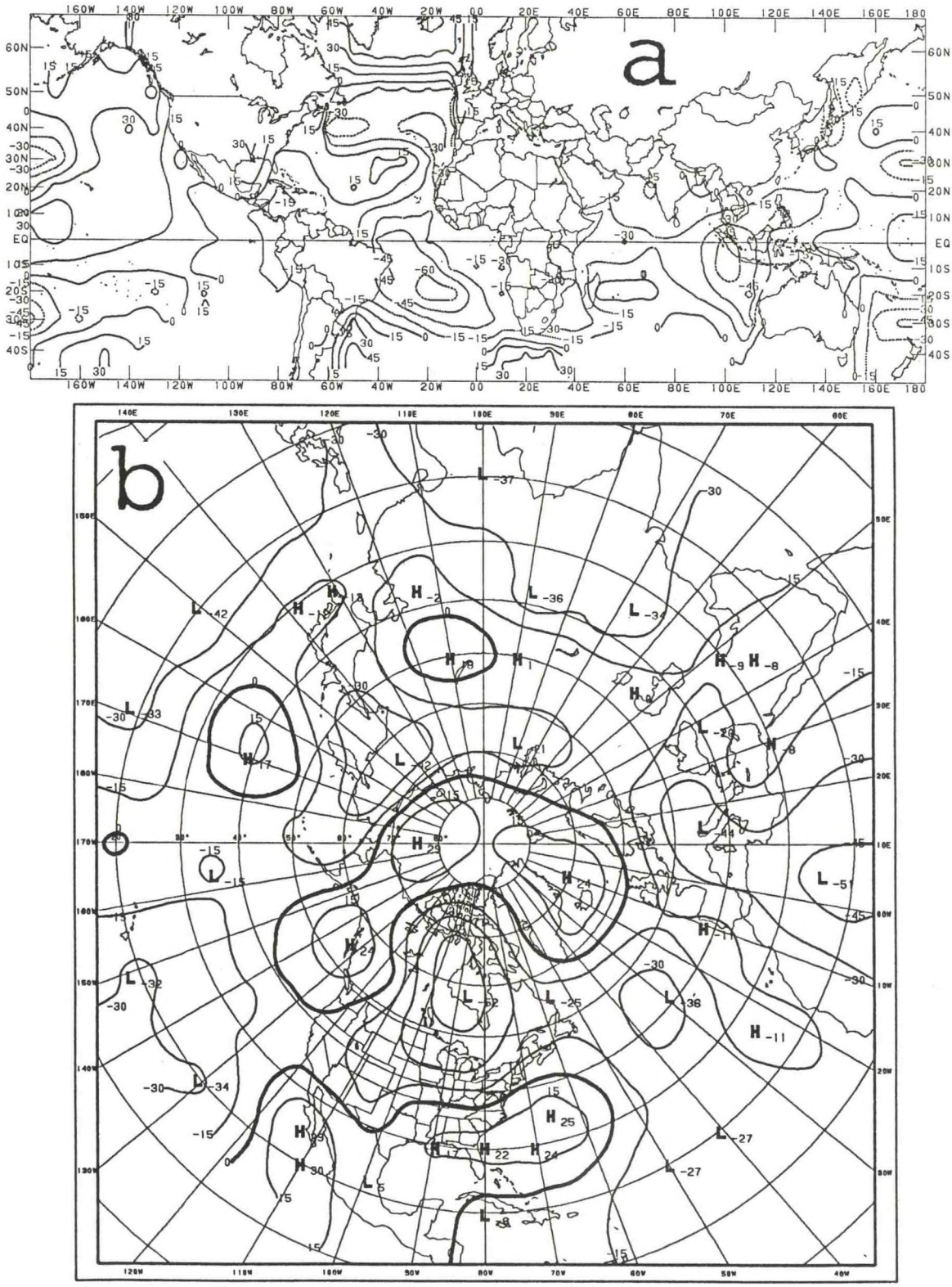

12. Part (a): As in Fig. 8 (SST predictor CCA loadings) except for mode 2, for the third (Jun-Jul-Aug) predictor period. Part (b): As in part (a), except for third period 700 mb predictors. Part (c): The principal predictand loading pattern for mode 2 for prediction of Jan-Feb-Mar U.S. surface temperature at 1 month lead.

C

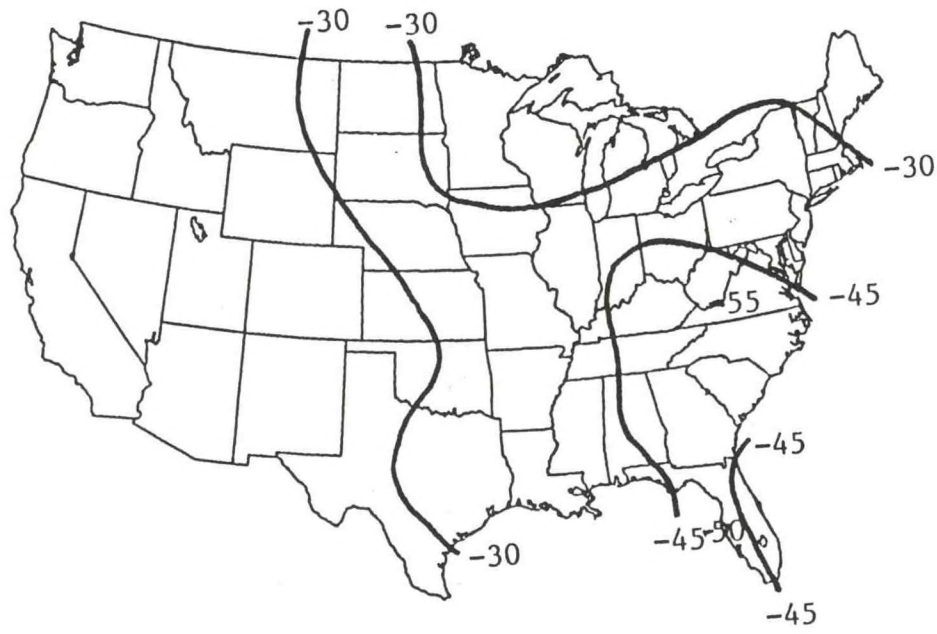

SST and 700 mb loading patterns, respectively; the weaker 700 mb loading pattern for the final period (fall) is omitted. The U.S. temperature predictor loading pattern for periods 1 and 2 (prior winter and spring) are shown in Fig. 15, and the U.S. temperature predictand loading pattern for mode 3 is shown in Fig. 16. The ENSO event (with cold Pacific SST, here) is strongly present in all three predictor fields during the prior winter and spring, with 700 mb and U.S. temperature patterns (Figs. 14 and 15) highly similar to those found related to the Southern Oscillation in Ropelewski and Halpert (1986), Barnston et al. (1991), and elsewhere. The SST loading patterns (Fig. 13) show rapid dissipation of the ENSO event from spring through fall, but a persistence of like-signed SST anomalies in the Indian Ocean and a development of same in the Atlantic in spring and summer. The summer 700 mb predictor loading pattern is weak but shows an SZ-like pattern with negative values at low latitudes, reinforcing the idea suggested in mode 2 of a relationship in the NH summer between tropical SST anomalies in at least two of the three major oceans and subtropical NH 700 mb height anomalies of the same sign at a majority of the longitudes. The mode 3 principal predictand pattern (Fig. 16) indicates positive (negative) anomalies in much of the eastern portion (particularly the Northeast) of the U.S. and negative (positive) anomalies along the California coast during the Jan-Feb-Mar period a year after a mature cold (warm) water ENSO event. This roughly suggests a counter-clockwise rotation of the ENSO related U.S. temperature pattern for the year following an ENSO event; however, appearing as the third mode, the reliability of this rule must be considered cautiously. The canonical component time series associated with mode 3 (not shown) is moderately well correlated with that of mode 1 (Fig. 11) when the two series are offset by one year, but are orthogonal (by definition) without the temporal offset.

All three leading modes described above link predicted Jan-Feb-Mar U.S. temperature to very recent (and suggested concurrent) or past (up to 13 months earlier) tropical SST anomalies. Modes 1 and 3 describe differently timed ENSO events, while mode 2 involves the SST in the tropical Atlantic and Indian Oceans.

The strongest centers on the principal predictand loading maps for modes 1, 2 and 3 (Figs. 10, 12c, 16) carve out most of the areas shown in Fig. 7a to be most skillfully forecast using the three modes (plus some weaker higher order modes). It is expected that in the formation of an actual forecast, projections of the observed antecedent patterns onto these modes may partially or substantially offset one another in some regions.

Seasonal forecasts made at longer leads than 1 month, or for different but overlapping target periods, retain similar CCA predictor and predictand loading pattern scenarios to those described above, taking movement of the predictor time window into account. For example, the loading pattern diagnostics for mode 1 for a 4 month lead forecast for the same Jan-Feb-Mar period (the SST portion of whose predictor patterns is shown in Fig. 17) shows the development of an ENSO event in similar fashion to that for the 1 month lead forecast, except that the lead-

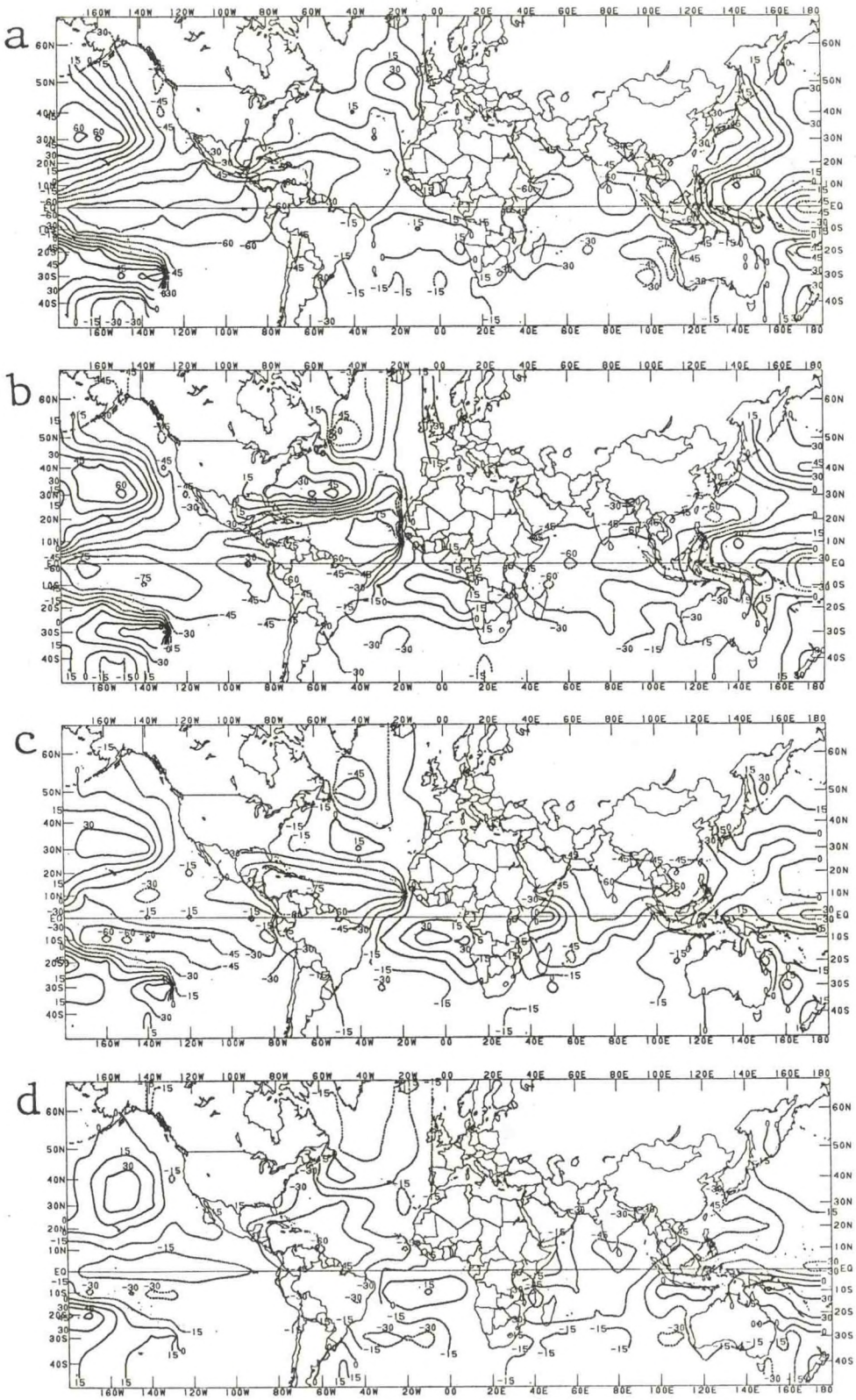

13. As in Fig. 8, except for mode 3. Parts (a), (b), (c), and (d) show loadings for the first (Dec-Jan-Feb), second (Mar-Apr-May), third (Jun-Jul-Aug) and fourth (Sep-Oct-Nov) predictor periods, respectively.

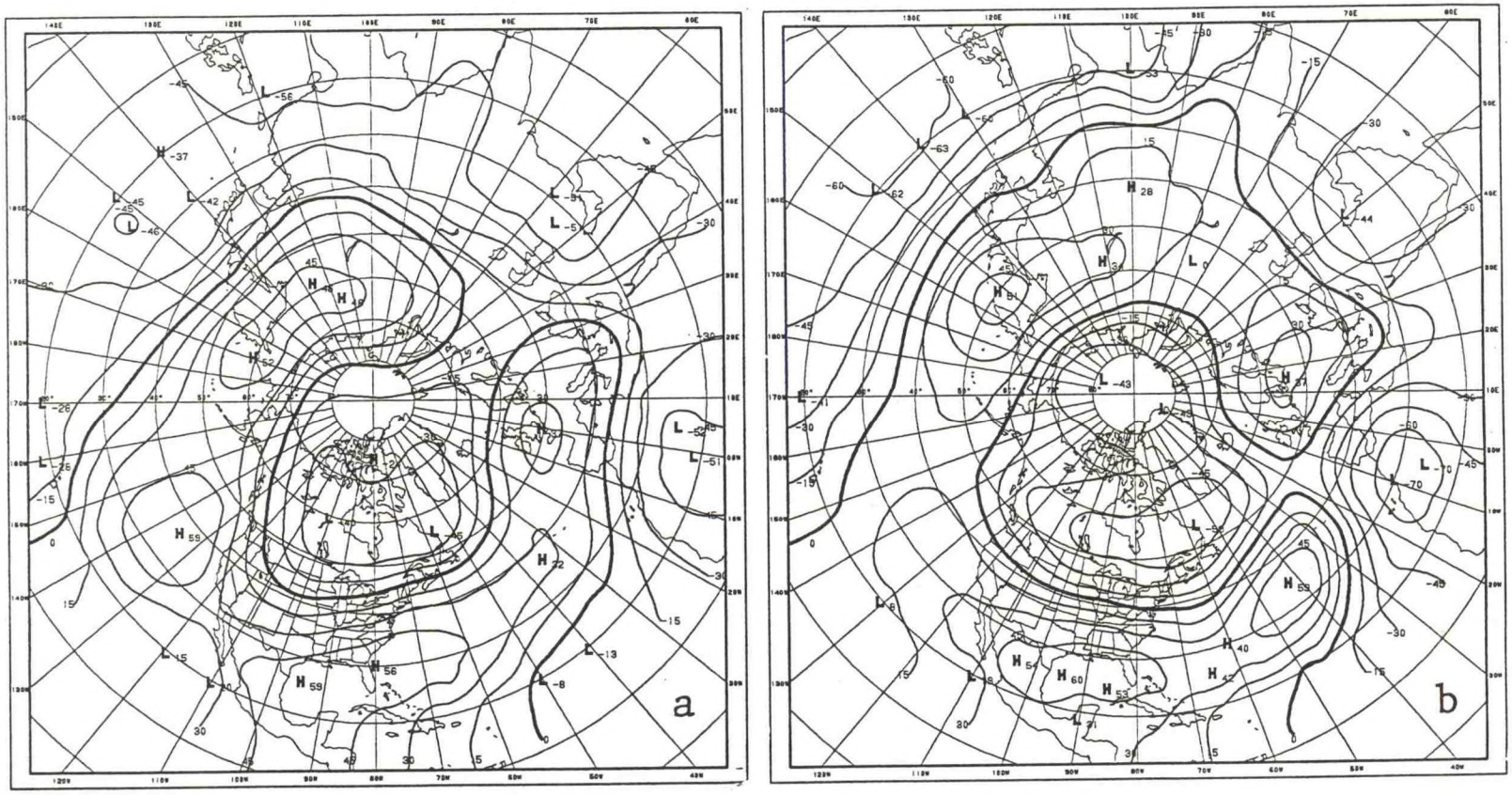

14. As in Fig. 13 except for 700 mb predictor loadings for (a) the first, (b) second, and (c) third predictor periods.

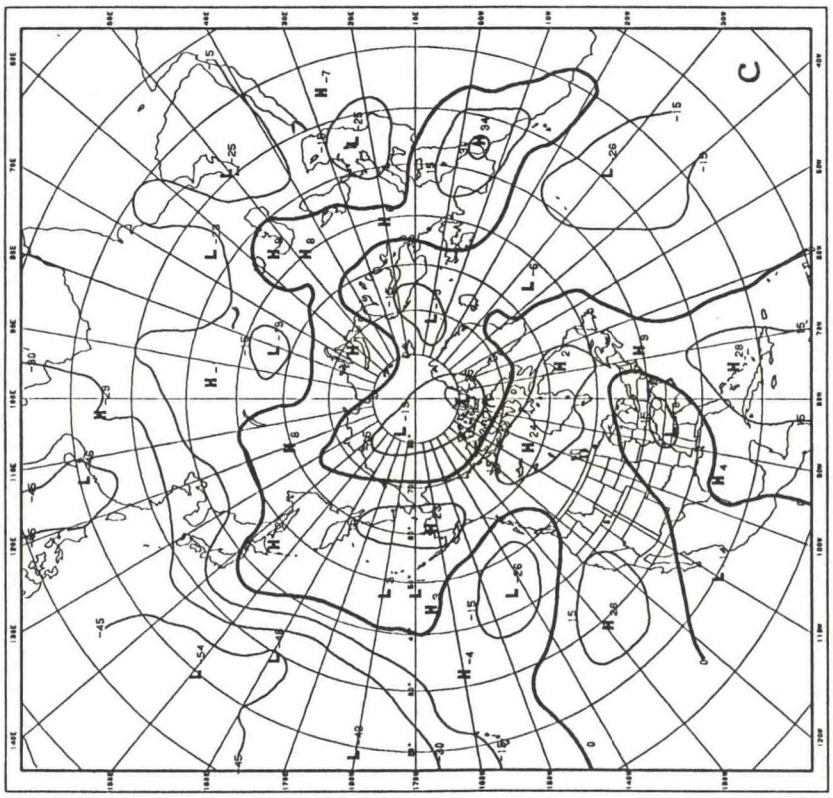
C

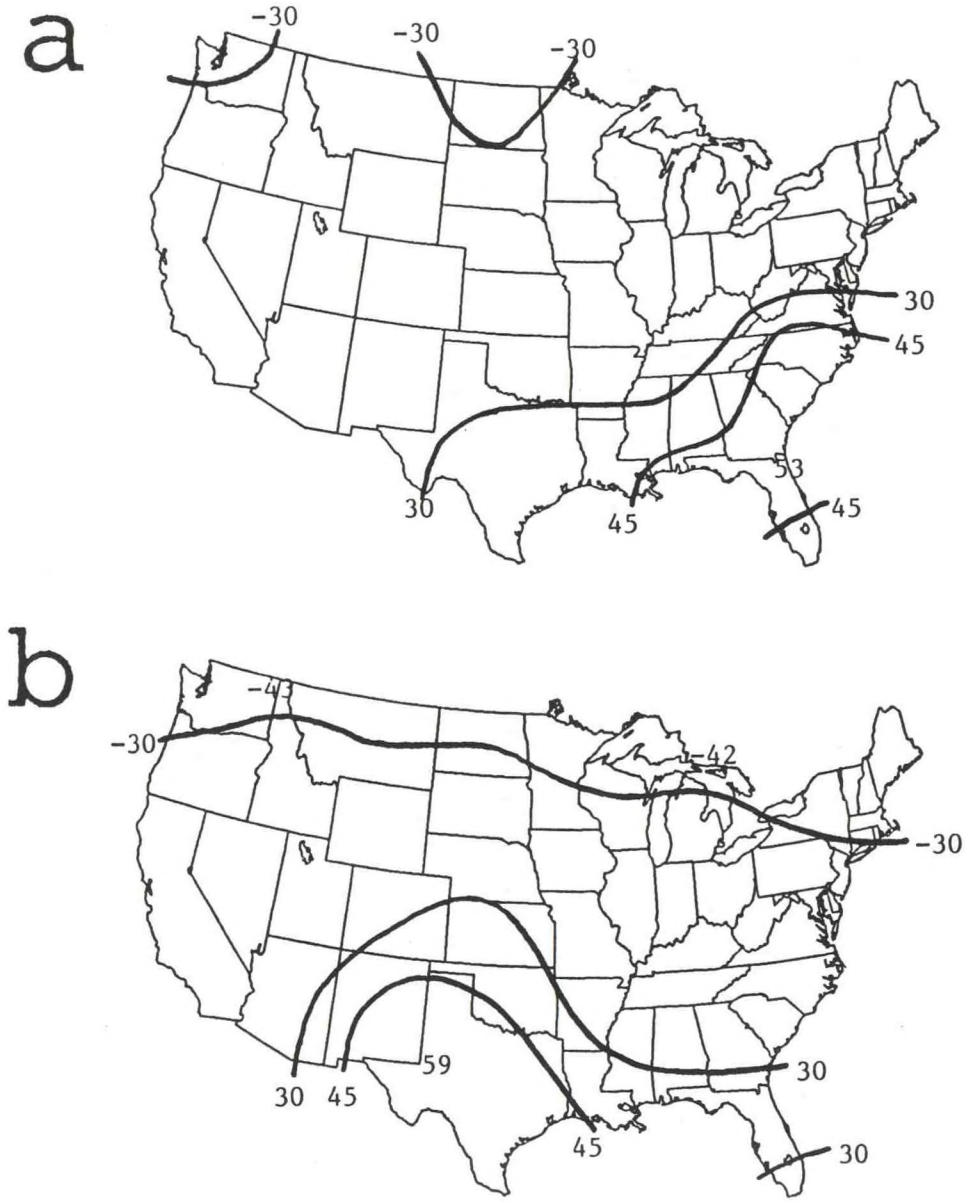

15. As in Fig. 13 except for the U.S. surface temperature predictor loadings for (a) the first and (b) second predictor periods.

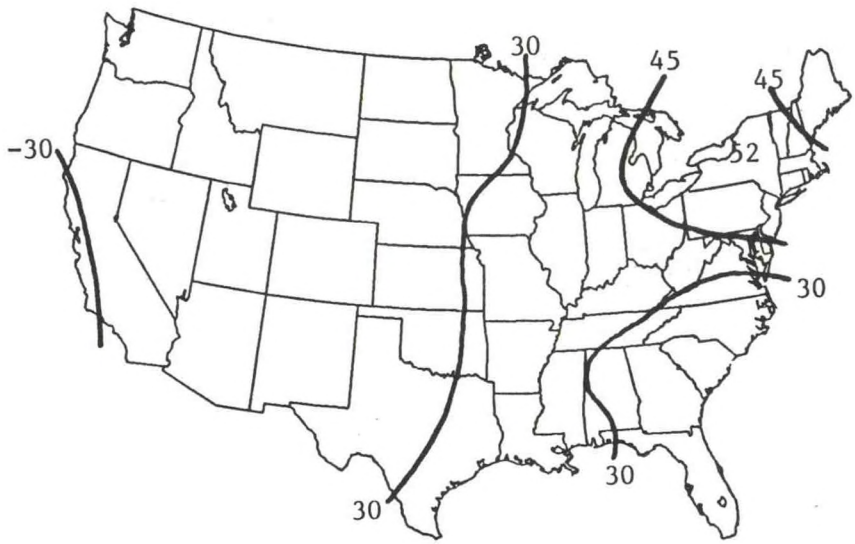

16. The principal predictand loading pattern for mode 3 for the prediction of Jan-Feb-Mar U.S. surface temperature at 1 month lead.

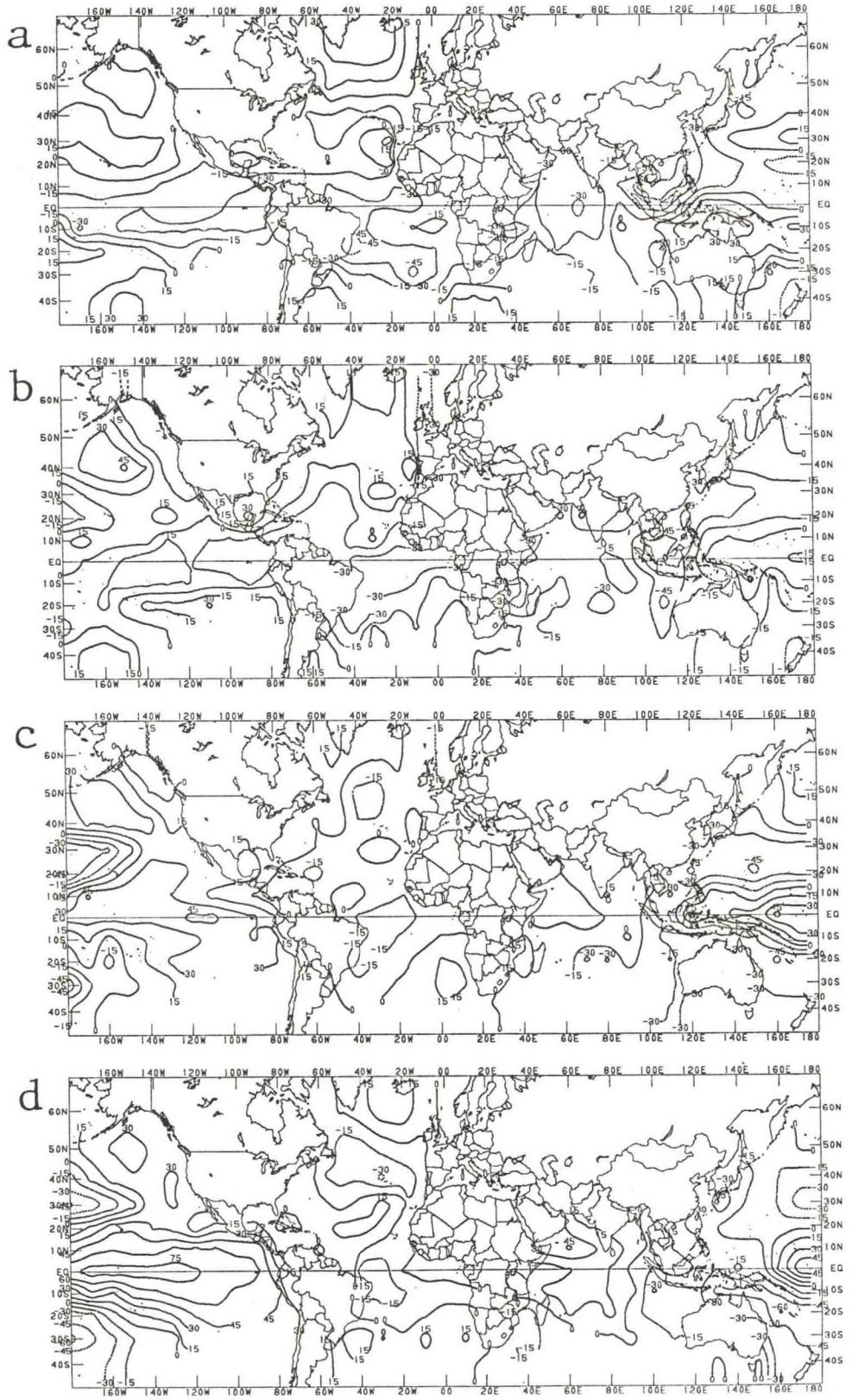

17. SST predictor CCA loadings for mode 1 for prediction of Jan-Feb-Mar U.S. surface temperature at 4 months lead. Parts (a), (b), (c), and (d) show loadings for the first (Sep-Oct-Nov more than a year prior), second (Dec-Jan-Feb), third (Mar-Apr-May), and fourth (Jun-Jul-Aug) predictor periods, respectively.

ing fall is no longer included and the fall a year earlier is included. The backward movement of the predictor window makes for a slightly less accurate anticipation of the ENSO event, since the critical predictor behavior is captured only in the latter portion of that window. The mode 1 principal predictand map for the 4 month lead case (not shown) has a weaker version of the same northern versus southern tier dipole seen in Fig. 10. Modes 2 and 3, while less similar to their counterparts in the 1 month lead experiment, reflect some of the same associations in different combinations, in addition to some of the remainder from mode 1. That the skill of the 4 month lead forecast is not significantly less than that of the 1 month lead (Fig. 6) suggests that seasonal temperature forecasts for the U.S. in winter/early spring are generally determinable (with modest skill) several months prior to the beginning of the winter. Such forecasts appear to depend on the low frequency component of climate variability such as tropical SST, whose behavior over a long period ending several months prior to forecast time appears to be nearly as useful as that ending much closer to forecast time. Figure 6 shows that such long lead possibilities generally exist for any of the target seasons having relatively high predictive skill for 1 month lead--i.e., those in winter through early spring and summer through early fall.

(b) WARM SEASON 3-MONTH PREDICTABILITY

The skill of mid-June through mid-September forecasts made in the middle of May (target period 17 at 1 month lead) is 0.29 both for the originally weighted (Fig. 4a) and double weighted SST (Fig. 6). Because sources of skill in forecasting summer U.S. temperature are not common (empirical or dynamical) knowledge (in contrast to the role of ENSO in winter forecasting), the skill sources of the forecasts are examined with little prior expectation.

Figure 18 shows the geographic distribution of the skill for mid-June through mid-September forecasts using double weighted SST predictors. The pattern is widespread and somewhat scattered, with highest skill in southern Texas, the northern Rockies/northwestern Plains, central Midwest, and southern Appalachians. The first three canonical modes explain 16, 4 and 3 percent respectively of the original predictand variance in a hindcast sense. In this case mode 1 has marked dominance and can be assumed to contribute heavily to the skill pattern appearing in Fig. 18.

The SST predictor loading patterns for the four consecutive 3 month predictor seasons (mid-May to mid-Aug, mid-Aug to mid-Nov, mid-Nov to mid-Feb, and mid-Feb to mid-May--to be called summer, fall, winter and spring, respectively, in this discussion) for mode 1 are shown in Fig. 19. All four predictor periods present a like-signed anomaly of moderate intensity in <u>all three</u> tropical oceans, with remarkable uniformity in loading intensity across oceans and periods. There is a tendency for the tropical Pacific to be most strongly involved in the first

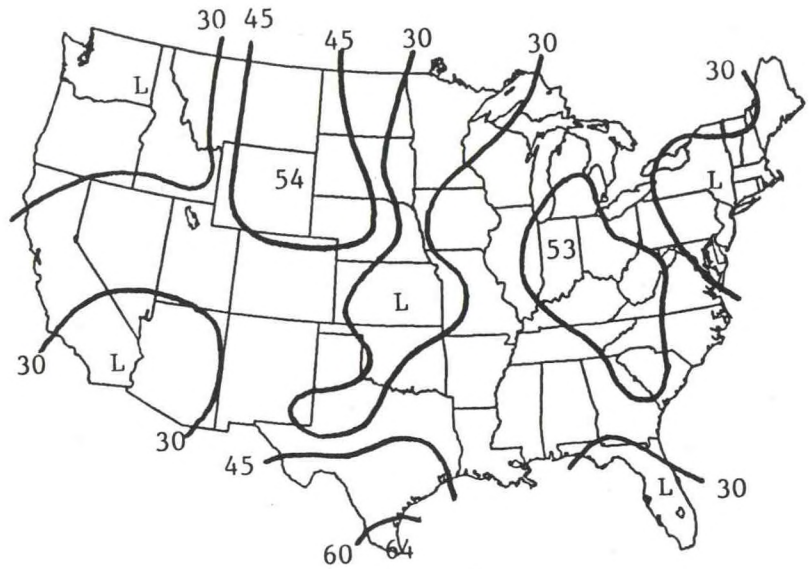

18. Geographical distribution of CCA skill in forecasting 3-month mean U.S. surface temperature at 1-month lead with double-weighted SST predictors for mid-Jun to mid-Sep.

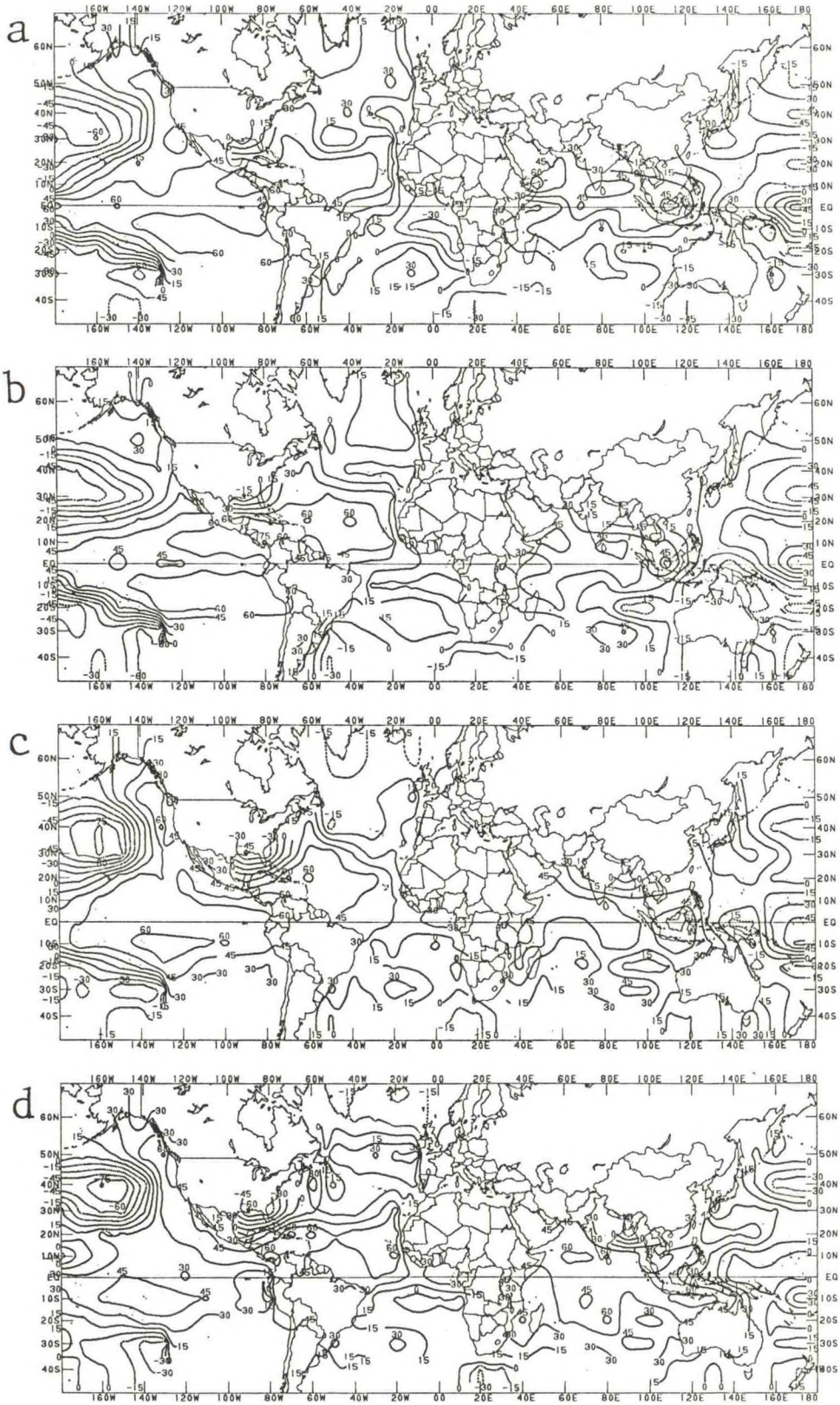

19. SST predictor CCA loadings for mode 1 for prediction of mid-Jun to mid-Sep U.S. surface temperature at 1 month lead. Parts (a), (b), (c), and (d) show loadings for the first (mid-May to mid-Aug, or "summer"), second (mid-Aug to mid-Nov, or "fall"), third (mid-Nov to mid-Feb, or "winter") and fourth (mid-Feb to mid-May, or "spring") predictor periods, respectively.

(summer) predictor period and for its involvement to gradually diminish over the following three seasons.

The corresponding 700 mb height predictor loading patterns are shown in Fig. 20. In the prior summer and fall (parts a and b) strong Subtropical/Zonal (SZ) patterns are noted, with low latitude anomalies of like sign to that of the tropical SST noted in Fig. 19. In winter and spring (parts c and d) there appears a Pacific/North American pattern (PNA; Wallace and Gutzler 1981, Horel 1981, Esbensen 1984, Barnston and Livezey 1987) with a suggestion also of a Tropical/Northern Hemisphere pattern (TNH; Mo and Livezey 1986, Livezey and Mo 1987, Barnston and Livezey 1987), with polarities compatible with the sign of the SST loadings in the tropical Pacific (Fig. 19c,d) to be associated with an ENSO episode. Even in these latter two maps there is an SZ signature, with the same anomaly sign across all subtropical longitudes except near Mexico.

Figure 21 shows the mode 1 principal predictand pattern associated with the mid-June through mid-September forecasts. While much of the U.S. has at least modest involvement, the strongest "centers of action", all of the same polarity, appear in the northern Rockies and Great Basin, with a secondarily active area in portions of the Midwest and eastern states. The mode 2 and 3 predictand loading maps (not shown) are considerably weaker and less coherent, and of no interest. Their contributions can be noted as part of the difference between Fig. 21 and Fig. 18.

The canonical component time series associated with the mode 1 predictors is shown in Fig. 22. This plot reflects both a 3 to 5 year cycle (with a weak to moderate linkage to ENSO) and an interdecadal cycle in which values tend to be high in the late 1950s and very early 1960s, lower from the mid-1960s through mid-1970s, and higher again from around 1980 through the early 1990s. This implication of very low frequency climate change for the summer target period has been noted in Barnett and Preisendorfer (1987) with somewhat different phasing for a non-monopole U.S. temperature principal predictand pattern, using somewhat different SST predictors and a different period of record. The monopole temperature pattern obtained here is compatible with results in Jones et al. (1982), who found the Northern Hemisphere average temperature to be lowest from the middle 1960s through the middle to late 1970s, preceded and followed by warmer temperatures. The cause of such a global climate change is unknown.

The fact that there is interannual autocorrelation in the U.S. summer temperature implies a violation of the independence assumption required for optimally representative use of cross-validation. However, direct calculation of the autocorrelation shows it to be weak when the other sources of total variability are included: The mean 1-year autocorrelation over the 59 stations is 0.09 (see also Fig. 9 in Van den Dool et al. 1986) with only 8 stations having statistically significant (i.e., >0.35) autocorrelations, occurring in Florida, south Texas, the southern Rockies and the desert southwest. The CCA results are therefore

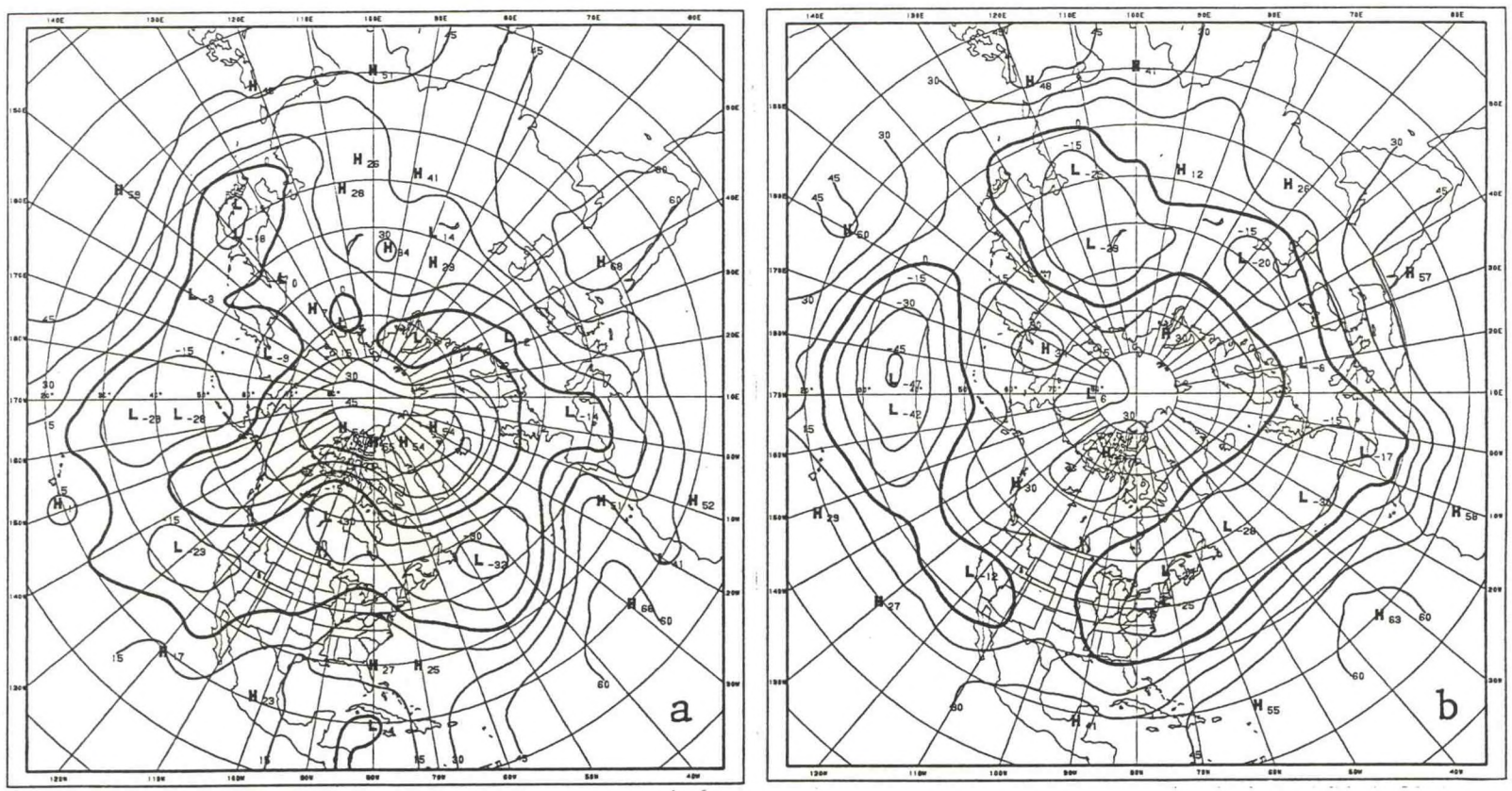

20. As in Fig. 19, except for 700 mb predictor loadings for forecasts of mid-Jun to mid-Sep U.S. surface temperature.

c
d

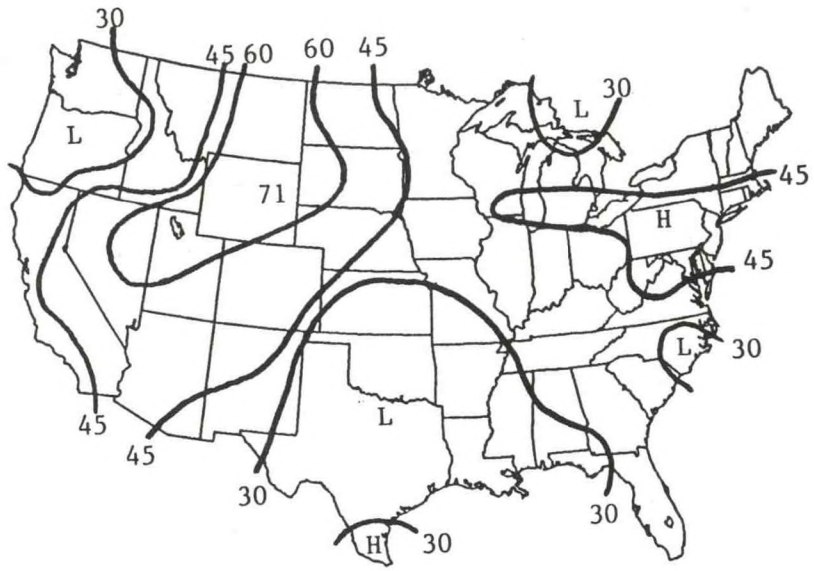

21. The principal predictand loading pattern for mode 1 for the prediction of mid-Jun to mid-Sep U.S. surface temperature at 1 month lead.

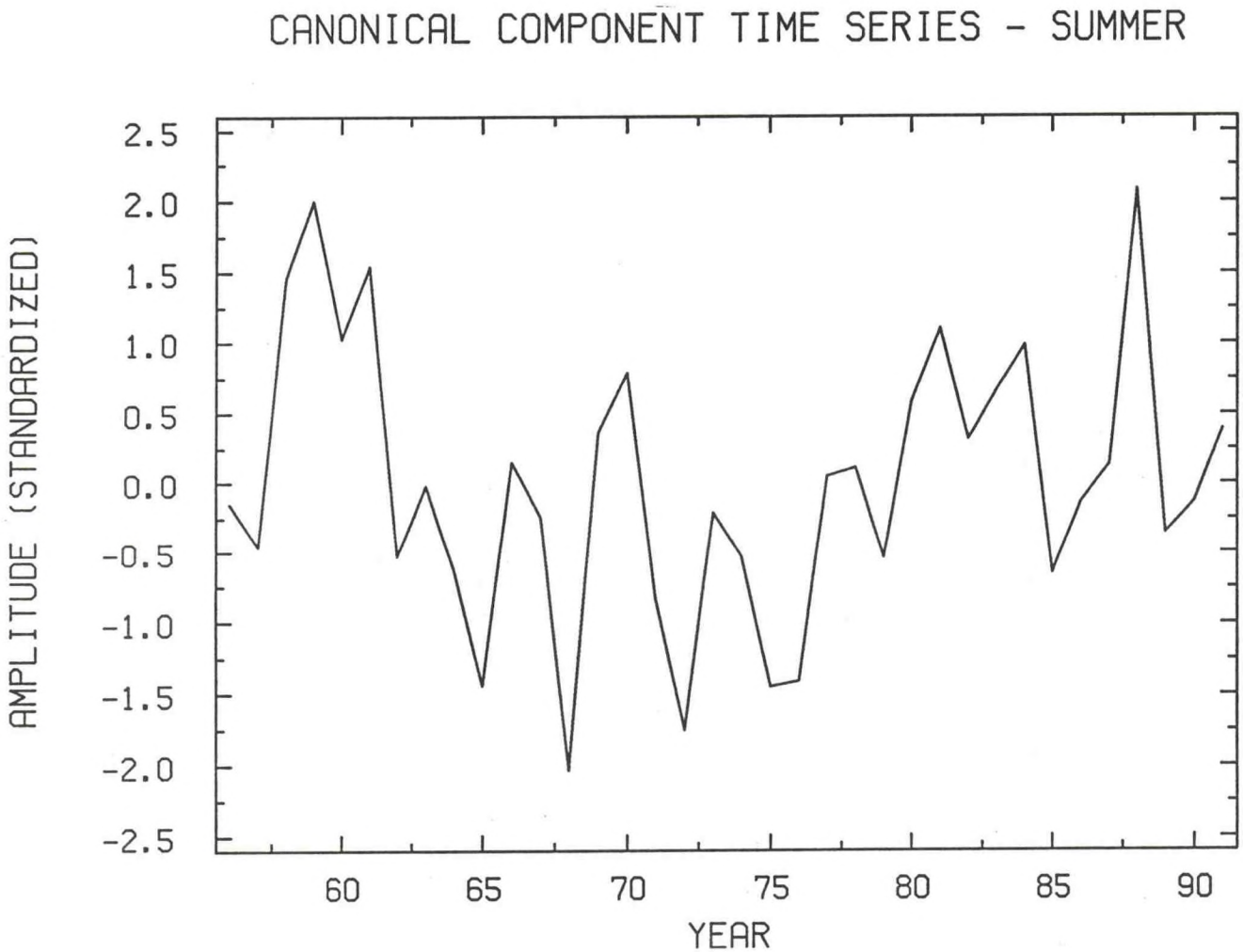

22. The canonical component predictor time series for mode 1 for prediction of mid-Jun to mid-Sep U.S. surface temperature.

likely representative in terms of the general scenario and pattern characteristics, but the associated forecast skill estimates may be slightly inflated, particularly along the southern border of the country.

While cross-validated skill results are highlighted in Fig. 7 for the eight 1.5-month-apart 3 month seasons, such results were also examined for all 24 overlapping seasons. In the skillful portion of the cold season the geographic distributions of skill for adjacent overlapping periods are quite similar, as are the CCA predictor loading maps and principal predictand maps for the leading one or two modes. In the skillful portion of the summer this is the case for the predictor loading maps, but not for the principal predictand maps or the skill patterns. To illustrate, we compare results for Jul-Aug-Sep to those for mid-Jun to mid-Sep which were just described. The predictor loading patterns for the Jul-Aug-Sep forecasts are quite similar to those shown in Figs. 19 and 20 for mid-Jun to mid-Sep; ENSO effects appear slightly more prominently for Jul-Aug-Sep. The geographical distributions of skill for the two forecasts, however, are substantively different (compare Fig. 18 for mid-Jun to mid-Sep to Fig. 7e for Jul-Aug-Sep). In Jul-Aug-Sep the skill is centered not in the northern Rockies, but in the lee of the Rockies and Midwest. The principal predictand loading pattern for mode 1 (Fig. 23) reveals a broad active area in much of the eastern and central U.S., in contrast with the comparable map for mid-Jun to mid-Sep (Fig. 21). The predictand loading patterns for subsequent modes are weak and do not compensate for the mode 1 differences.

The common factor between the two warm season cases is the general tendency for the same temperature anomaly sign across much of the U.S. as the SST anomaly in the prior year across much of the tropical ocean belt (including the Pacific, where it is associated with ENSO). The 700 mb height at low latitudes assumes the same anomaly sign as that of the SST in the predictor periods. This is most clearly noted in prior warm seasons; in cold seasons meridionally amplified wave patterns (e.g. the PNA) may coincide with or possibly obscure the zonal symmetry. The focus of the like-signed resulting mid-to-late summer U.S temperature anomaly cannot be predicted, but has greatest likelihood of occurring in the Midwest, southern Texas, or the northern Rockies/northern Plains, and least likelihood in the four "corners" of the country (the Pacific Northwest, New England, Florida and the desert Southwest). The relationship described here is reminiscent of a similarly vague relationship shown by Erickson (1983), in which zonally averaged subtropical NH 700 mb height anomalies in the preceding winter and spring were found to predict summer temperature anomalies of the same sign <u>averaged over the U.S.</u> Here we note, on the basis of the comparable magnitudes of the SST and the 700 mb height predictor loadings, that the worldwide tropical SST may be responsible for the process, with subtropical geopotential height responding largely passively.

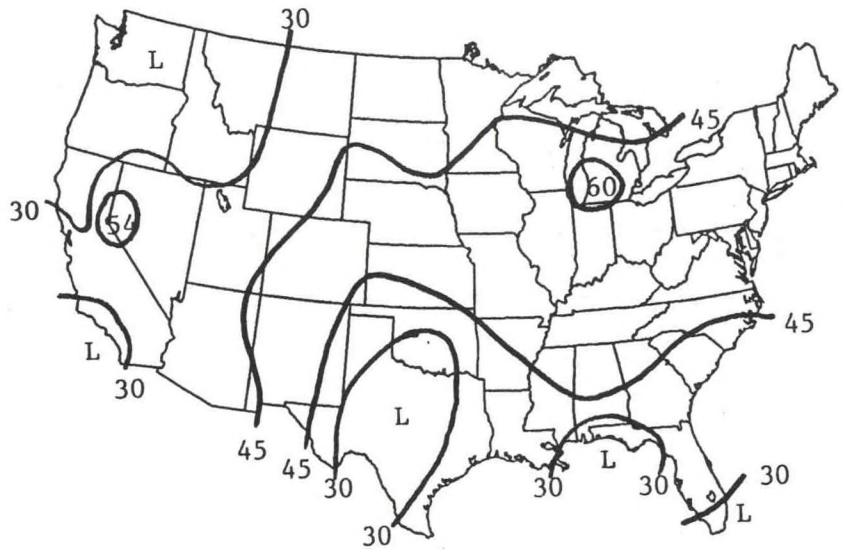

23. The principal predictand loading pattern for mode 1 for the prediction of Jul-Aug-Sep U.S. surface temperature at 1 month lead.

This cluster of tropical and subtropical predictor factors relating to U.S. summer temperature will be visited again in the discussion of 1 month mean predictions, where the predictor time window is shortened by a factor of three for a closer (month-by-month) look at the predictor patterns spanning through the prior spring.

2) PREDICTION OF 1-MONTH MEANS

In performing the CCA experiments on the 1 month time scale, each of the four consecutive predictor periods is 1 month in duration; one-half month is used as the minimum lead time and one month as the lead increment. The origins of skill usually turn out to be no more than somewhat noisier versions of what is already found for 3 month means at the same time of year. There are instances, however, in which qualitative differences are noted in the predictor patterns.

The correlation skills for 1 month mean predictor and target periods made at leads of 1/2, 3/2, ..., 9/2 months with double SST weight are shown in Fig. 24a in similar format to Fig. 6. A tendency for modest skill is found in middle and late winter, and, more sharply, just after mid-summer. It is noted that the skill averaged over the entire annual cycle is lower for 1- than 3-month mean periods, both because of the lower 1-month winter skill peak and the shorter duration of the summer peak. This suggests that stronger predictive signals are generally found at lower frequency, perhaps because "weather noise" related to the atmosphere's internal dynamics (which depends mainly on initial conditions) loses prominence relative to boundary condition (e.g. SST) effects. Increasing the lead time from 0.5 to 4.5 months shows no evidence of diminishing the 1 month skill levels. This is consistent with the lack of a substantial decrease in the skill of the 3 month forecasts from the 1 to the 4 month lead (Fig. 6). The corresponding plot of cross-validated persistence skill (Fig. 24b) shows skills generally equal to or lower than those of Fig. 24a, with the exception of 1/2-month lead forecasts for target period 18 (forecasts for September made at mid-July) for which a persistence skill of 0.18 is obtained.

Figures 25 and 26 show CCA forecast skill results for the 1 month mean target period with variations in predictor composition. In Fig. 25 the original rather than doubled SST weight is used, to determine whether the 700 mb height is relatively more valuable for forecasts with the shorter time frame. Comparison of Figs. 25 and 24a shows that greater forecast skill occurs with doubling of the SST weight, but to a somewhat lesser extent than for 3 month forecasts.

In Fig. 26 double weighted SST is used, but the four consecutive predictor periods are 3 months in duration rather than 1 month (i.e. they span over 1 year as in the 3 month experiments). A comparison of Fig. 26 versus Fig. 24a shows some improvement with the longer and earlier predictor periods, especially for cold season forecasts made at short lead times. However, obtain-

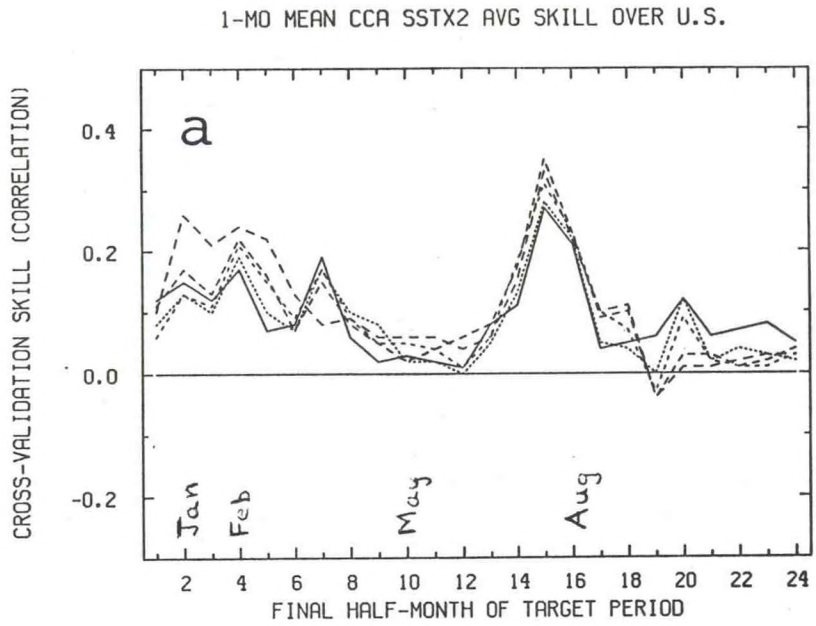

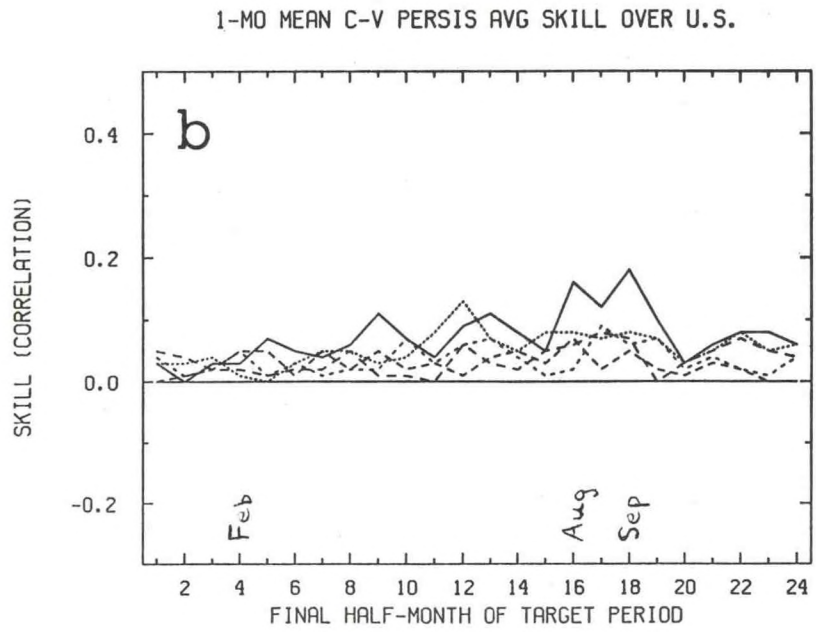

24. **Part (a): CCA forecast skill averaged over the U.S. for 1 month mean temperature for each of 5 lead times, with the SST field weighted double. Each of the four predictor periods is one month in duration. Part (b): As in part (a) except for persistence forecasts.**

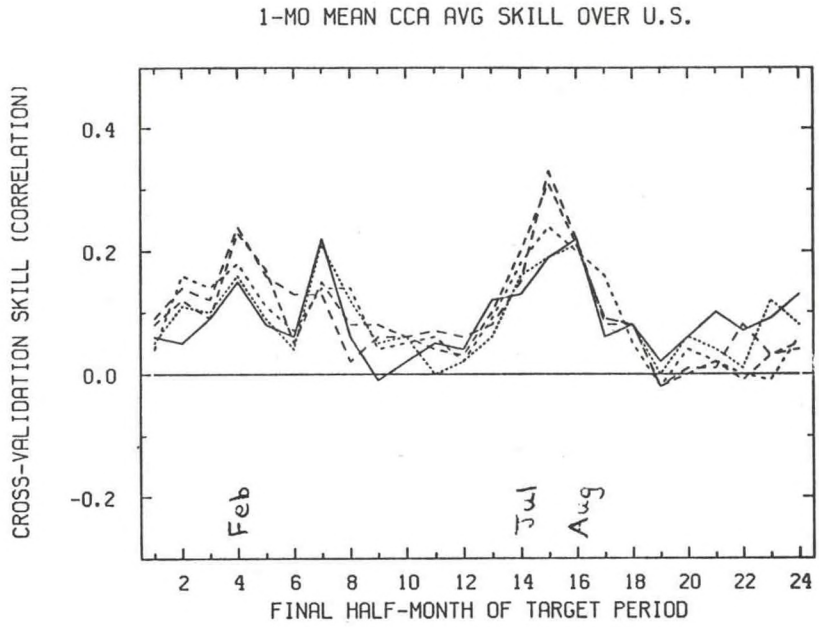

25. As in Fig. 24a, except with original (natural) SST weight.

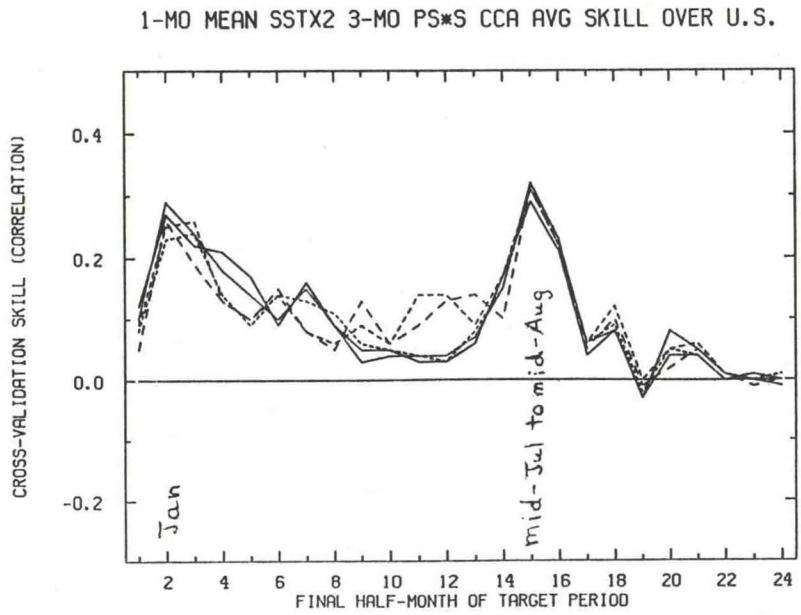

26. As in Fig. 24a (with double weighted SST) except that each of the four predictor periods is three months in duration.

ing the broad late winter skill peak of about 0.30 for 3 month mean forecasting (Fig. 6) apparently requires longer predictand as well as predictor time means--i.e. the signal is largely low frequency on both sides. The warm season skill peak, on the other hand, is just as great in 1 as in 3 month mean forecasting; however, elongating the 4 month total predictor time window increases short lead forecast skill still farther. The former feature suggests that warm season predictability either may involve a higher frequency signal or a higher signal-to-noise ratio than for the cold season; the latter feature suggests that it depends on events that take place more than 4 months prior to forecast time (e.g. the previous winter). This last idea implies that not only are long lead forecasts sometimes just as skillful as shorter or zero lead forecasts, but that in some cases there is a specific skill-optimizing nonzero lead time. In the present case it is suggested that the skill of mid-July to mid-August U.S. temperature predictions is optimized with the inclusion of tropical and subtropical climate information from earlier than the previous March.

Inspection of the predictor and predictand canonical loading patterns (not shown) for the two cold season 1 month target periods having highest cross-validated skill (seasons 4 and 7; Fig. 24a) indicates that, despite differences in some of the details, the origins of skill are similar to those found for 3 month means at the same time of year--i.e. largely ENSO and other mainly tropical ocean effects. The fact that these associations occur more clearly for predictand periods 4 and 7 than the intervening 1 month periods may be a reflection of the noisy character of 1 month periods, where the overall tropical SST effects are masked by shorter-lived strong fluctuations such as those related to the 30-60 day waves (Madden and Julian 1971) or the internal dynamics of the extratropical atmosphere.

The skill of end-of-June forecasts for mid-July to mid-August (target period 15 at 1/2-month lead) has the highest skill score (0.27; Fig 24a) among 1/2-month lead forecasts and is explored for comparability to the 3 month forecasts for the same time of year (seasons 17 and 18; Figs. 18-23) described earlier. Figure 27 displays the geographic distribution of the skill for these forecasts, revealing relatively high skill in much of the East, Midwest, central Plains and southern Rockies. CCA mode 1, explaining 11 percent of the original predictand variance, is the source of much of the organized skill structure. The SST and 700 mb predictor loading patterns for mode 1 are shown in Figs. 28 and 29. The four panels of predictor SST and 700 mb height in these two figures represent the March, April, May and June climate states, respectively, leading in a canonical sense to the U.S. surface temperature predictand pattern for mid-July to mid-August (Fig. 30). The latter monopole pattern is largely congruent with the high skill regions shown in Fig. 27. The SST predictor loading patterns (Fig. 28) leading to the generally warm (cold) mid-July to mid-August surface temperatures shown in Fig. 30 include the gradual waning of a warm (cold) ENSO episode (positive [negative] SST anomalies in the east tropical Pacific and negative [positive] SST anomalies south of the Aleutian

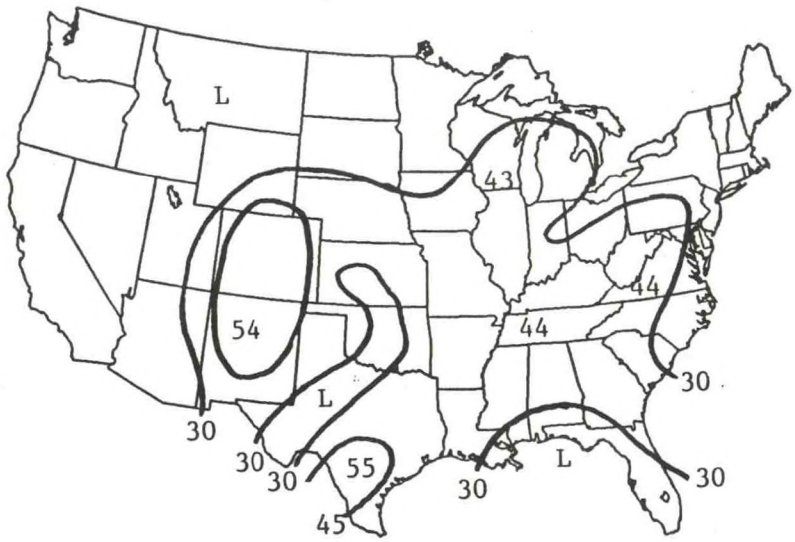

27. Geographical distribution of CCA skill in forecasting 1-month mean U.S. surface temperature at 1/2 month lead with double-weighted SST predictors for mid-Jul to mid-Aug.

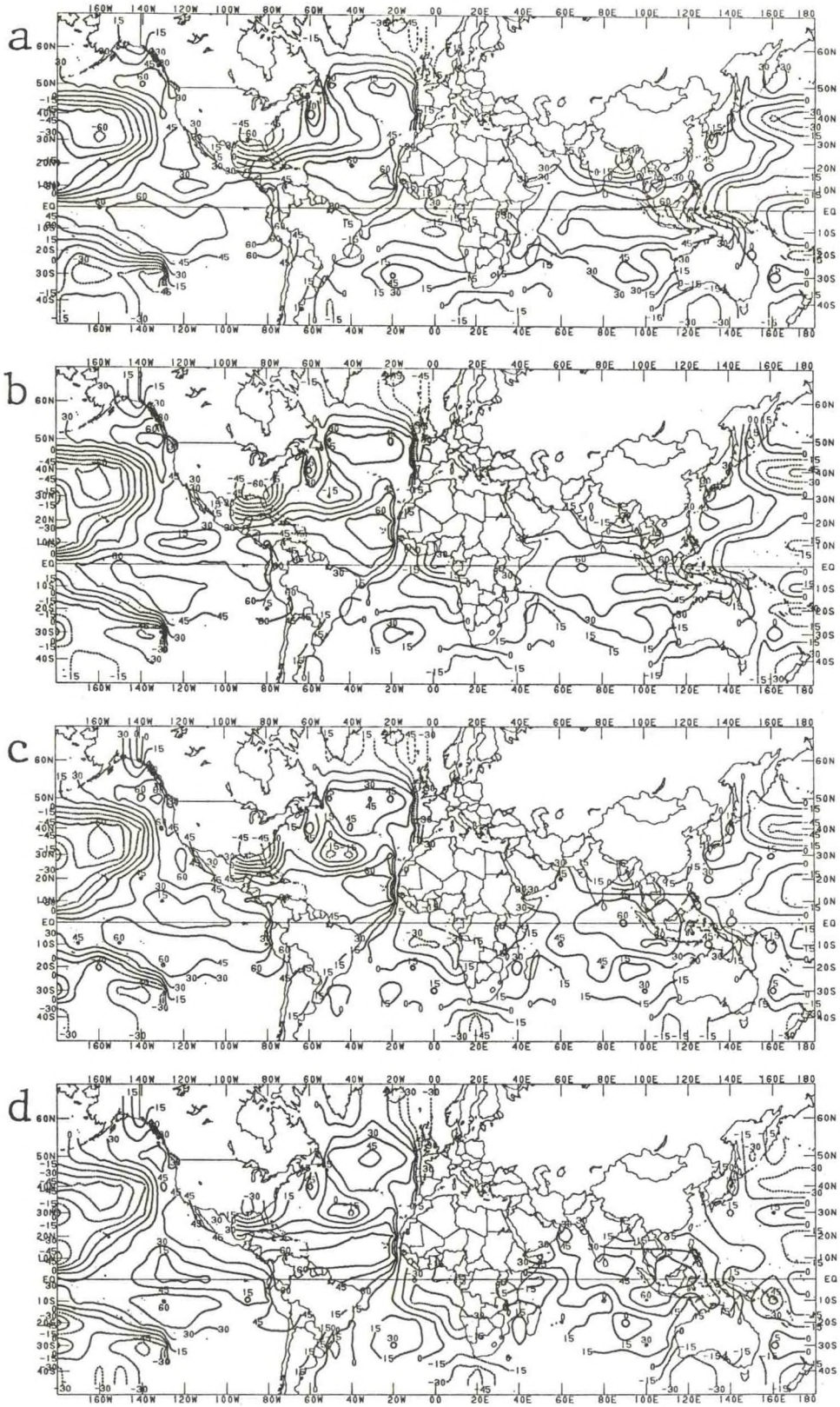

28. SST predictor CCA loadings for mode 1 for prediction of mid-Jul to mid-Aug U.S. surface temperature at 1/2 month lead. Parts (a), (b), (c), and (d) show loadings for the first (Mar), second (Apr), third (May) and fourth (Jun) predictor periods, respectively.

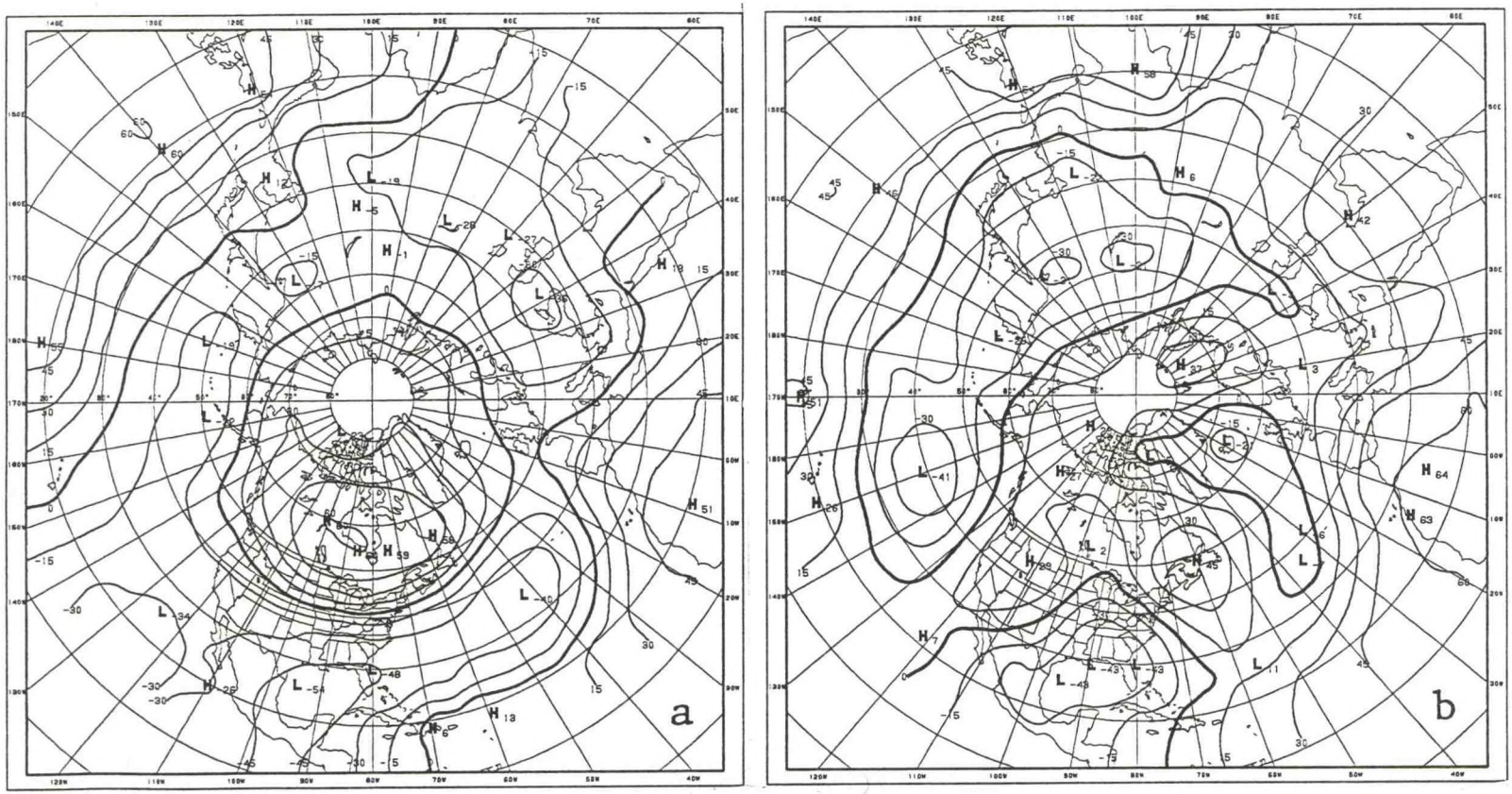

29. As in Fig. 28, except for 700 mb predictor loadings for forecasts of mid-Jul to mid-Aug U.S. surface temperature.

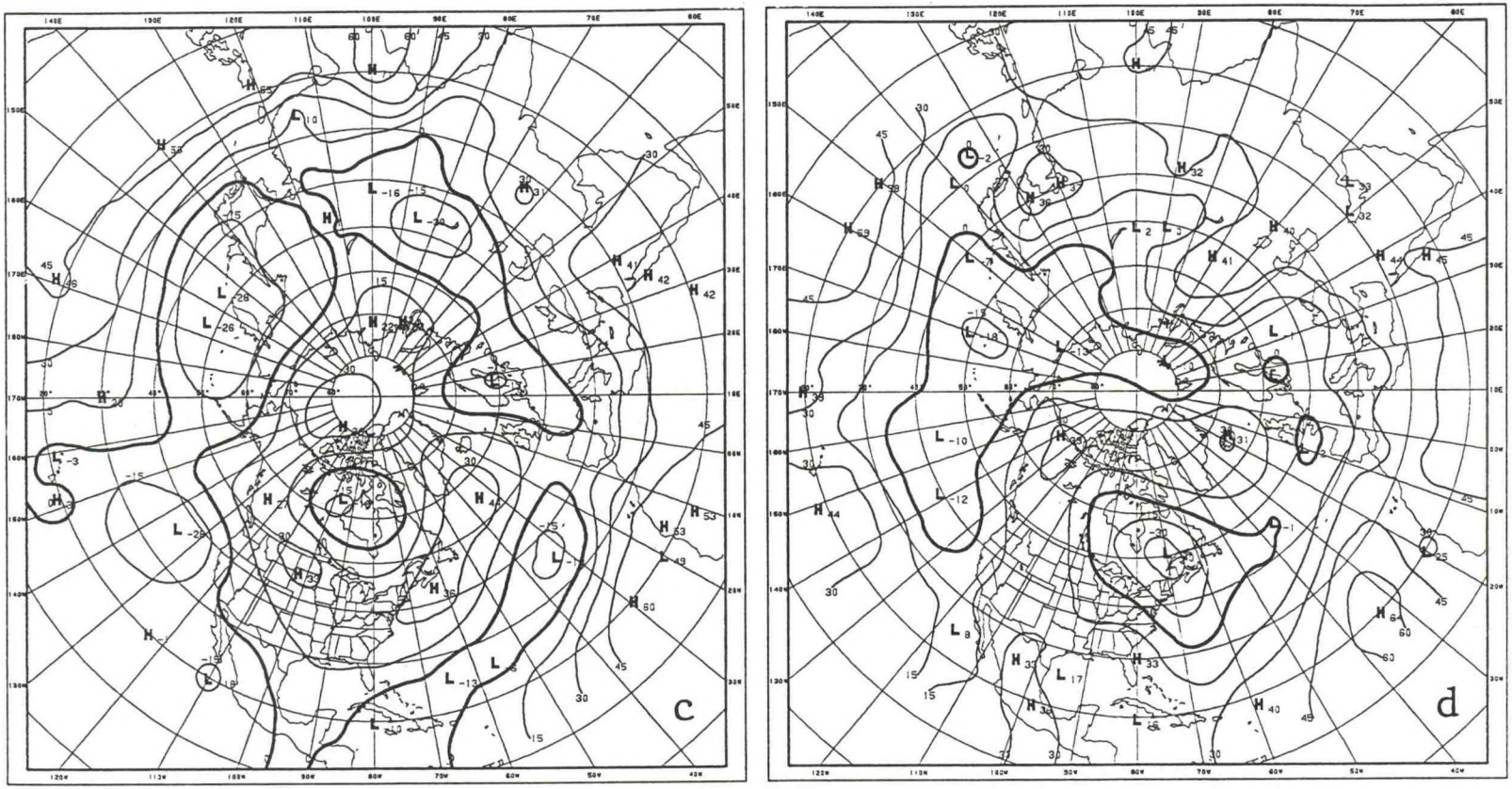
c
d

Islands), as well as Indian Ocean warmth (coldness) that declines only slightly throughout the predictor period. Moreover, warm (cold) tropical Atlantic SST is found with essentially unchanging strength from April to June following slightly lower strength in March, located just north of the equator with maximum intensity near 10^{o}N, 30^{o}W (off the African coast) with a westward extension across the Atlantic into the Caribbean Sea. The 700 mb height predictors indicate ENSO responses in March and April (with a strong TNH/WPO and a weak PNA pattern, respectively). Additionally, all four predictor periods exhibit the SZ pattern with positive (negative) loadings at low latitudes, particularly in the Pacific and eastern Atlantic/North Africa regions.

This scenario has similarity to that described for the 3 month warm season target period (mid-June to mid-September) using 3 month predictor periods at one month lead (section 4a(1[b])). In fact, the associated canonical component time series (not shown) strongly resembles that for mid-June to mid-September (Fig. 22), including the interdecadal variation. The annual march of CCA skill shown in Fig. 24a for mid-July to mid-August forecasts (target season 15) indicates that longer lead forecasts have slightly greater skill than the half month lead forecasts. To determine the sources of the longer lead forecast skill, we examine the loading patterns for the 3.5 month lead forecasts made at the end of March, which produces the highest (0.35) cross-validated skill. The geographical distribution of forecast skill is shown in Fig. 31, and the predictor loading patterns for SST and 700 mb predictor and the principal predictand canonical loading pattern for mode 1 are shown in Figs. 32, 33, and 34, respectively. The spatial distribution of skill (Fig. 31) is similar to that of the 1/2 month lead forecasts for the same target period (Fig. 27). The predictor loading maps (Figs. 32, 33) also show a series of events similar to those for the shorter lead forecasts. With the 3 month earlier predictor window (covering December, January, February and March), the mature ENSO event is caught at its peak. The SST anomaly in the Indian Ocean is already well developed throughout winter and early spring, but the Atlantic does not strongly follow suit until March (Fig. 32d). The 700 mb predictor loadings (Fig. 33) indicate effects of ENSO primarily in the form of strong TNH or WPO patterns in January, February and March, but only with a weak PNA pattern in December. The corresponding principal predictand loading map (Fig. 34) is roughly similar to that for the 1/2 month lead forecasts (Fig. 30). It can be speculated that forecasts for mid-July to mid-August contain their best skill when the predictor period can determine whether (1) a major Pacific SST anomaly took place in the prior winter, with the Indian Ocean mimicking that anomaly at least into spring, and whether (2) the Atlantic later also assumes the same anomaly sign, beginning by early spring. That the longer lead forecasts using December through March predictors outperform those using March through June suggests either that the events the previous winter are of greater predictive importance for the coming summer than those of the later spring, or, if the events of later spring are at least as important, they are accompanied by a proportionately greater increase in irrelevant variability (noise). This is further

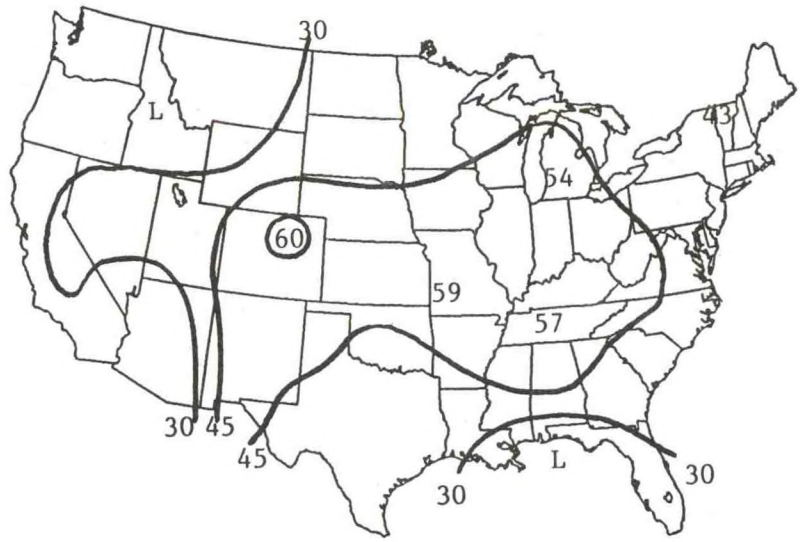

30. The principal predictand loading pattern for mode 1 for the prediction of mid-Jul to mid-Aug U.S. surface temperature at 1/2 month lead.

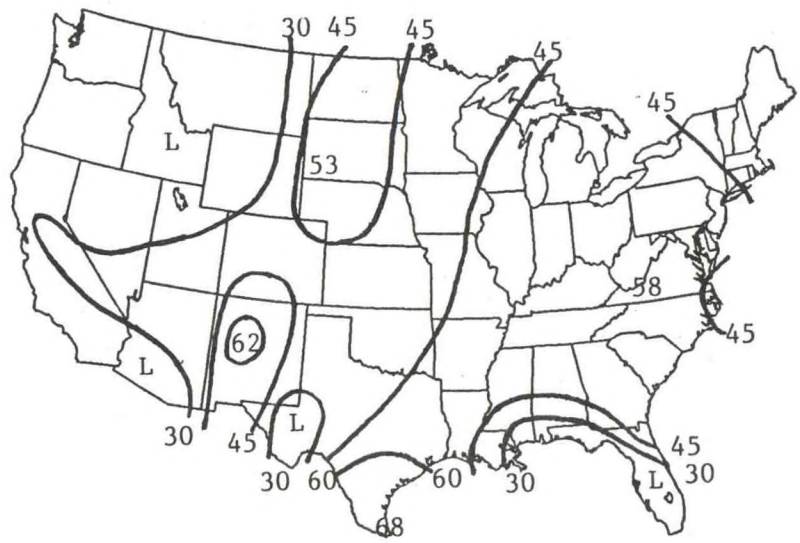

31. Geographical distribution of CCA skill in forecasting 1-month mean U.S. surface temperature at 3.5 month lead with double-weighted SST predictors for mid-Jul to mid-Aug.

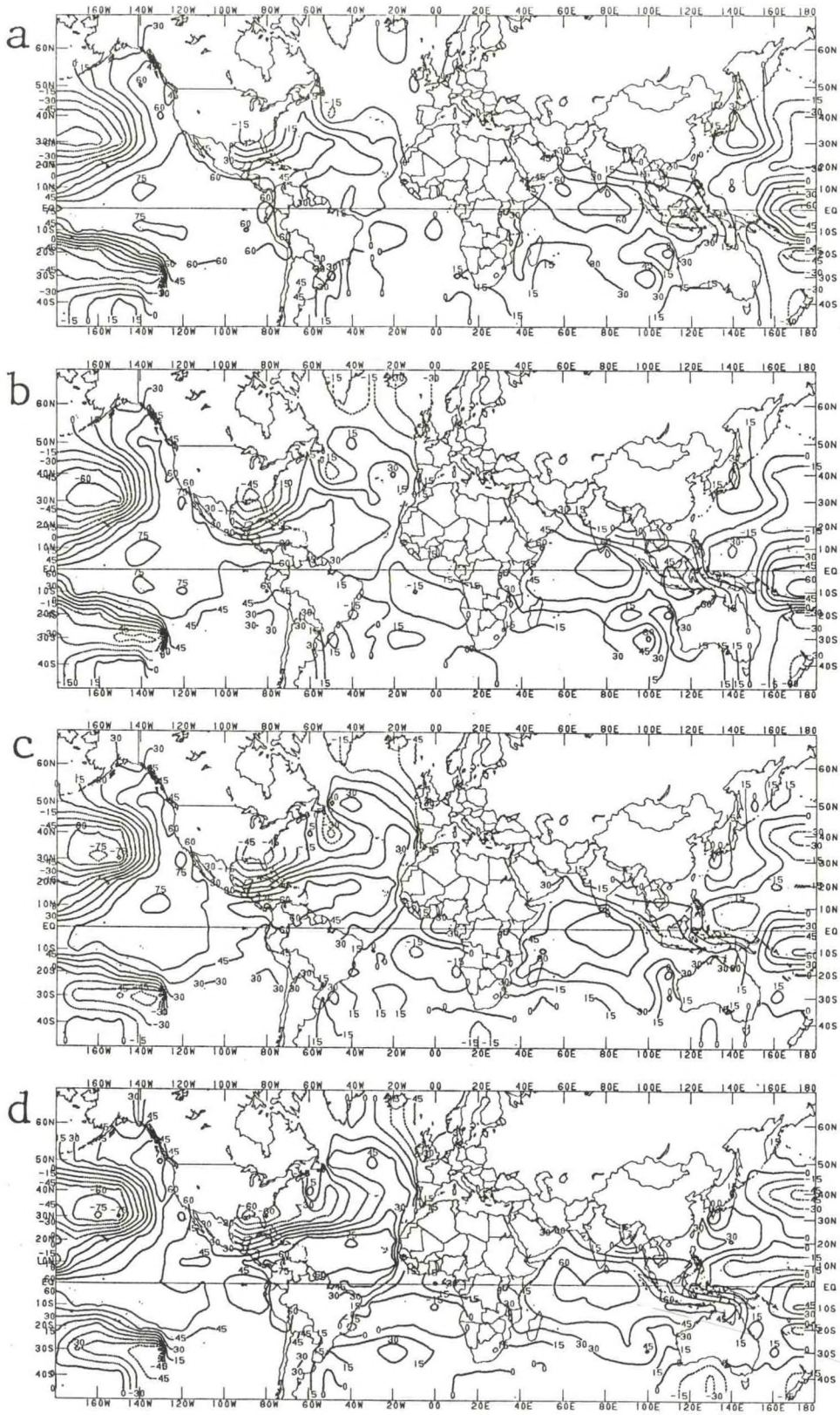

32. SST predictor CCA loadings for mode 1 for prediction of mid-Jul to mid-Aug U.S. surface temperature at 3.5 month lead. Parts (a), (b), (c), and (d) show loadings for the first (Dec), second (Jan), third (Feb) and fourth (Mar) predictor periods, respectively.

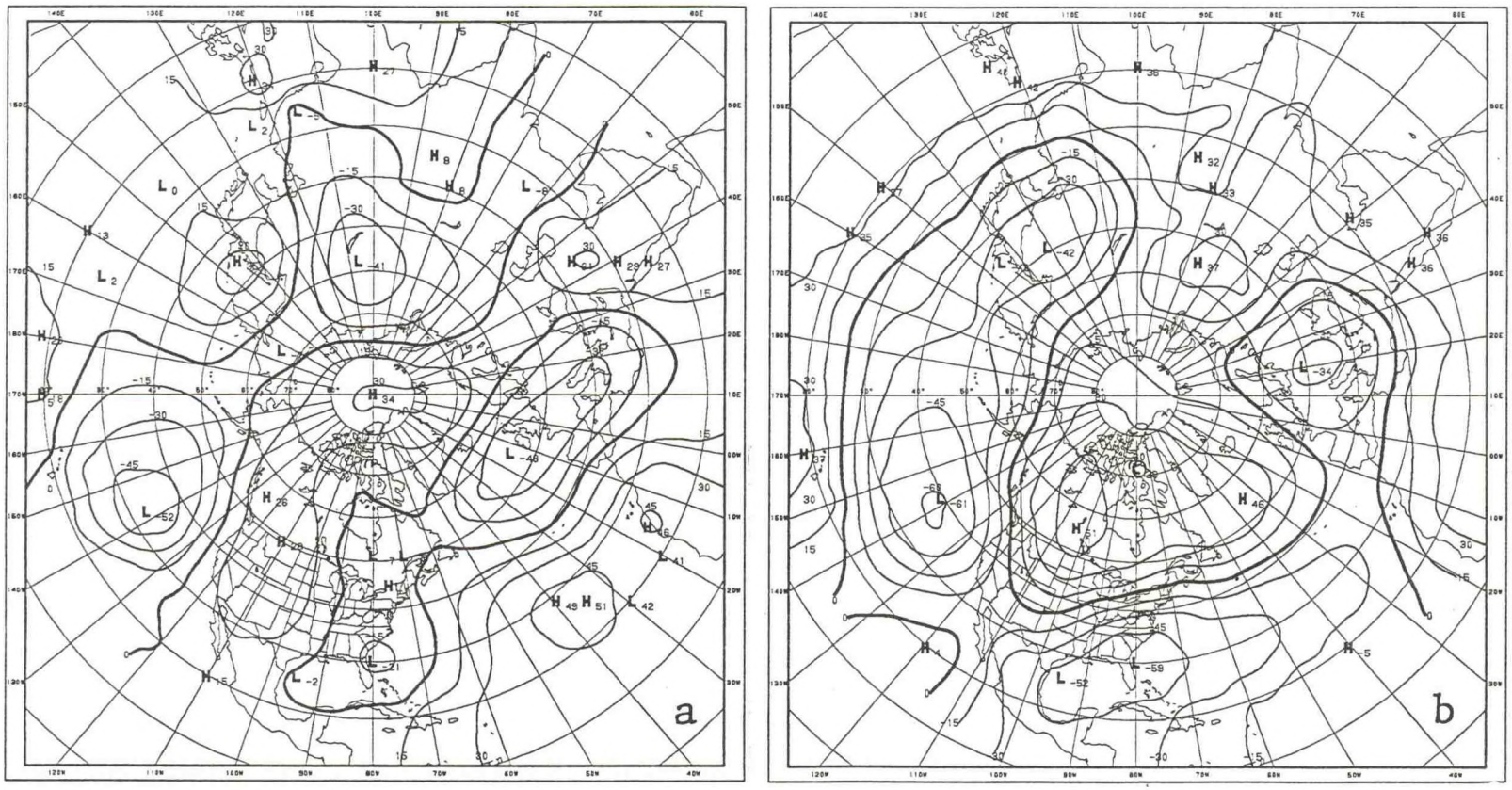

33. As in Fig. 32, except for 700 mb predictor loadings for 3.5 month lead forecasts of mid-Jul to mid-Aug U.S. surface temperature.

c
d

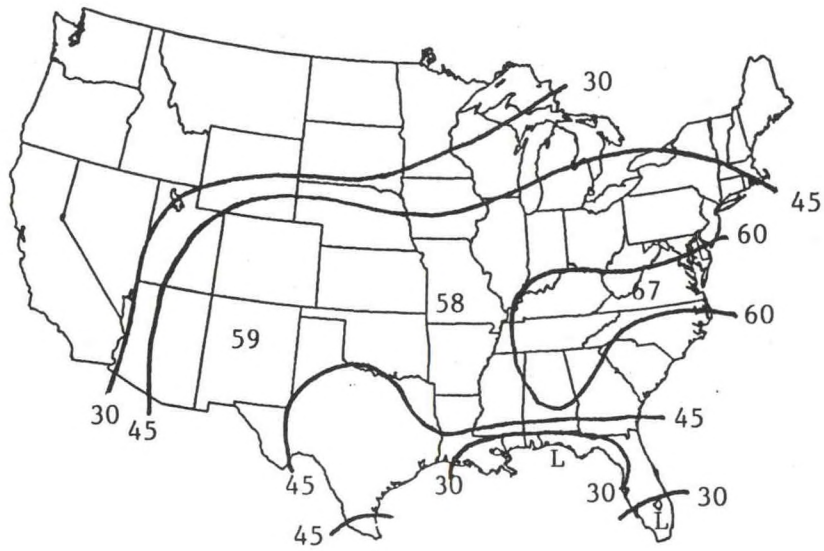

34. **The principal predictand loading pattern for mode 1 for the prediction of mid-Jul to mid-Aug U.S. surface temperature at 3.5 month lead.**

indicated by the stronger predictor loading magnitudes found in the winter periods (e.g. the tropical Pacific SST in December and January; Fig. 32a,b) than in any period contained in the shorter lead predictor times (Figs. 28, 29).

(3) AFTEREFFECTS OF ENSO IN THE OTHER TROPICAL OCEANS

The predictor loadings for the most skillful warm season forecasts of both 1 and 3 month mean periods portray the tropical Pacific and Indian oceans as having the same sign of temperature anomaly in the preceding winter. In spring, the Pacific anomaly wanes (marking the end of a warm or cold ENSO event), while the Indian Ocean anomaly continues, perhaps only beginning to gradually dissipate. Meanwhile, the tropical Atlantic, which had only shown a weak like-signed anomaly in winter, develops an anomaly in the spring. In summer the Pacific anomaly is much weaker if not completely gone, the Indian Ocean anomaly is still present but weakening, and the Atlantic anomaly is strongly present and just beginning to wane.

To explore whether this scenario is a regularly expected worldwide SST feature rather than an occasionally occurring construct linked to the U.S. temperature predictand as defined in an individual CCA mode, the 1955-1991 SST data set was used to compute lag correlation fields between the SST at all grid box locations and the January mean SST in 7 ENSO related tropical Pacific grid boxes (105-175^{o}W, 5^{o}N-5^{o}S). Three month lag intervals prior to, during and following the January reference time were used. Figure 35 shows the results for the eight 3 month intervals beginning with the January 12 months prior to the reference January (part a), and ending with the October 9 months afterwards (part h). The first four panels show a nearly stationary development of an east-central Pacific anomaly pattern associated with ENSO. The one year prior map (part a) suggests that ENSO was weakly of the opposite phase, both in the main anomaly in the tropical Pacific and in the oppositely signed anomaly in the North Pacific at 40^{o}N. By October and January (parts d and e) the Indian Ocean appears already to be adopting the Pacific anomaly to a moderate extent, but the Atlantic does not show much correlation despite a weak suggestion in October. In the April following the reference winter (part f) both the Atlantic and Indian ocean SSTs show as strong a lag correlation with the tropical Pacific SST 3 months earlier as does the tropical Pacific itself. This timing of warmings (coolings) among the three oceans has been documented in other studies, such as Kiladis and Dias (1989). In July (part g) all correlations are weaker; however, the Atlantic correlations, which formed last, are strongest. By the following autumn (part h) all lag correlations are close to zero.

The CCA-depicted relationship between winter and spring SST anomalies in each of the three oceans and the forthcoming summer U.S. surface temperature is more conveniently organized in Table 1, in which monthly mean SST in portions of the tropics in each of the three oceans[2] is lag correlated with monthly mean U.S.

surface temperature averaged over all except Florida and the western quarter of the country. Mean temperature in much of the U.S. in late summer (particularly July and August) is positively correlated with tropical SST in the Pacific the preceding winter through early spring (which was partly investigated by Douglas 1989), the Indian Ocean in late winter and early spring, and in the Atlantic in late spring and early summer.

Table 2 illustrates these relationships on a case-by-case basis for the spring and summer following warm and cold mature ENSO event winters defined by Ropelewski and Jones (1987), where the category of the mean of the monthly standardized anomalies (see Table 2 caption) of each of the three tropical oceans at their critical times of the year is listed with the category of Jul-Aug-Sep mean surface temperature in much of the U.S. (with U.S. area as defined above for the Table 1 correlations). The tendency for negative anomaly signs across the oceans and the summer U.S. temperature is quite clear for cold events, where even the strength of the anomalies appears somewhat consistent within events. For warm events the relationship is much weaker. It can be speculated that during cold events the tropical ocean SST anomaly is communicated between oceans and from ocean to the extratropical atmosphere mainly through sensible heating. During warm events, where latent heating plays a major role in the heat transfer, the speed and spatial configuration of the transfer is more complicated and unpredictable, being dependent on the positions of the subtropical jets, the locations of the strongest SST anomalies, etc. Perhaps, therefore, the tropical Pacific SST anomaly is less likely to be faithfully communicated to the other two oceans and then to the extratropical atmosphere during warm than cold events. It should be noted that the 1992 data, which is not used here but became available during this writing, does not support the relationship between winter tropical Pacific SST and U.S. summer temperature: A warm ENSO event occurred in winter of 1991-92, but the U.S. temperature was below normal in summer 1992 despite the antecedent winter positive SST anomalies in the tropical Pacific and Indian (but not Atlantic) oceans. (The Mt. Pinatubo eruption may have contributed to the cool U.S. summer.)

---

[2]The portions were chosen to be rough representations of the SST predictor loadings for the 1 and 3 month summer U.S. temperature forecasts discussed above. They are as follows. In Pacific: 5N-5S,105-175W; in Atlantic: 5-25N from Africa to the Americas; in Indian: 5N-5S, 55-105E.

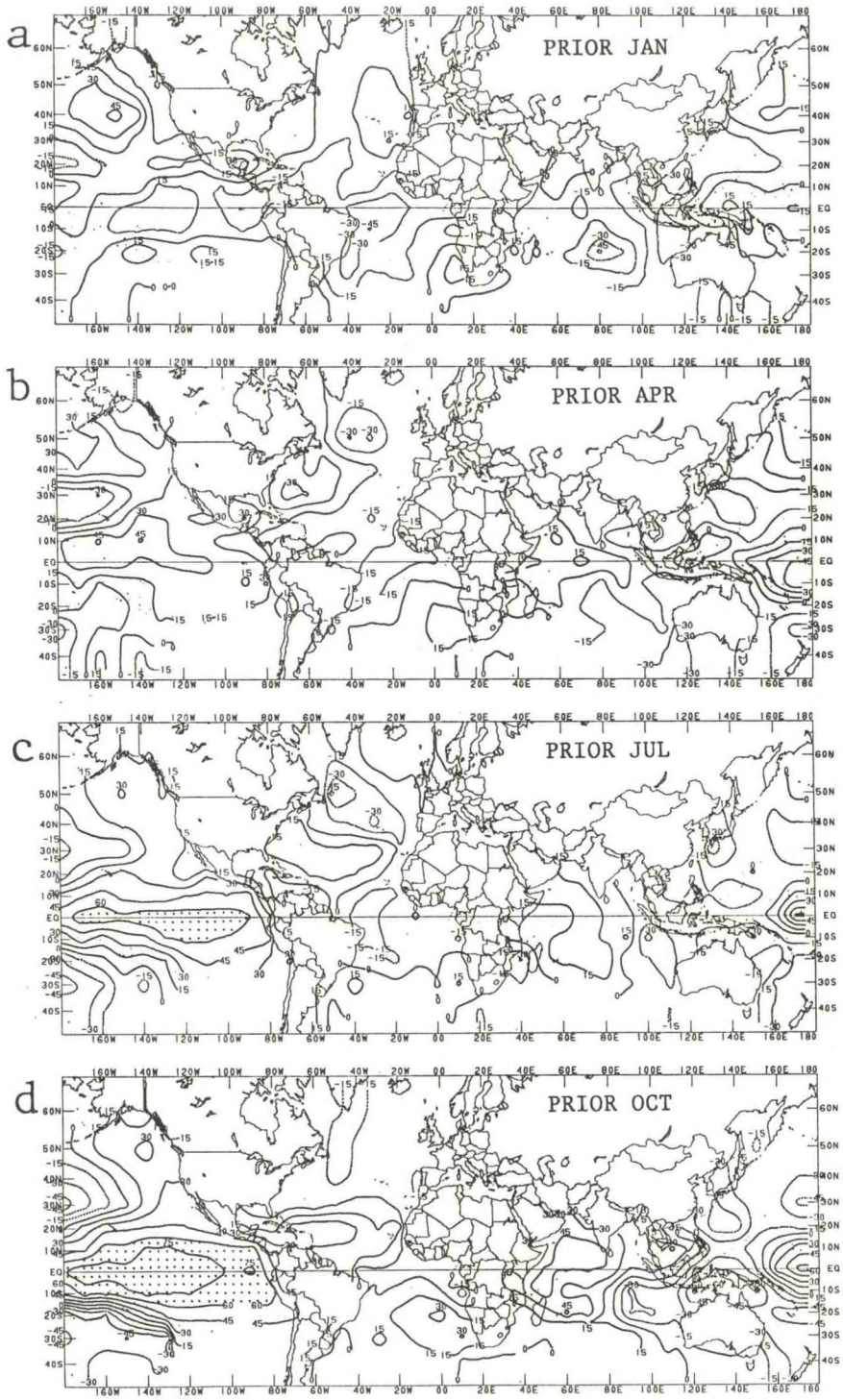

35. Lag correlation field (X100) for SST over much of the globe at prescribed times and the SST averaged over 105-175W, 5N-5S in January (to be called the "reference"). The prescribed times are (a) January, a year prior to the reference, (b) April, 9 before reference, (c) July, 6 months before, (d) October, 3 months before, (e) January, the reference time itself, (f) April, 3 months following reference, (g) July, 6 months following, and (h) October, 9 months following.

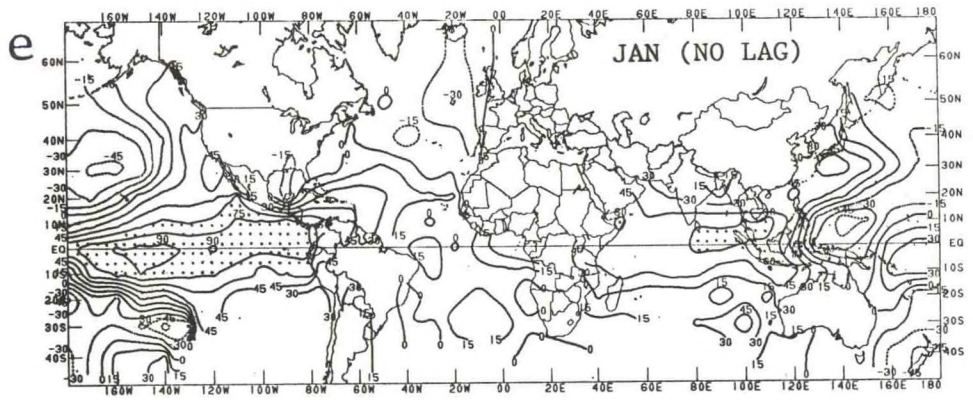
e
JAN (NO LAG)

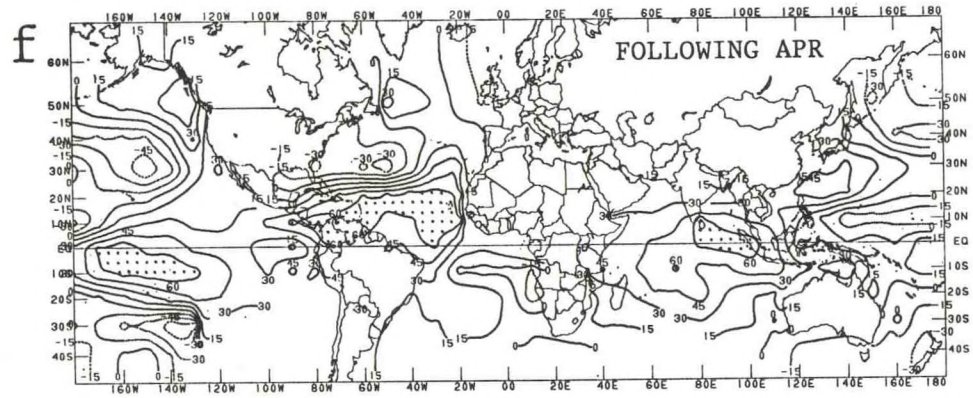
f
FOLLOWING APR

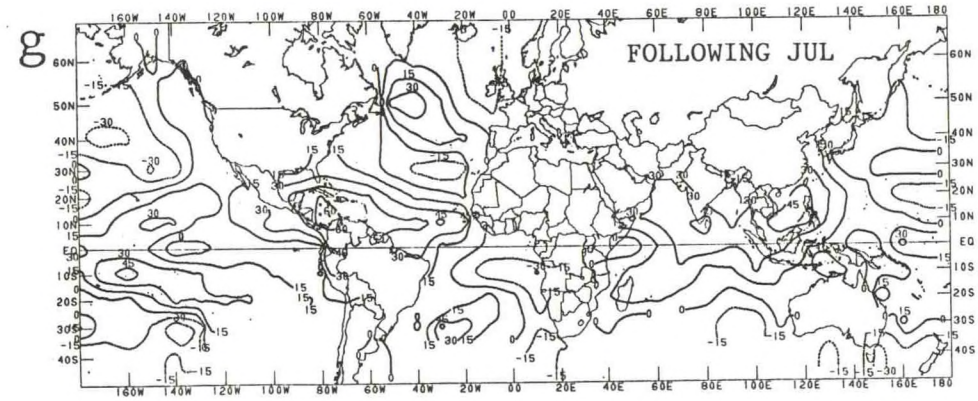
g
FOLLOWING JUL

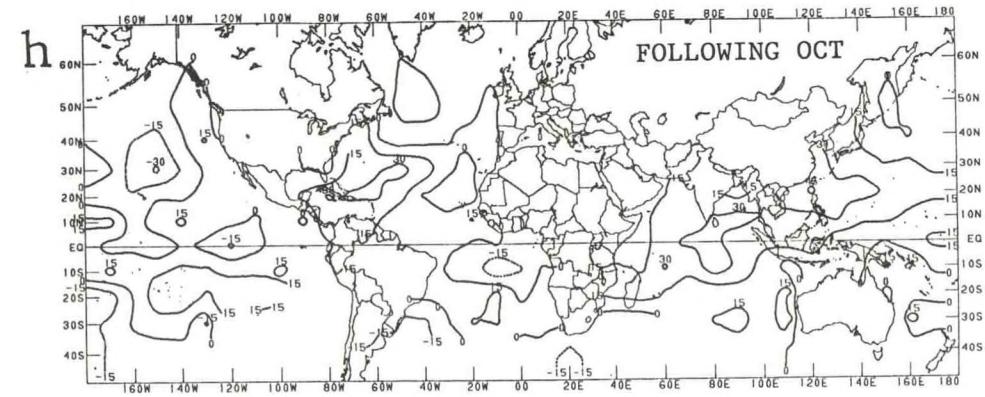
h
FOLLOWING OCT

PACIFIC OCEAN

		---Monthly Mean SST----					
		Jan	Feb	Mar	Apr	May	Jun
	May	16	14	03	04	02	01
U.S.	Jun	08	09	04	-05	-14	-26
	Jul	43	37	36	23	06	04
TEMP	Aug	48	48	41	29	13	-09
	Sep	44	35	39	29	22	06
	Oct	-16	-19	-25	-25	-22	-26

INDIAN OCEAN

---Monthly Mean SST----					
Jan	Feb	Mar	Apr	May	Jun
05	00	03	10	13	05
26	25	27	25	22	34
27	36	39	18	26	14
38	41	45	31	30	20
40	51	40	38	27	20
01	-17	-23	-16	-15	-24

ATLANTIC OCEAN

		---Monthly Mean SST----					
		Jan	Feb	Mar	Apr	May	Jun
	May	10	15	13	03	10	19
U.S.	Jun	24	15	8	-02	08	-06
	Jul	1	14	21	21	34	44
TEMP	Aug	30	32	36	43	40	35
	Sep	31	41	38	45	54	40
	Oct	27	17	1	-1	-11	-18

*** ALL THREE OCEANS ***

---Monthly Mean SST----					
Jan	Feb	Mar	Apr	May	Jun
16	13	8	7	10	11
25	19	15	7	7	1
30	35	37	25	28	28
49	48	47	41	35	21
49	51	45	44	43	30
5	-7	-18	-16	-20	-30

Table 1. Correlation (X100) between monthly mean tropical SST for the month specified along the top of each block and monthly mean surface temperature in most of the eastern three-quarters of the U.S. for the month specified along the left side. Shown for specific large portions (see footnote 2 in text) of the tropical Pacific, Indian, Atlantic, and the mean of all three oceans.

Warm ENSO Events

Year (+1)	Jan-Feb Pacific	Feb-Mar Indian	Apr-May Atlantic	Jul-Aug-Sep Temperature Eastern 2/3 of U.S.
1958	4	-1	4	-1
1966	3	1	2	-1
1970	2	2	3	2
1973	4	3	1	1
1977	2	-1	-1	3
1983	4	4	2	3
1987	3	3	2	1

Cold ENSO Events

1956	-2	-1	-3	-1
1957	-1	-1	-2	1
1965	-2	-3	-2	-2
1971	-4	-2	-3	-2
1972	-2	-2	-2	-2
1974	-4	-5	-5	-3
1976	-4	-4	-4	-2
1989	-4	-1	-3	-1

Table 2. Categorically defined means of monthly standardized anomalies of the tropical Pacific, Indian and Atlantic oceans at empirically derived critical locations and times of the year during and following a warm or cold ENSO winter, and of the surface temperature in the eastern two-thirds of the U.S. in Jul-Aug-Sep. Means of the monthly standardized anomalies (which have less than unit standard deviation--especially for U.S temperature) are categorized as follows:
1 .00 - .50 2 .50 - 1.00 3 1.00 - 1.50
4 1.50 - 2.00 5 >2.00 (and similarly for negatives)

The ocean-ocean and ocean-U.S temperature lag correlational data and the 1 and 3 month CCA relationships shown above imply a role of ENSO episodes for North American climate even for summer. The important physical question of how the anomalies in the tropical Atlantic and Indian oceans tend to occur with Pacific ENSO events may be treated in modelling experiments. Another aspect of this warm season phenomenon is its interdecadal component of variability: While the seasonal timing of the warm (cold) SST anomalies across the oceans is as shown here, the tendency for general warmth (coldness) throughout the worldwide tropical SST occurs partly on an interdecadal time scale, as illustrated by the canonical component time series for prediction of warm season U.S. temperature (Fig. 22).

(4) ATTEMPT AT INCORPORATING LATE SUMMER PERSISTENCE SKILL

While the skill of simple persistence forecasts is typically weak when lead times are included in the forecast format, Fig. 24b indicates noticeable skill (0.18) for 1 month forecasts made at half month lead for September. The geographical distribution of persistence skill for these forecasts is shown in Fig. 36. Much of the skill is concentrated along the Gulf coast and inland, as well as along the immediate Pacific coast, where low level flow consistently communicates the anomalies of the nearby upwind SST. This same distribution of persistence skill is found to a lesser degree in the two previous target seasons (not shown). When the half month lead time is removed, persistence skill is noticeably enhanced and a winter skill peak appears in addition to the warm season peak (not shown). Thus, at zero lead there are more instances in which persistence outperforms CCA--especially for 1-month mean target periods.

Part of the skill of warm season persistence is explained by the interdecadal component of the variability, as illustrated in the canonical component time series for predicting mid-Jun to mid-Sep U.S. temperature (Fig. 22). The associated 1-year autocorrelation of the temperature is least buried by other sources of variation during summer. Thus, some of the persistence skill is attributable to multi-year regimes and not to shorter term climate fluctuations.

In hopes of increasing predictive skill above the levels attained by CCA alone, persistence forecasts were combined with CCA forecasts in two ways: (1) using CCA with predictand data that are expressed as the change from the predictor to the predictand period, and (2) using station-wise multiple regression with the CCA forecast and the persistence forecast as the two predictors. The second method is similar to that used in Livezey et al. (1990) with analog forecasts and persistence. For both methods the overall cross-validated result was not as favorable as that using CCA alone. (Only a couple of stations near the Gulf of Mexico that have high persistence skill benefited somewhat from the combination algorithms in the September forecasts.) When CCA is run using as predictors only U.S. surface temperature itself in the fourth predictor period (not shown), skill is lower

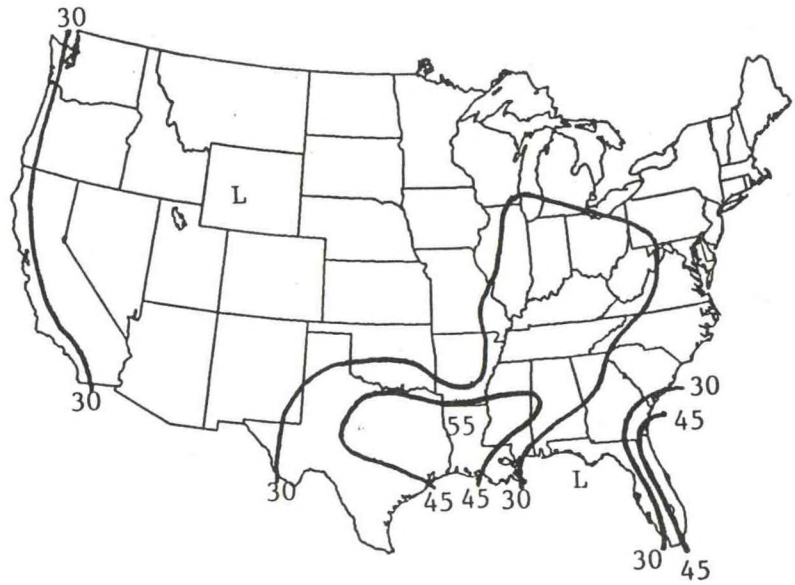

36. Geographical distribution of persistence skill in forecasting mean U.S. surface temperature in Sep at 1/2 month lead.

than that of simple persistence. Apparently the truncation of information in the pre-orthogonalization, as well as that within the CCA eigenanalysis itself, filters some of the local station information that is preserved in simple station-wise persistence.

b. Prediction of United States Surface Precipitation

The CCA experiments were performed also for precipitation, using SST and 700 mb height as predictors with SST predictors weighted double as was found to increase skill for temperature forecasts. The seasonal cycle of cross-validated correlation skill in predicting the 3 month total precipitation (not shown) at the same U.S. stations used for temperature (Fig. 1c) contains considerably weaker mean skills than those for temperature (Fig. 6). A suggestion of modest skill appears in late winter/early spring as for temperature, but a late summer skill peak is nearly absent. In an attempt to filter some of the noise present in the station data, another trial was performed using climate division monthly mean data (NOAA 1983) at the 59 divisions most closely colocated with the stations. A slight improvement in skill occurs, particularly in the late winter. However, skills are still weak, as shown in Fig. 37. For both station and climate division precipitation it is found that when the SST field is not weighted double, skill is no lower. The skill of persistence forecasts using climate division data (not shown) is lower than for CCA forecasts, never reaching 0.10. Figure 38a presents the geographical distribution of skill for season 6 (Jan-Feb-Mar) CCA forecasts for 1 month lead for climate division precipitation, with mean skill of 0.15. Highest skill pockets are noted in the southeastern and south central states (particularly in southern Texas and Florida) and in the northern Great Lakes. The mode 1 canonical predictor loading patterns for SST and 700 mb height associated with this skill (not shown) are very similar to those shown for Jan-Feb-Mar U.S. surface temperature (Figs. 8, 9) in that a cold (warm) ENSO event develops and becomes strong by the fourth (fall) predictor season. The principal predictand loadings for the leading mode (Fig. 38b) reveal a roughly north-south dipole pattern with precipitation deficits (excesses) in the South and excesses (deficits) in the North and Midwest. The effects in the South have been documented elsewhere (Douglas and Englehart 1981, Ropelewski and Halpert 1986, Epstein 1992). The northward extension of the South's anomaly sign into Nebraska and the occurrence of the opposite sign of anomaly in or just east of the Midwest were noted in Epstein (1992; see his Fig. 1).

Predictive skill for 3 month mean precipitation is barely found in the warm season (Fig. 37). The distribution of local skill and the predictor and predictand loading maps associated with Jun-Jul-Aug forecasts at several leads (not shown) weakly suggest a tendency toward summer dryness (wetness) along the eastern seaboard and wetness (dryness) along the west coast following several seasons with anomalously cold (warm) SSTs in the tropics of all three major oceans.

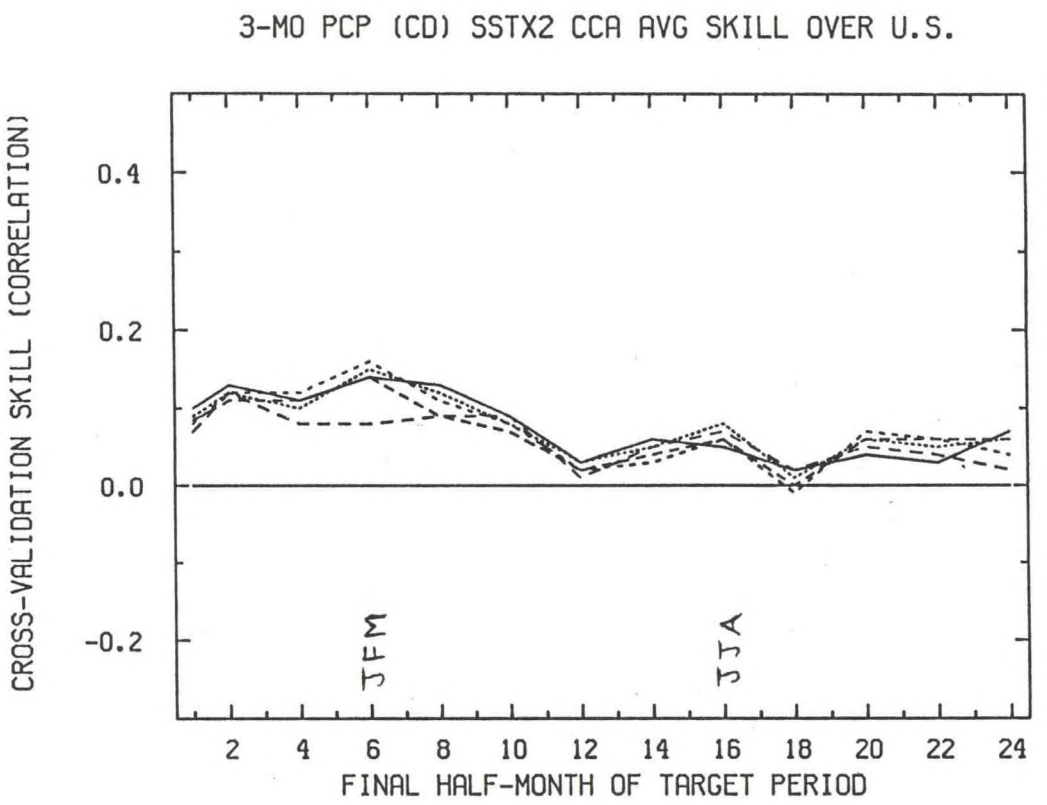

37. CCA forecast skill averaged over the U.S. for 3 month mean precipitation for each of 5 lead times, with the SST field weighted double. Each of the four predictor periods is three months in duration. Climate division precipitation data are used rather than station data. Results for 12 seasons are represented.

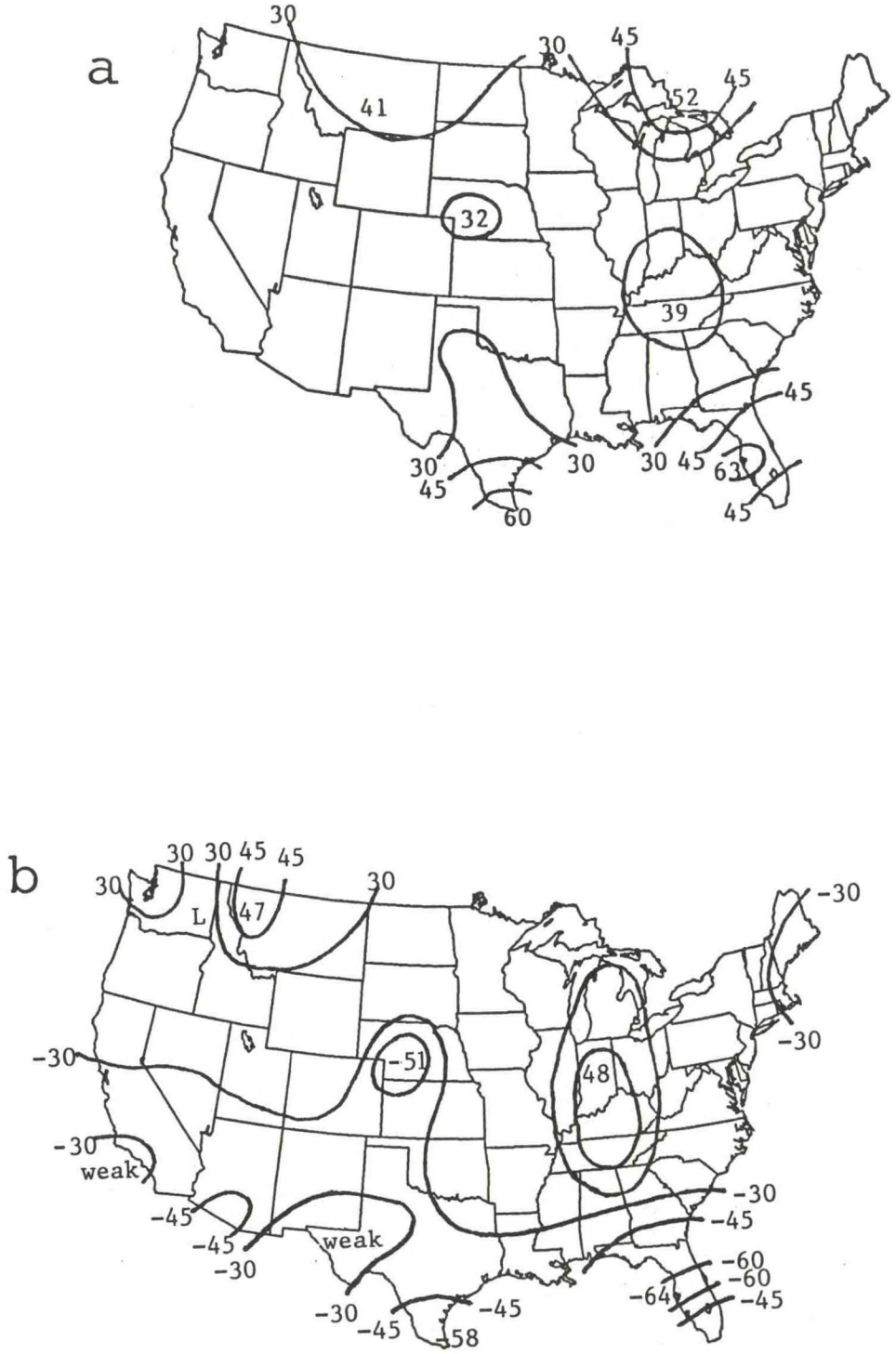

38. Part (a): Geographical distribution of CCA skill in forecasting 3-month mean U.S. surface precipitation at climate divisions at 1 month lead with double-weighted SST predictors, for Jan-Feb-Mar. Part (b): The principal predictand loading pattern for mode 1 for Jan-Feb-Mar precipitation prediction.

One month mean precipitation forecast skills (not shown) are generally lower than those for 3 month means and have similar seasonality. Persistence skills are not noticeably higher with the shorter averaging period, with half-month lead skills rarely showing a skill surplus compared with the longer leads.

Because 1 and 3 month total precipitation has a somewhat positively skewed distribution (but much less so than for shorter periods), CCA skills were determined for the logarithm as well as the 0.667 and 0.800 powers of the precipitation totals. While results were slightly improved for some sectors, overall differences were negligible.

From the forecasts performed here it is apparent that precipitation remains a very difficult parameter to predict in the mid-latitudes. However, the occurrence of an ENSO event provides noticeable winter through mid-spring mean predictive skill that is concentrated most heavily in Florida and Texas.

c. Prediction of 700 mb Height in the PNA Region

An approximately equal-area 59-point grid of 700 mb height in the Pacific/North American region with approximate borders of 20-70^{o}N, 50-180^{o}W (Fig. 39) was used as the CCA forecast target. The skill of 700 mb height forecasting is assessed because of a tacit assumption that much of the climate variability at the earth's surface occurs in association with upper air patterns. The fluctuations aloft in some ways are simpler to understand, being comparatively removed from additional complications at the surface such as terrain, horizontal gradients in heat capacity and albedo, etc. We ask whether higher statistical predictability is possible above the surface where the achievement of predictive potential is based on fewer critical variables.

The sets of predictors explored here are (1) NH 700 mb height and quasi-global SST, with the latter double-weighted as before, (2) 700 mb height alone, and (3) SST alone. The mode truncation point for the pre-orthogonalization as well as the CCA itself is held at 6 modes (as used for U.S. temperature and precipitation prediction) based on examination of eigenvalue curves and cross-validated skill sensitivity trials.

Figure 40a shows the seasonal cycle of skill in predicting 3 month mean 700 mb height on the basis of previous 700 mb heights and double-weighted quasi-global SST, averaged over the 59 predictand points. The profile appears generally similar to that for U.S. surface temperature (Fig. 6) in that there is a broad skill peak in the latter part of the cold season and a secondary maximum in late summer. However, the 700 mb height profile is less sharply seasonally dependent. One aspect of this is the relative lack of a brief, relatively strong warm season skill peak. The decay of skill with lead time is similar to that for U.S. temperature prediction.

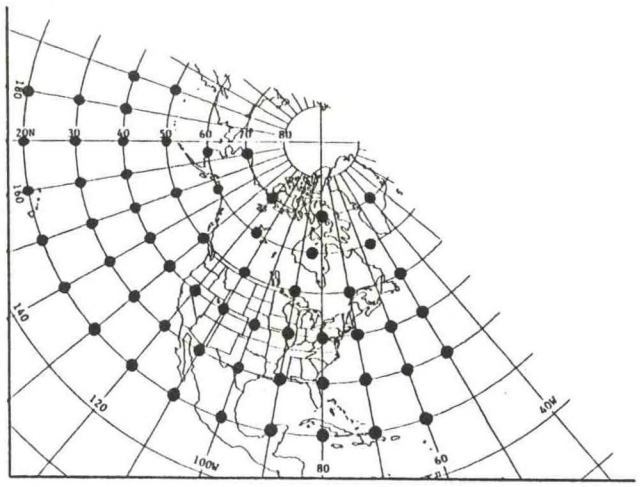

39. The grid of 59 points of 700 mb height over the Pacific/ North American (PNA) region.

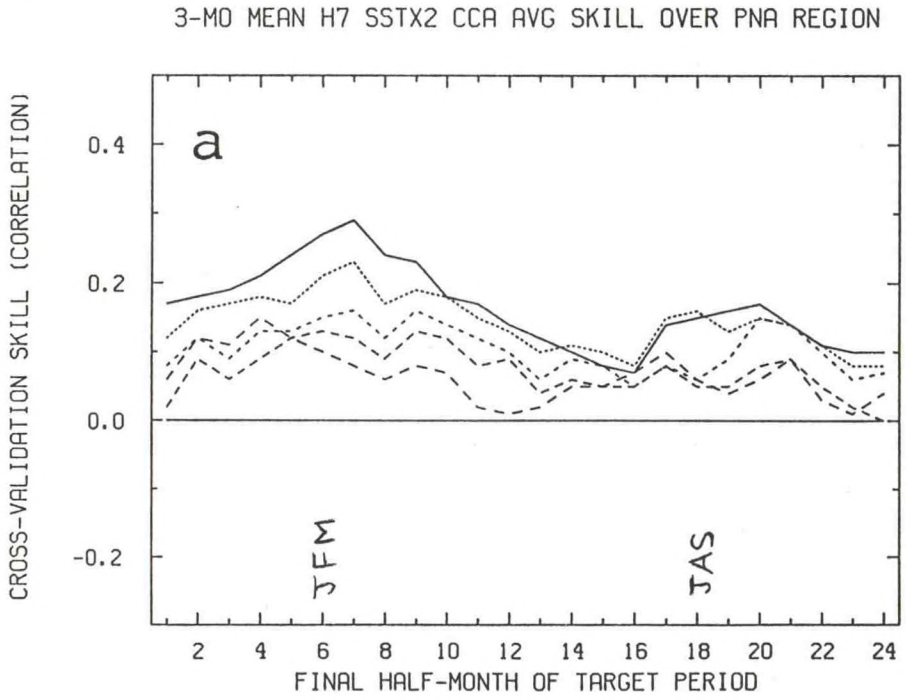

40. Part (a): Seasonal variation of CCA forecast skill averaged over the PNA region for each of five lead times for 3-month mean 700 mb height. Each of the four predictor periods is three months in duration. Double-weighted SST and NH 700 mb height are used as predictor fields. Part (b): As in part (a) except using SST as the only predictor field. Part (c): As in part (a) except using 700 mb as the only predictor field. Part (d): As in part (a) except for persistence forecasts.

When the above experiment is rerun using only SST predictors, resulting skill is essentially unchanged, as shown in Fig. 40b. When the only predictors are NH 700 mb height, skill declines markedly (Fig. 40c). Finally, the skill of point-wise persistence of the 700 mb height from predictor to predictand periods is shown in Fig. 40d, with the 1 month lead scores showing a skill level generally higher than that for CCA forecasts using only hemispheric 700 mb height predictors and lower than forecasts using only SST predictors in winter and spring but higher in summer and fall. The loss of skill realized with the change from SST to 700 mb height predictors is more general than that found for U.S. surface temperature prediction (Figs. 5a and 5b); in the latter case the cold season skill is most greatly affected, whereas for predicting 700 mb height the effect is noted more uniformly throughout the annual cycle. The relative lack of a late summer skill peak in predicting 700 mb height may be due partly to the larger predictand area, containing several "zero lines" in addition to the marginally predictable areas in between, as opposed to the smaller U.S. area which can be mostly filled by a single anomaly area centered in the interior in summer heat wave versus coolness regimes [see sections 4a(1[b]) and 4a(2)]. There may also be a relative lack of a forced tropical signal in summer in the PNA area as compared with winter.

The seasonal march of the geographical distribution of 1 month lead cross-validated skills for the PNA region 700 mb height experiments using hemispheric 700 mb height and double weighted SST as predictors is presented in Fig. 41 for eight overlapping 1.5-month-apart 3 month seasons (Jan-Feb-Mar, mid-Feb to mid-May, etc.). The late winter and late summer forecasts have highest mean skill, the latter being the secondary maximum. In late spring and late fall the patterns are weaker, more poorly defined, and show little continuity with the adjacent higher skill season patterns.

The forecasts for Jan-Feb-Mar made at the end of November (1 month lead) have one of the highest cross-validated skill of the forecast sets shown in Fig. 40a (mean skill is 0.27; only the following overlapping season has higher skill of 0.29), and also in Fig. 40b for SST predictors alone (mean skill also 0.27, and unsurpassed). The geographical distribution of skill (Fig. 41a) indicates skill centers in the subtropical Pacific (near and west of Hawaii), in the North Pacific (near and southwest of the Aleutians), in Canada/north-central U.S., and along the southern tier of U.S. states. The corresponding predictor canonical loading patterns for the leading CCA mode (not shown) are very similar to those for predicting Jan-Feb-Mar U.S. surface temperature (Figs. 8, 9); i.e. the SST predictor loading patterns show the development of an ENSO event in the tropical Pacific over the previous spring and summer, clearly enduring through the fall and (presumably) the predictand period, and the 700 mb height predictor loading pattern for the leading fall shows a PNA-like pattern with the expected polarity for the sign of the SST anomaly. The principal predictand loading map for this mode (Fig. 42a) has a high magnitude pattern markedly congruent to that of the skill map resulting from the combination of 6 modes, revealing the

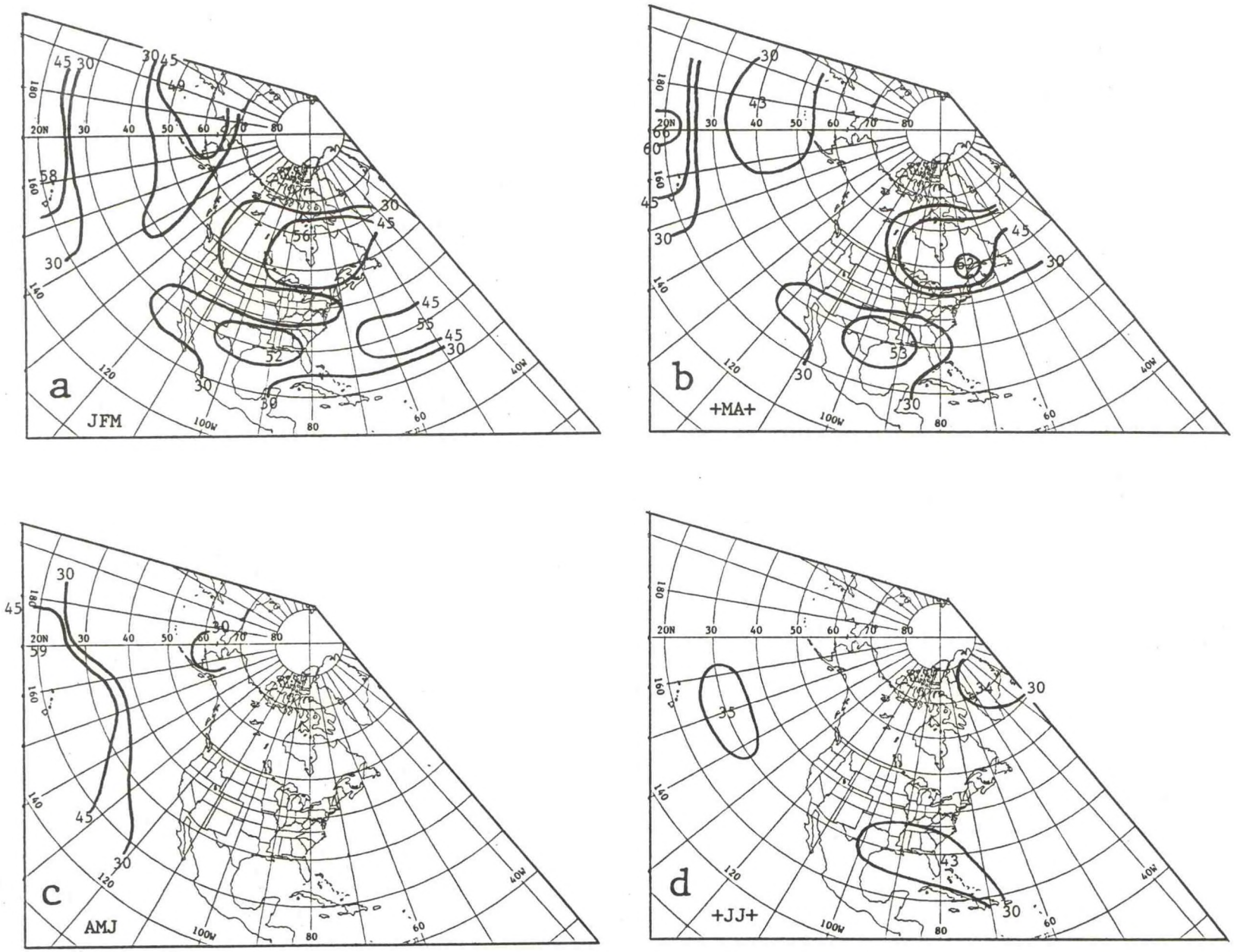

41. Geographical distribution of CCA skill in forecasting 3-month mean 700 mb height in the PNA region at 1-month lead using the 700 mb height and double-weighted SST fields as predictors for (a) JFM, (b) +MA+, (c) AMJ, (d) +JJ+, (e) JAS, (f) +SO+, (g) OND, and (h) +DJ+, where the "+" denotes the adjacent half of the neighboring month.

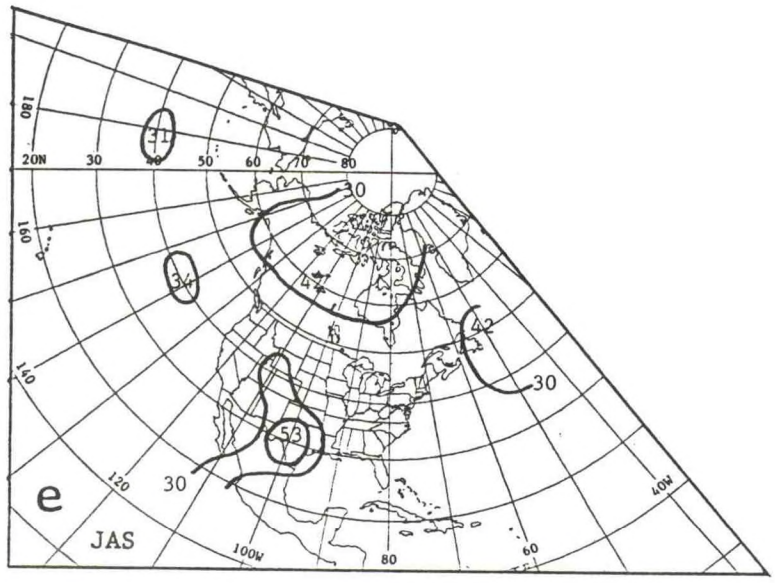
e
JAS
180
20N
30
40
50
60
70
80
160
140
120
100W
40W
31
30
34
42
30
53
30

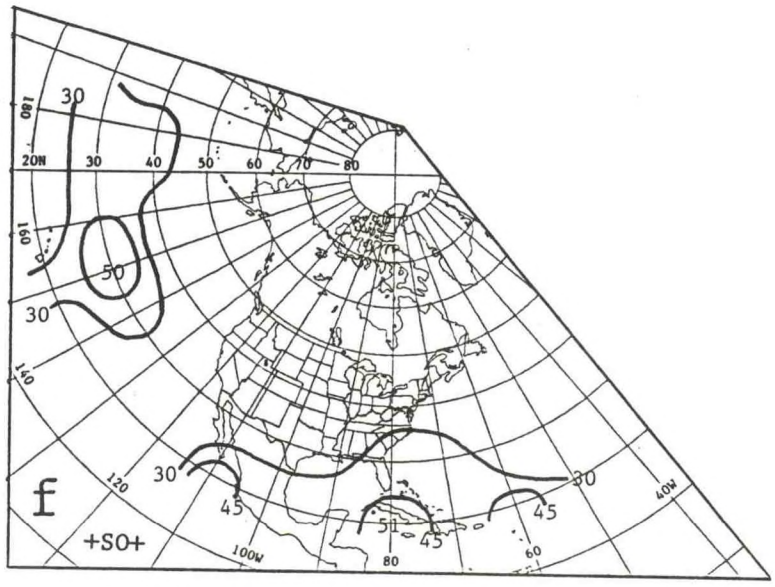
f
+SO+
180
20N
30
40
50
60
70
80
160
140
120
100W
40W
30
50
30
30
45
51
45
45
30

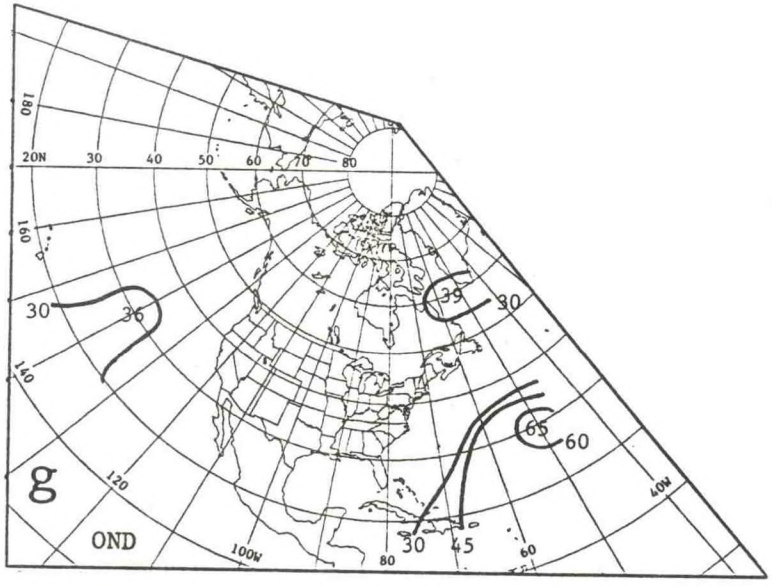
g
OND
180
20N
30
40
50
60
70
80
160
140
120
100W
40W
30
36
39
30
65
60
30
45

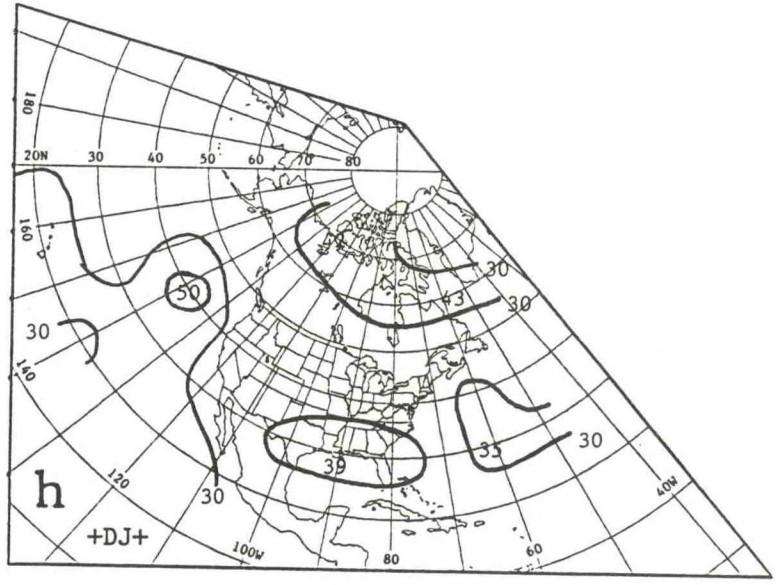
h
+DJ+
180
20N
30
40
50
60
70
80
160
140
120
100W
40W
50
30
43
30
30
39
35
30

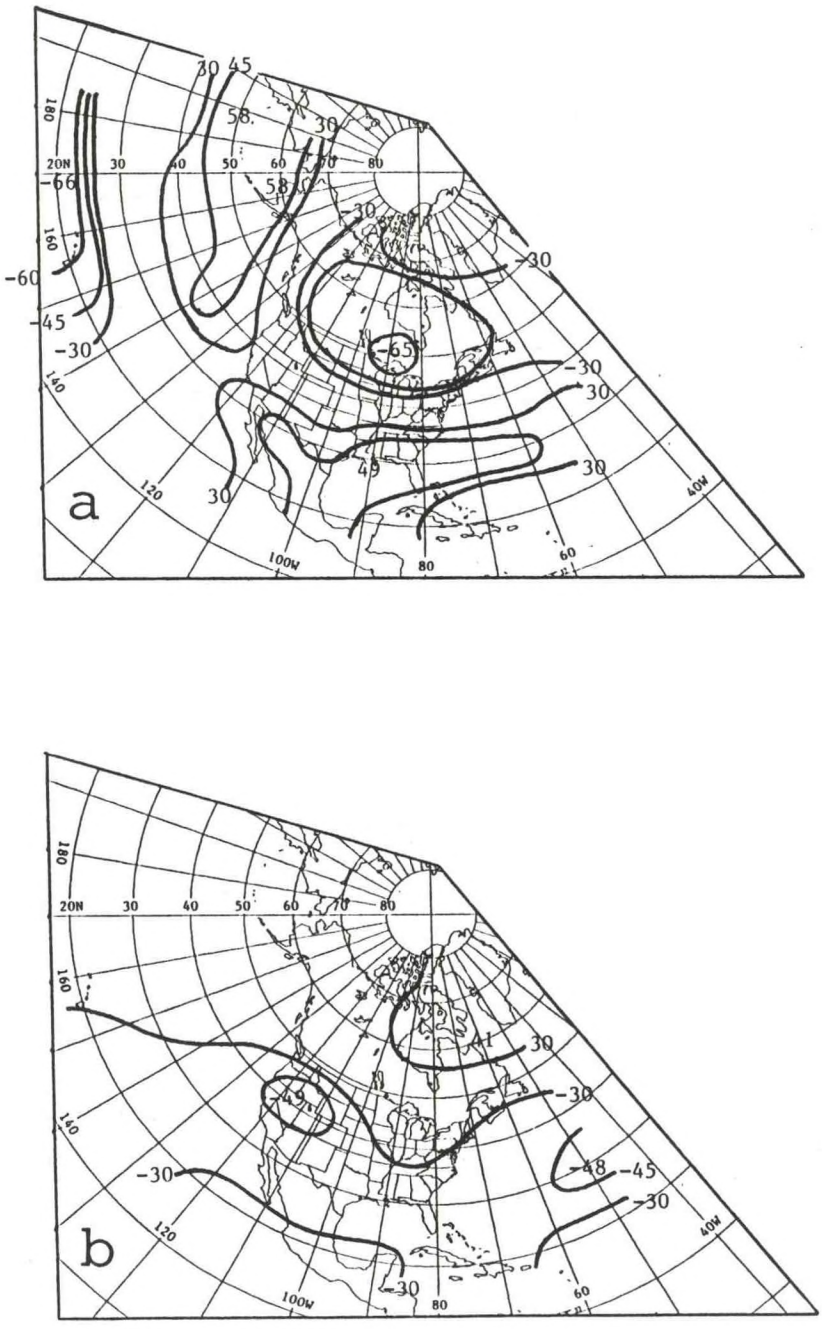

42. Part (a): The principal predictand loading pattern for mode 1 for the prediction of Jan-Feb-Mar 700 mb height in the PNA region at 1 month lead. Part (b): As in part (a) except for mode 2.

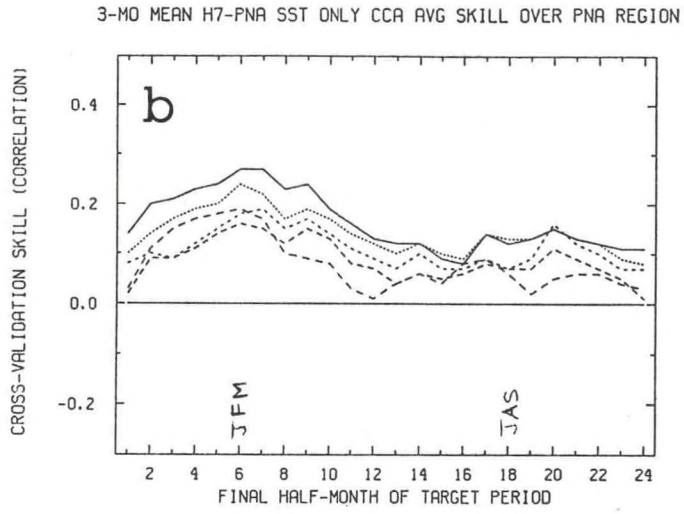
3-MO MEAN H7-PNA SST ONLY CCA AVG SKILL OVER PNA REGION
b
CROSS-VALIDATION SKILL (CORRELATION)
0.4
0.2
0.0
-0.2
JFM
JAS
2 4 6 8 10 12 14 16 18 20 22 24
FINAL HALF-MONTH OF TARGET PERIOD

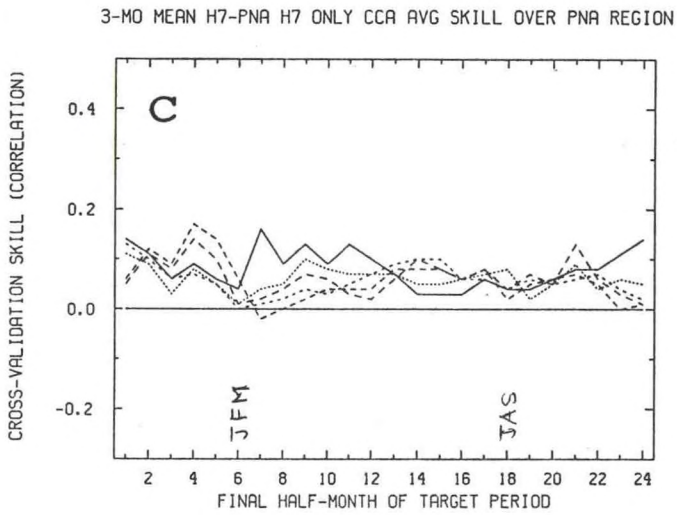
3-MO MEAN H7-PNA H7 ONLY CCA AVG SKILL OVER PNA REGION
c
CROSS-VALIDATION SKILL (CORRELATION)
0.4
0.2
0.0
-0.2
JFM
JAS
2 4 6 8 10 12 14 16 18 20 22 24
FINAL HALF-MONTH OF TARGET PERIOD

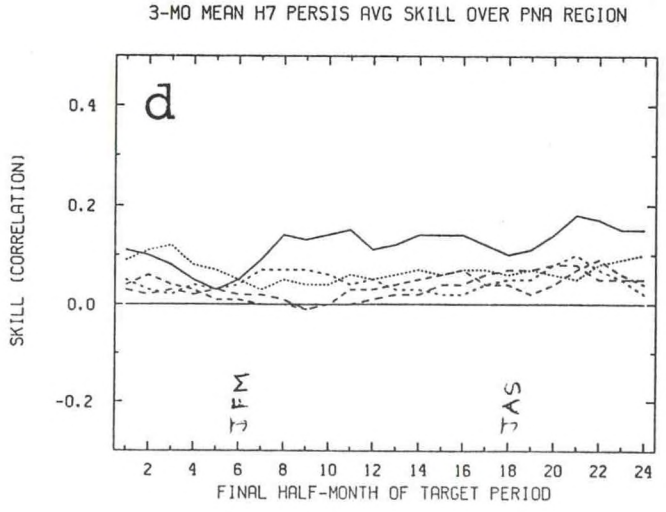
3-MO MEAN H7 PERSIS AVG SKILL OVER PNA REGION
d
SKILL (CORRELATION)
0.4
0.2
0.0
-0.2
JFM
JAS
2 4 6 8 10 12 14 16 18 20 22 24
FINAL HALF-MONTH OF TARGET PERIOD

relative importance of mode 1. The polarity as well as configuration of signs of the predictand loading map's "centers of action" is suggestive of known extratropical ENSO effects, with a north-south WPO dipole in the Pacific, and a TNH-like dipole over the North American continent. In fact, Fig. 42a markedly resembles a map of simple correlation for the cold season between a Southern Oscillation Index and 700 mb height, such as that shown in Fig. 1 of Barnston et al. (1991). Such a pattern contains components of teleconnection patterns such as (in order of dominance) the TNH, WPO, PNA, and NAO or WA (Wallace and Gutzler 1981, Horel 1981, Barnston and Livezey 1987), as well as the leading unrotated principal component of winter Northern Hemispheric 700 mb height (shown in Fig. 11d in Barnston and Livezey 1991). As will become evident in the experiments predicting entire NH height (in section 4d), the pattern shown in Fig. 42a, as well as the resulting realizable skill (Fig. 41a), represent a strikingly large proportion of the total cold season hemispheric predictability.

Part of the skill magnitudes shown in Fig. 41a is not accounted for by the principal predictand map for mode 1 (Fig. 42a)--namely in locations south of Greenland (the eastern extension of the Hudson Bay skill center) and over the Atlantic at 30°N (the eastern extension of the southern U.S. skill band). Most of the remaining skill appears to come from CCA mode 2, whose principal predictand loading map (Fig. 42b) reveals a North Atlantic Oscillation (NAO) pattern with a strong North American extension of the negatively (or, alternatively, positively) signed southern lobe of the dipole. The predictor patterns associated with mode 2 (not shown) suggest a cold (warm) ENSO event the preceding winter (with a like-signed SST anomaly in the tropical Indian Ocean as in the tropical Pacific) followed by like-signed spring and summer SST anomalies in the tropical Atlantic accompanied by the SZ 700 mb height pattern with like-signed anomalies at low latitudes.

Forecasts for Jul-Aug-Sep made at the end of May (1 month lead) are part of a secondary maximum of cross-validated skill of the forecast sets shown in Fig. 40a, with mean skill of 0.15. The geographical distribution of skill (Fig. 41e) indicates a skill center over Texas in the south central U.S. (peak skill 0.53) and several weaker centers elsewhere in the PNA region. The scenario described in sections 4a(1[b]) and 4a(2) above for late summer 1 and 3 month mean U.S. surface temperature predictability (involving spring warming [cooling] of the tropical and NH subtropical Atlantic with a declining warm [cold] ENSO event) might be expected to be associated with the present predictand pattern. However, this appears only as mode 3, with different relationships described in the leading two modes. Thus the mean 700 mb height in the larger PNA region does not share the same predictive relationships found for summer U.S. surface temperature. Besides the different respective areal coverages, this could be caused by phenomena affecting the surface and boundary layer without significantly affecting the upper atmosphere.

Table 3 documents the predictor and predictand scenarios for 8 overlapping three month seasons for all modes giving rise to local cross-validated skill peaks of 0.4 or higher. Aside from diluted versions of the cold and warm season relationships highlighted above for adjacent seasons, a sequence of events leading to an NAO pattern in late fall (OND) is listed. This sequence is more completely isolated in the NH prediction experiments discussed below, in which the predictand includes all of the Atlantic region rather than only the western half.

Table 3. Summary of CCA predictor and predictand scenarios, described by loading patterns, for skill-producing 1 month lead forecasts of 700 mb height anomalies in the Pacific/North American (PNA) region for eight overlapping three month seasons. The four predictor periods are listed in leftmost column beneath the predictand season and areal (PNA region) mean cross-validated skill. "Winter" refers to DJF, "late winter" to +FM+, etc. Polarities of centers of loading patterns are defined relative to one another rather than in an absolute sense, as a collective reversal of signs would be equally representative. "ENSO signature" in SST loadings refers to an anomaly in the eastern half or the east-central portion of the tropical Pacific Ocean. Indian Ocean anomalies of same sign may also appear. New or unexpected major non-summer and non-winter results are underscored.

Season/ Areal average skill/ The four predictor seasons	Predictor and Predictand Loading Patterns	Regions with Cross-Validated Skill of 0.4 or Greater; [ ] Indicates Mode of Origin
	MODE 1:	
	SST: Strong ENSO signature in spring, summer and fall, with anom. sign of Pacific SST appearing in Indian Ocean in summer and fall.	South-Central Canada [1]
JFM	700mb: PNA pattern, with western North American anom. of same sign as trop. Pacific SST, in fall.	Southern U.S. [1] to west-central Atlantic at 30N [2]
0.27	Predictand: Strong TNH/PNA pattern with southern Canadian anom. of same sign as trop. Pacific SST.	Subtrop. Pacific from Hawaii westward [1]
winter spring summer fall	MODE 2:	
	SST: ENSO signature winter and spring, and like-signed SST in tropical Atlantic and Indian Oceans spring and summer, and in East China Sea in fall.	South and west of Aleutians [1]

	700mb: SZ pattern in winter with subtrop. anom. sign like trop. Pacific SST anom. PNA/TNH in spring with Canadian anom. of same sign as trop. Pacific SST. Predictand: Extended North American/Atlantic NAO pattern with anom. sign like trop. Pacific SST over Atlantic at 30N and western U.S.	
---	---	---
	MODE 1: SST: Strong ENSO signature mostly east of 150W. 700mb: PNA pattern in late fall with western North American center having anom. sign like trop. Pacific SST. However, there is "opposing" NAO (no PNA center in southeast U.S., but NAO center of conflicting sign). Predictand: Strong TNH/PNA pattern with Canadian center of anom. sign like trop. Pacific SST.	South-Central Canada, east to Atlantic coast [1 and some 2] Southern U.S., Mexico, Gulf of Mexico [1]
+MA+ 0.24 late winter late spring late summer late fall	MODE 2: SST: Trop. Atlantic anom. late spring; same anom. sign in East China Sea late fall with opposite sign anom. south of Aleutians. 700mb: Previous late winter PNA, western Canadian anom. sign like trop. Atlantic SST. However, there is "opposing" NAO (no PNA center in southeast U.S., but NAO center of conflicting sign). PNA/TNH of analogous polarity in late spring. Predictand: NAO pattern with 30N anomaly of sign like trop. Atlantic SST.	Subtrop. Pac. from Hawaii westward [1] South of Aleutians [1]

AMJ 0.14 spring summer fall winter	MODE 1: SST: Northern trop. Pacific anom. (centered 20N,140W) in spring, summer and fall, with opposing anom. in East China Sea in fall. 700mb: Anom. north of Hawaii of opposite sign as SST in fall and winter. Predictand: Anomaly at 30N, 140-160W with sign of SST and 700mb predictors. MODE 2: SST: ENSO signature all four predictor periods, waning in final winter. No trop. Atlantic anomaly. 700mb: PNA/TNH/WPO patterns in spring and following winter with subtrop. Atlantic extended center of same sign as southern Canadian center and trop. Pacific SST. Predictand: Short wavelength PNA/TNH pattern of same polarity as predictor 700mb.	Subtrop. Pac. (130W-180) [1, with western part from 2]
---	---	---
+JJ+ 0.08 late spring late summer late fall late winter	MODE 1: SST: Large anom. at 50-60N from southwest Aleutians to Kamchatka in late winter. 700mb: WPO pattern in late fall and late winter with northern center of same sign as SST anom. Predictand: WPO pattern, where southeast US has same anom. sign as SST.	Southeast U.S. [1]

	MODE 1: SST: Trop. Atlantic anom. (including Caribbean) in winter and spring; same sign anom. had appeared in trop. Pacific in summer and somewhat in fall. 700mb: PNA/TNH in fall, winter with polarity compatible with trop. Pacific SST anom. Predictand: Anom. with sign like trop. SST in eastern and central North Pacific (35-40N) and off northeast US/southeast Canadian coast; anom. with opposite this sign at 20-30N across North America and in Alaska.	South-central US [1] West-central Canada [some 1] Off west coast of North America at US/ Canadian border [3] Off east coast of North America at U.S./ Canadian border [1 and some 3]
JAS 0.15 summer fall winter spring		
	MODE 2: SST: Anom. in all four predictor periods off east U.S. coast; same sign anom. in fall and spring at 20S at western South American coast; same sign anom. 10-20N in eastern Atlantic and eastern Indian Ocean summer and fall; opposite sign anom. centered 20N,90E (east of India) in winter and spring. 700mb: Subtropical Zonal (SZ) pattern all four predictor periods (weakest in winter) with subtrop. anom. with sign same as SST off east US coast. Predictand: Weak to moderate anom. (of same sign as SST off east US coast) across much of PNA region, especially southwest of California and near 40N in eastern U.S.	
	MODE 3: SST: ENSO signature summer, fall, winter, waning in spring as trop. Indian and Atlantic oceans develop same sign anom. Opposite sign anom. throughout all four predictor periods south of Aleutians and at similar longitude in the mid-latitude Southern Hemisphere. 700mb: PNA in fall (with polarity consistent with SST ENSO event); strong PNA/TNH/WPO winter and spring of consistent polarity. Predictand: Anom. of same sign as ENSO-related trop. Pacific SST over south-central and Gulf region of U.S. as well as eastern Alaska; opposite sign anom. western North America near US/Canadian border, eastern North America near US/Canadian border, and in central Paci-	

	fic at 30-40N.	
	MODE 1: SST: Moderate ENSO signature late summer and late fall, switching to opposite ENSO phase by late spring. 700mb: PNA/TNH pattern with polarity consistent with early trop. Pacific SST (with Canadian center of same sign as SST) in late fall and late winter. Predictand: Anom. of sign opposite late spring trop. Pacific SST south of Aleutians, and of sign opposite to this in Alaska and western Canada. MODE 2: SST: Anom. in Atlantic at 40N,60W in late fall through late spring; anom. of same sign at 20S just off South American coast in late winter and late spring. 700mb: SZ pattern with anom. sign same as Atlantic SST at subtrop. latitudes in late summer and following late spring. Predictand: Anom. of same sign as Atlantic SST over southeast U.S., Caribbean, and Gulf of Mexico; same anom. sign also over and to south of Alaska.	Caribbean, Mexico [2] North Pacific south-southeast of Aleutians, south to 30N [1]
+SO+ 0.15 late summer late fall late winter late spring		
	MODE 1: SST: ENSO signature develops in summer. 700mb: Anom. of sign like trop. Pacific SST over subtrop. Atlantic in winter, spring and summer. Predictand: Weak PNA-like pattern with strongest center in eastern U.S. and off coast with sign opposite trop. Pacific SST. MODE 2: SST: Anom. in North Atlantic at 40N,60W in winter, spring and summer; same sign anom. off South American west coast at 20S in fall, spring and summer, and off Baja California (20N,110W) in sum-	Central and western Atlantic at 20-30N [2]
OND 0.10 fall winter spring summer		

	mer. Opposite sign of anom. south of Aleutians in fall and the following summer. 700mb: SZ pattern with anom. with sign like SST off South American coast at subtrop. latitudes in fall and the following summer, especially in Atlantic and North Africa. Predictand: NAO-like pattern with anom. of sign like SST off South American west coast, across Atlantic at 20-30N and south-central U.S. and Gulf of Mexico; opposite anom. sign over Greenland.	
	MODE 3: SST: ENSO signature in fall, winter and spring, dissipating in summer. Same sign anom. in Indian Ocean all four periods, and in trop. Atlantic in spring and summer. 700mb: Combined WPO and TNH patterns in winter with anom. of sign like trop. Pacific SST over Canada. Combined WPO, TNH and NAO in spring with anom. of sign like trop. Pacific SST over Canada and south of Greenland. Predictand: Weak north-south dipole in Pacific (20N vs. 40N) at 130W, with southern pole of sign like trop. Pacific SST.	
---	---	---
	MODE 1: SST: Anom. of same sign in trop. Atlantic and trop. Pacific, north of equator, in all four predictor seasons, but weaker in late summer in Atlantic. 700mb: PNA pattern with anom. sign in western U.S and Canada like tropical SST, in late fall and late winter. Predictand: TNH-like pattern with anom. of sign like tropical SST over Hudson Bay eastward to south of Greenland, and opposite sign over Cuba and off southwest Canadian coast.	Pacific, off coast of California (40N, 130-140W) [1 and 3] Davis Strait (55W,60N) [1 and some 2] Northwest Canada [from none of 1, 2 or 3]
+DJ+ 0.20 late fall late winter late spring late summer	MODE 2: SST: Strong ENSO signature in late fall and late winter, weakening	Subtrop. Pacific (20N, 160W) [3]

but continuing in late spring and late summer. Indian Ocean assumes same anom. sign as trop. Pacific in all four predictor seasons, and trop. Atlantic does so in late winter and late spring.

700mb: PNA pattern in late fall with anom. sign over western North America like trop. Pacific SST; TNH-like pattern with analogous polarity in late winter. SZ pattern with subtrop. anom. sign like trop. Pacific SST in all four predictor periods (but weaker in late winter).

Predictand: NAO pattern with anom. sign like trop. Pacific SST in western Atlantic and much of U.S., and opposite sign over Greenland.

MODE 3:

SST: Strong ENSO signature in late spring and late summer.

700mb: Anom. of sign opposite trop. SST at subtrop. latitude in mid-Pacific in late winter, strengthening and moving northward to 30N by late spring and late summer.

Predictand: Combined TNH/PNA with anom. of same sign as trop. Pacific SST in south-central Canada.

d. Prediction of 700 mb Height in the Northern Hemisphere

CCA experiments were applied to the entire field of 358 grid points of NH 700 mb height, using the following three sets of predictors: (1) NH 700 mb height and quasi-global SST, with the latter double-weighted, (2) 700 mb height alone, and (3) SST alone. As before, set (1) performed best and was subsequently used. Because of the more extensive predictand field, sensitivity tests for the mode truncation point for the pre-orthogonalization as well as the CCA itself initially were carried out with more than 6 modes. Based on examination of eigenvalue curves and cross-validated skill, it was found that with a few exceptions, including more than 6 modes is not beneficial. Hence, 6 modes is uniformly used.

Figure 43 shows the seasonal cycle of cross-validated skill, using NH 700 mb height and double weighted SST predictors, in predicting the 3 month mean 700 mb height averaged over the NH at 1 month lead. Predictions are made for eight overlapping 3 month seasons progressing as JFM, +MA+, AMJ, ..., OND, and +DJ+, where the "+" symbol denotes the adjacent half of the neighboring month. The dashed line indicates cross-validated persistence skill. The profile shows less seasonal variation than the profiles for height in the PNA region (Fig. 40a) and U.S. surface temperature (Fig. 6). The geographical distribution of skill for each of eight overlapping 3 month periods is displayed in Fig. 44. The sequence of skill fields reveals a concentration of late winter and spring skill in regions associated mainly with the TNH, PNA, WPO, and even NAO patterns. The subtropical Pacific skill region extends westward as far as southeast Asia, an area showing skill independently of the Pacific at several other times of the year. The central North Atlantic is also included; this is somewhat east of the typical extent of the PNA pattern and suggests that a North Atlantic Oscillation (NAO) pattern (having a central Atlantic north-south dipole structure between about 30^{o}N and southern Greenland) may also be somewhat predictable. A broad area relatively lacking in predictive skill includes most of the Eurasian continent from 30^{o} northward. In late spring the regions of cold season predictability subside, creating a minimum in the temporal profile of skill until summer, when substantial skill appears in the subtropical eastern Atlantic, North Africa and the Arabian Penninsula. Weaker but noticeable summer skill is also found in parts of the United States, Canada, and the central North Pacific (Fig. 44d,e). The summer secondary skill peak declines somewhat in early fall (Fig. 44f), although some skill is retained in the subtropical Atlantic, North Africa and southeast Asia. The subtropical Pacific and extratropical TNH/PNA/WPO skill regions reappear with the approach of winter.

Table 4 lists the canonical eigenvalues in terms of percentage of total CCA-explained predictor-plus-predictand variance as a function of season and mode number for NH 700 mb height prediction. The seasons showing highest overall predictive skill (JFM, +MA+ and JAS) tend to have proportionally high variances explained by the leading 1 or 2 modes, suggesting only a small number of physical mechanisms underlying the predictability.

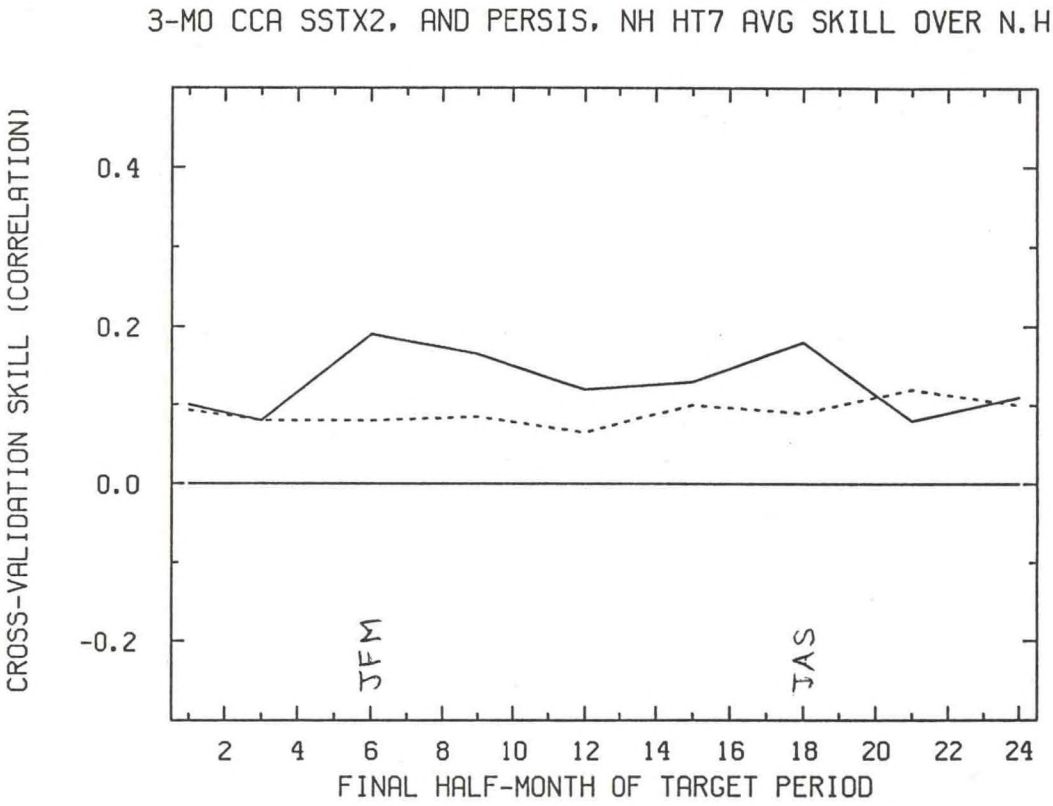

43. Seasonal variation of CCA forecast skill averaged over the Northern Hemisphere for 1 month lead time for 3-month mean 700 mb height (solid curve). Each of the four predictor periods is three months in duration. Double-weighted SST and NH 700 mb height itself are used as predictor fields. The skill of persistence forecasts is shown by the dashed curve.

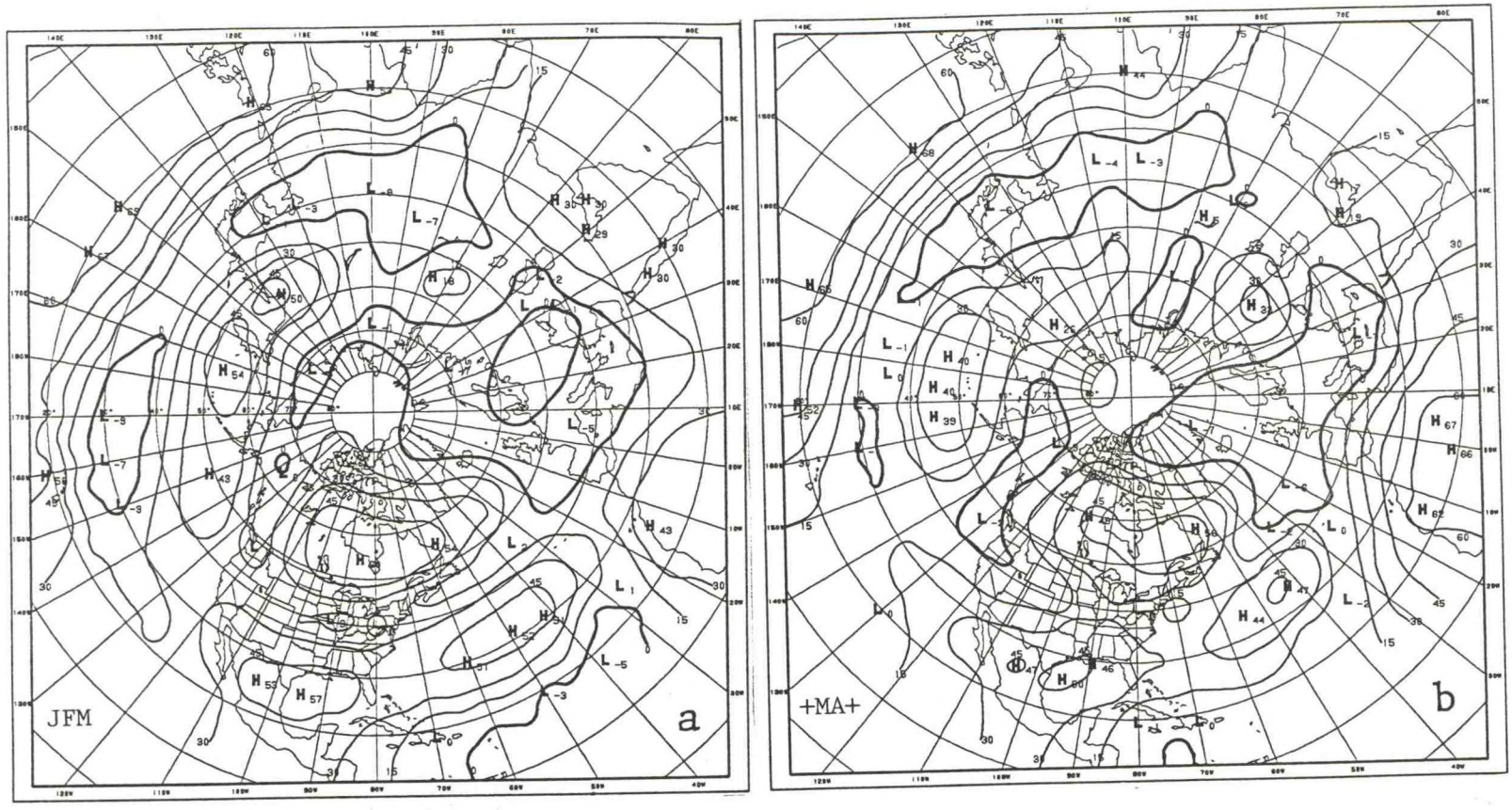

44. Geographical distribution of CCA skill in forecasting 3-month mean 700 mb height in the Northern Hemisphere at 1-month lead using the 700 mb height and double-weighted SST fields as predictors for (a) JFM, (b) +MA+, (c) AMJ, (d) +JJ+, (e) JAS, (f) +SO+, (g) OND, and (h) +DJ+, where the "+" denotes the adjacent half of the neighboring month.

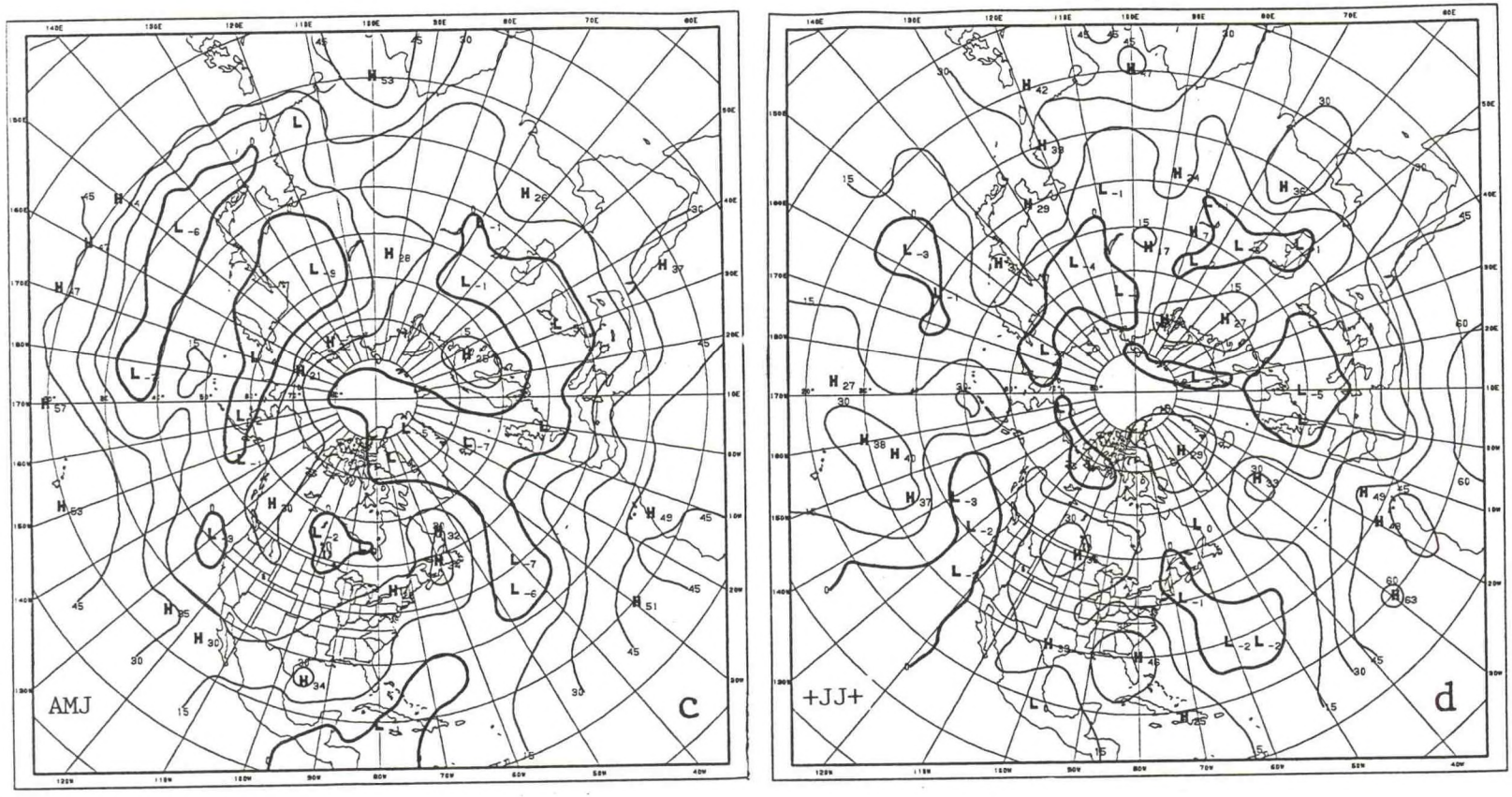
AMJ
c
+JJ+
d

JAS
e
+SO+
f

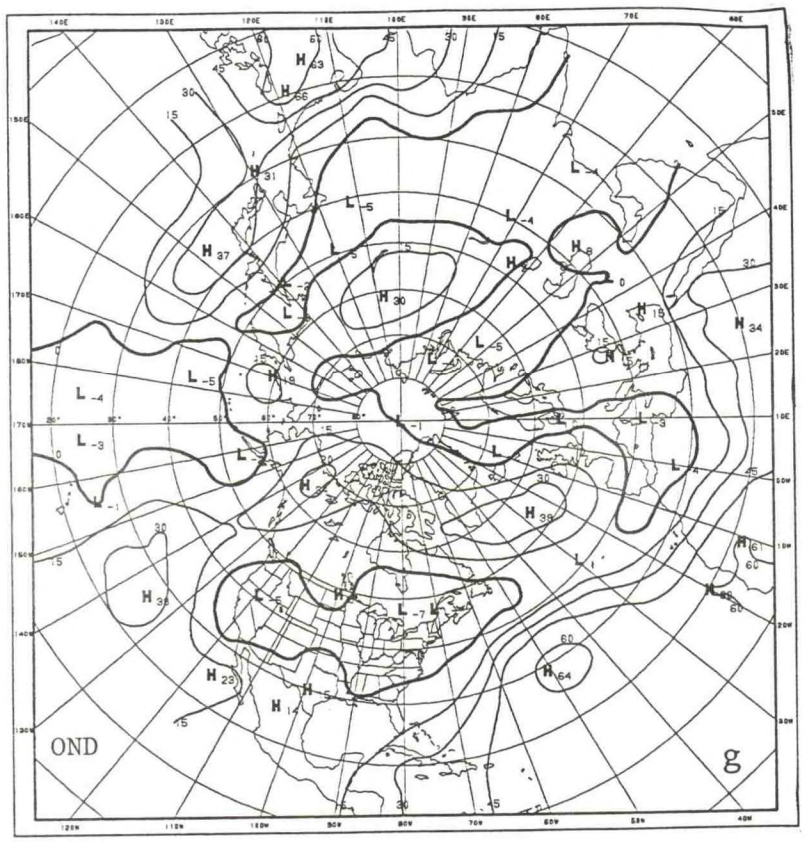
OND
g

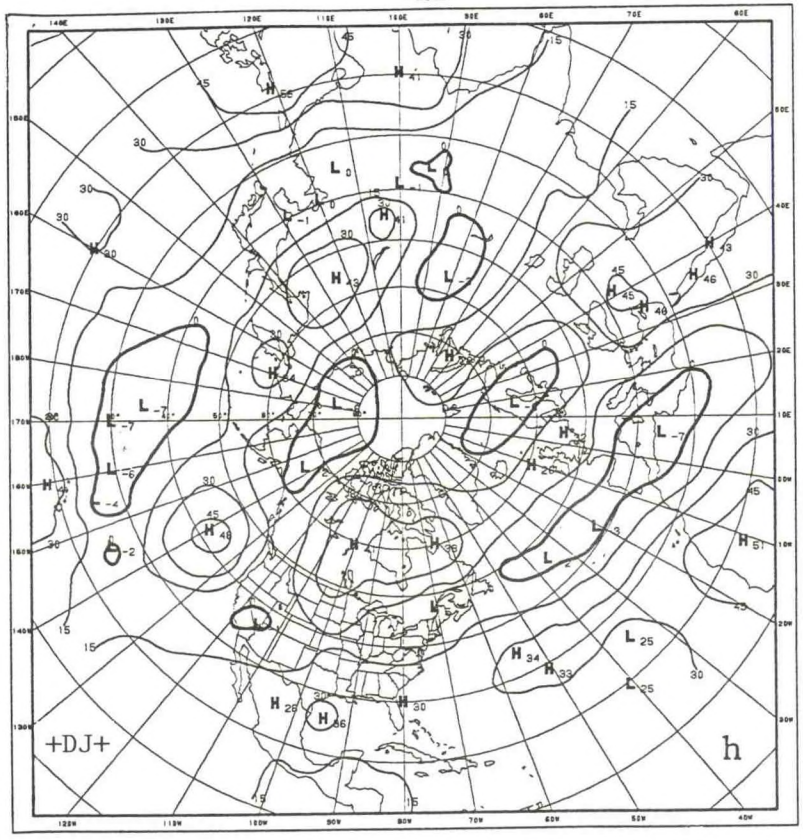
+DJ+
h

Season	CCA Mode Number					
	1	2	3	4	5	6
JFM	50	20	15	7	5	3
+MA+	52	31	13	3	1	
AMJ	38	29	18	10	4	
+JJ+	35	31	18	10	5	1
JAS	43	35	13	8	1	
+SO+	41	22	20	10	5	1
OND	43	35	13	6	3	1
+DJ+	30	26	23	12	5	4

Table 4. Percentage of total CCA-explained variance (using 5 or 6 modes) as a function of mode number for each of the eight 3-month target seasons in prediction of NH 700 mb height.

The skill for the January-February-March period (Figs. 43, 44a) is the highest of any time of the year. The CCA mode 1 principal predictand pattern is shown in Fig. 45. There is a close correspondence between the strongest centers of this pattern and the centers of highest cross-validated skill in Fig. 44a. Mode 1 contains 50 percent of the variance explained by all 6 modes, and 2.5 times the variance of the second mode (Table 4); this dominance is greater than for any of the other seasons. The leading season (Sep-Oct-Nov) SST and 700 mb height predictor patterns are shown in Figs. 46a,b. This is clearly a tropical Pacific ENSO situation (here, arbitrarily a cold event) with a strong equatorial versus mid-latitude Pacific SST anomaly dipole (Fig. 46a) and a PNA-like pattern (here, negatively phased) in the 700 mb height (Fig. 46b) in the preceding fall. The relatively lower magnitudes of the 700 mb height loadings (maximum of 0.64) than SST loadings (maximum >0.8) and the relative noisiness of the PNA height pattern underscores the comparatively greater predictive importance of SST than 700 mb height for subsequent hemispheric winter heights. The SST patterns show a progressive buildup of the cold water event in the loading patterns of the three earlier seasons (not shown), while the sequence of 700 mb height patterns are relatively uneventful. The scenarios of the substantially weaker modes 2 and higher are not of interest.

The predictive skill in Jul-Aug-Sep represents a secondary NH skill maximum (Fig. 43) whose geographic distribution is shown in Fig. 44e. In the late summer the subtropical latitudes of Africa and Asia, rather than the PNA region, are favored for predictability. The mode 1 principal predictand pattern is shown in Fig. 47a, with the third predictor period (Dec-Jan-Feb) SST and 700 mb height predictor patterns in Fig. 47b,c. The third period is chosen because it, along with the second period, has the strongest and most organized patterns. The principal predictand map (Fig. 47a) has a broad, strong center in southern Asia (identified as the monopole Asian Summer pattern in the rotated principal components study of Barnston and Livezey 1987), contributing to the eastern portion of the major skill area appearing in Fig. 44e. However, the predictand loading pattern is hemispheric in scale with a suggestion of a three-band zonally symmetric structure. Except in the Pacific, the subtropics tend to have positive loadings--especially in Asia, where they extend north to 50^{o}N to encompass the Asian skill center. (In the following discussion we use the polarities shown in the loadings, realizing that reversing their sign is equally valid.) The predictor loading patterns suggest a waning cold water ENSO event that could have peaked in the winter prior to the predictor window. The climate state in the included winter reveals only a weak cold SST signal in the tropical Pacific, but generally negative SST anomalies in the northern Indian Ocean, East China Sea, and parts of the tropical Atlantic (Fig. 47b). The associated 700 mb loading map (Fig. 47c) shows a weak pattern, including a negatively phased WPO and a northwestward-displaced PNA-like structure that sometimes accompany a cold ENSO event. The leading predictor period loadings (Mar-Apr-May; not shown) reveal a weakening of the SST pattern shown in Fig. 47b and a partial continuation of the 700 mb pattern noted in Fig. 47c. The two

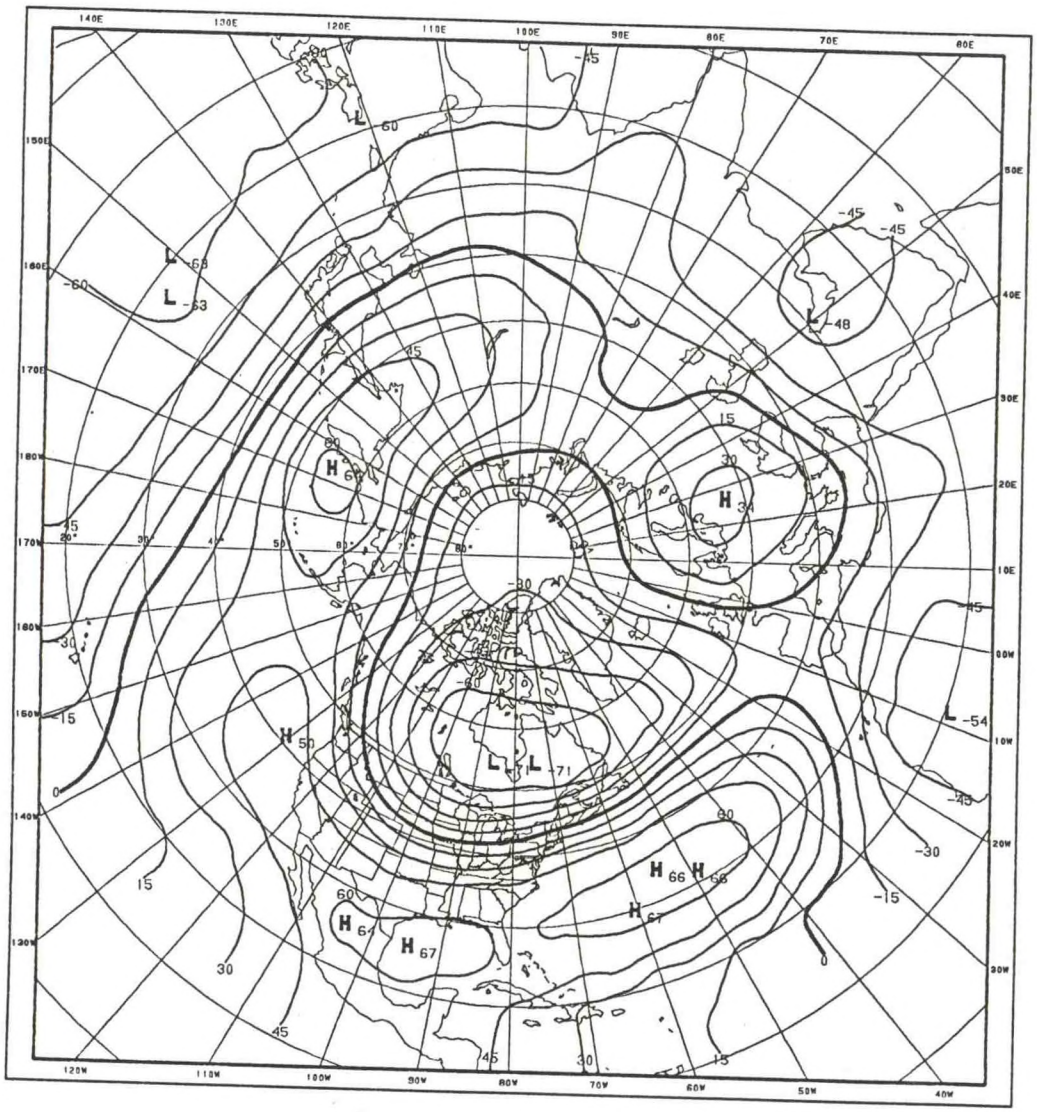

45. The principal predictand loading pattern for mode 1 for the prediction of Jan-Feb-Mar 700 mb height in the Northern Hemisphere at 1 month lead.

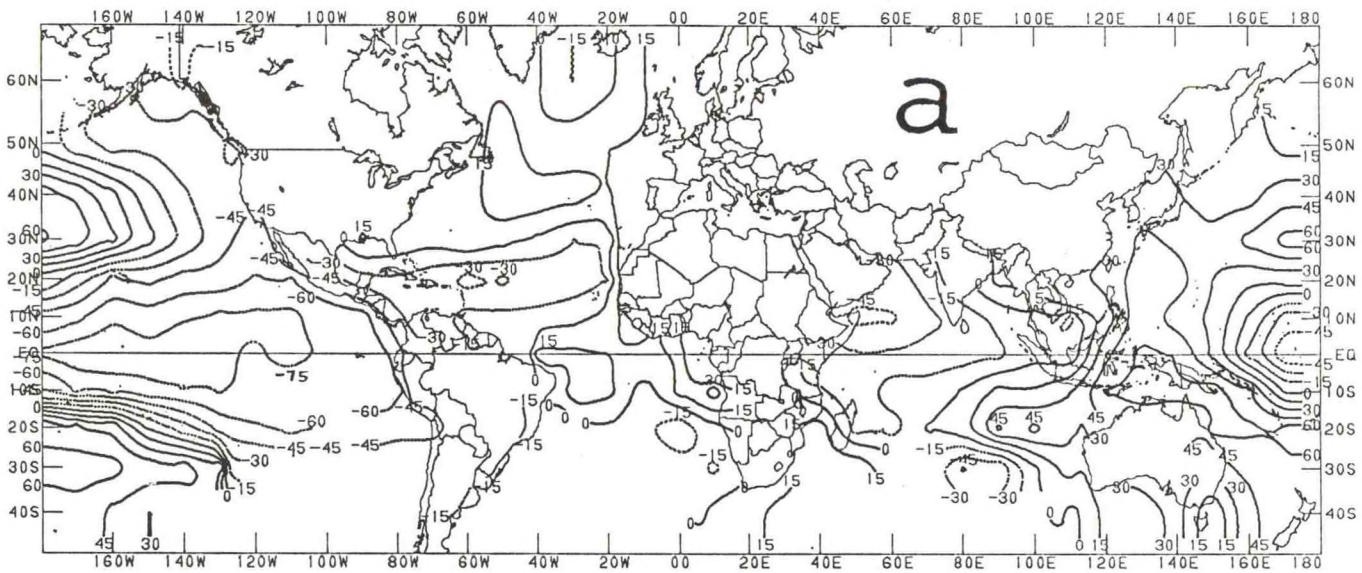

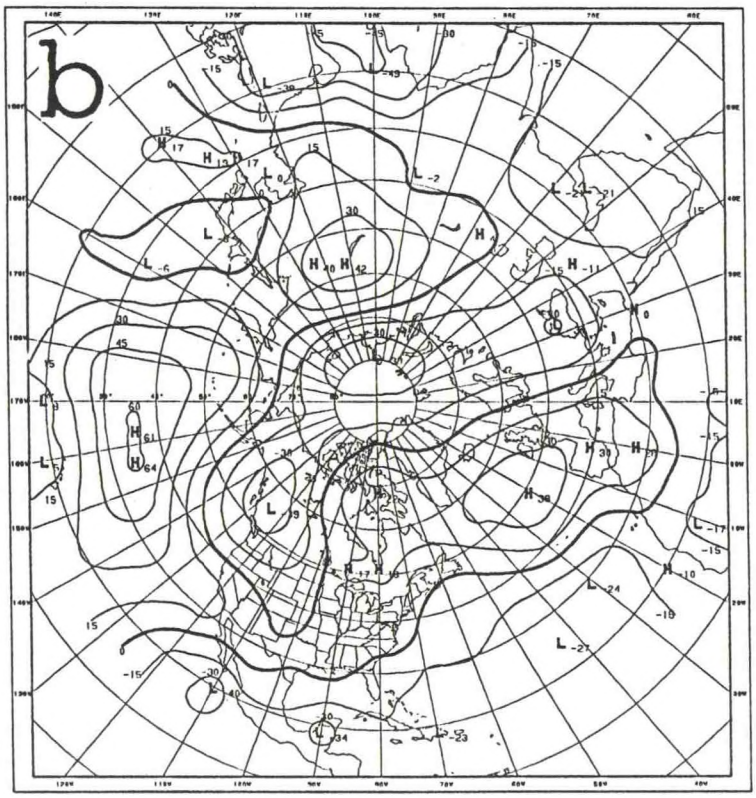

46. Part (a): SST predictor CCA loadings for mode 1 for prediction of Jan-Feb-Mar 700 mb height in the Northern Hemisphere at 1 month lead, for the fourth (Sep-Oct-Nov) predictor period. Part (b): As in part (a) except for 700 mb predictor loadings.

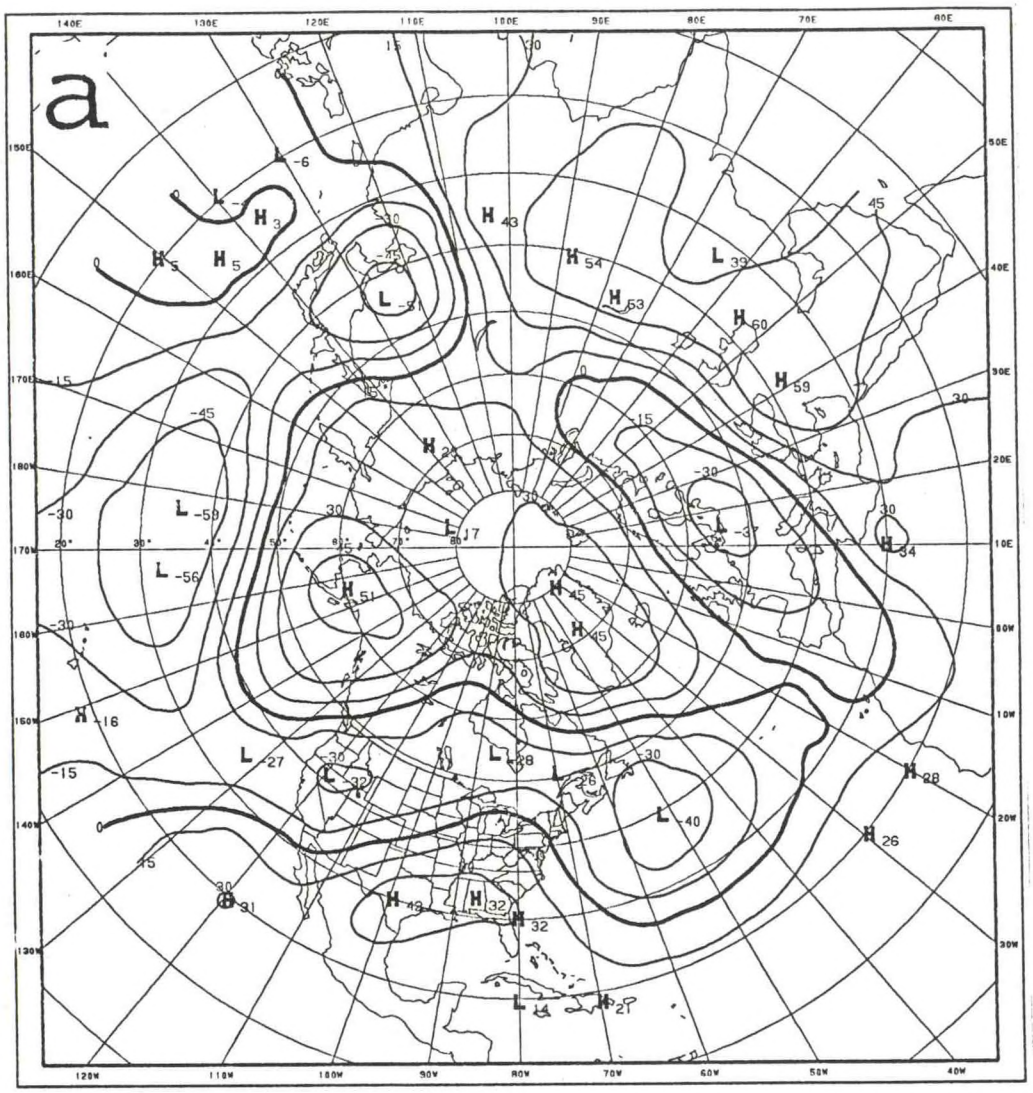

47. Part (a): The principal predictand loading pattern for mode 1 for the prediction of Jul-Aug-Sep 700 mb height in the Northern Hemisphere at 1 month lead. Part (b): SST predictor loadings for mode 1 for the third (Dec-Jan-Feb) predictor period. Part (c): As in part (b) except for 700 mb predictor loadings for the third period.

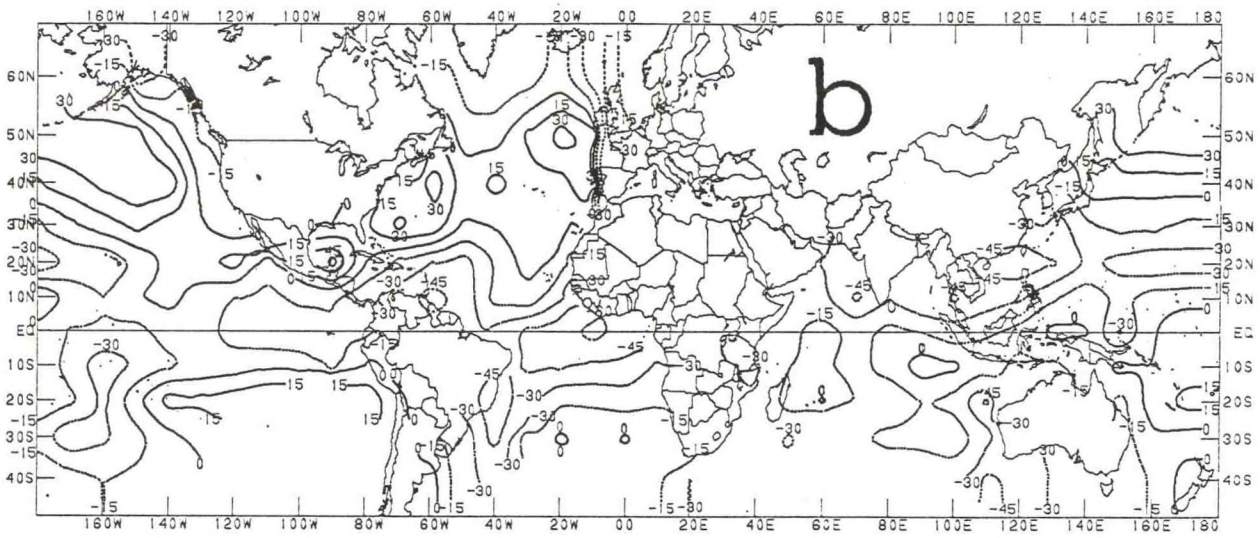
b
160W 140W 120W 100W 80W 60W 40W 20W 00 20E 40E 60E 80E 100E 120E 140E 160E 180
60N 50N 40N 30N 20N 10N EQ 10S 20S 30S 40S

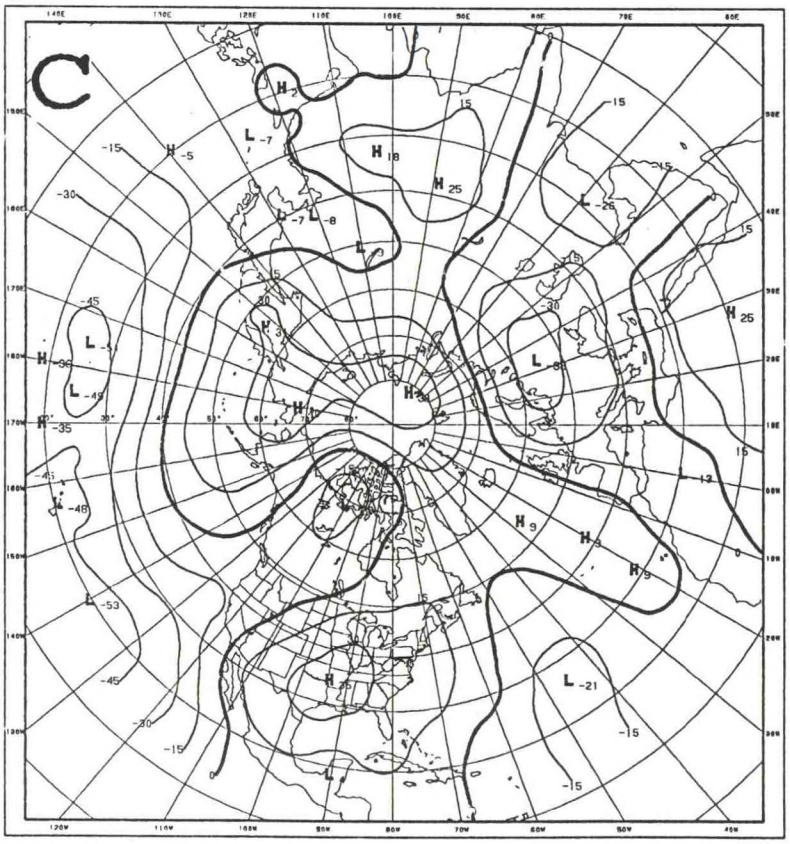
C

earliest predictor period loading patterns also show weaker SST anomalies in the Atlantic and Indian oceans than seen in Fig. 47b but a stronger cold ENSO event reflected by the tropical Pacific SST; the 700 mb patterns during these two periods are weak, with the fall (second) period having a negatively phased PNA pattern. This information suggests that positive (negative) late summer 700 mb height anomalies in south-central and southwestern Asia tend to follow negative (positive) SST anomalies in the northern Indian Ocean the previous winter. This cool (warm) SST condition, like that in the Atlantic and Caribbean, may be associated with the cessation of a cold (warm) ENSO event (see section 4a[3]).

The principal predictand pattern (Fig. 48a) and predictor loading patterns for the first (prior summer) and last (leading spring) predictor periods for mode 2 (Fig. 48b-e) reveal a rather stable zonally symmetric pattern of warmth (coldness) at low latitudes in the SST (Fig. 48b,c) as well as 700 mb height (Fig. 48d,e) in both predictor periods. The second and third predictor periods (not shown) have similar patterns, except for a noisier third period 700 mb height field. While weak ENSO features are noted, the warmth (coldness) includes the tropics of all three oceans. The regions of Jul-Aug-Sep 700 mb height best predicted by this regime (Fig. 48a) are roughly the same as those highlighted in the 700 mb predictors, and have the same anomaly sign--North Africa, the subtropical Pacific and subtropical Atlantic; the predictive skill (Fig. 44e) in these regions is enhanced by mode 2.

The principal predictand and 700 mb height predictor loading patterns strongly reflect the SZ warm season pattern discussed in Barnston and Livezey (1987) and elsewhere. It is suggested here that the SZ pattern in height is related to a like-signed similarly zonally symmetric tropical ocean anomaly pattern.

It is noted that the warm season relationships are weaker and less certain than the cold season ones. The regions of maximum predictive warm season skill occur in low latitude zonally elongated patterns, and their best predictors are of similar character. This is consistent with the relative lack of extratropical summer influence from ENSO, in contrast to the meridional propagation of ENSO responses in the Western Hemisphere in winter and spring.

The seasonality of the pockets of highest skill for prediction of NH 700 mb height is summarized in Fig. 49, in which the locations of the cross-validated skill centers for eight 1.5-month-apart seasons are plotted for two levels of skill: >0.45 (part a) and >0.60 (part b). This same picture could have been provided by the strongest centers of the principal predictand maps for the leading 1 or 2 modes for each season. However, the skills are the quantity of ultimate interest, representing the cumulative influence of all 5 or 6 CCA modes and subjected to the cross-validation process. In winter and spring, the locations of highest skill, being largely ENSO related, include the subtropical central and western Pacific, the central North Pacific near

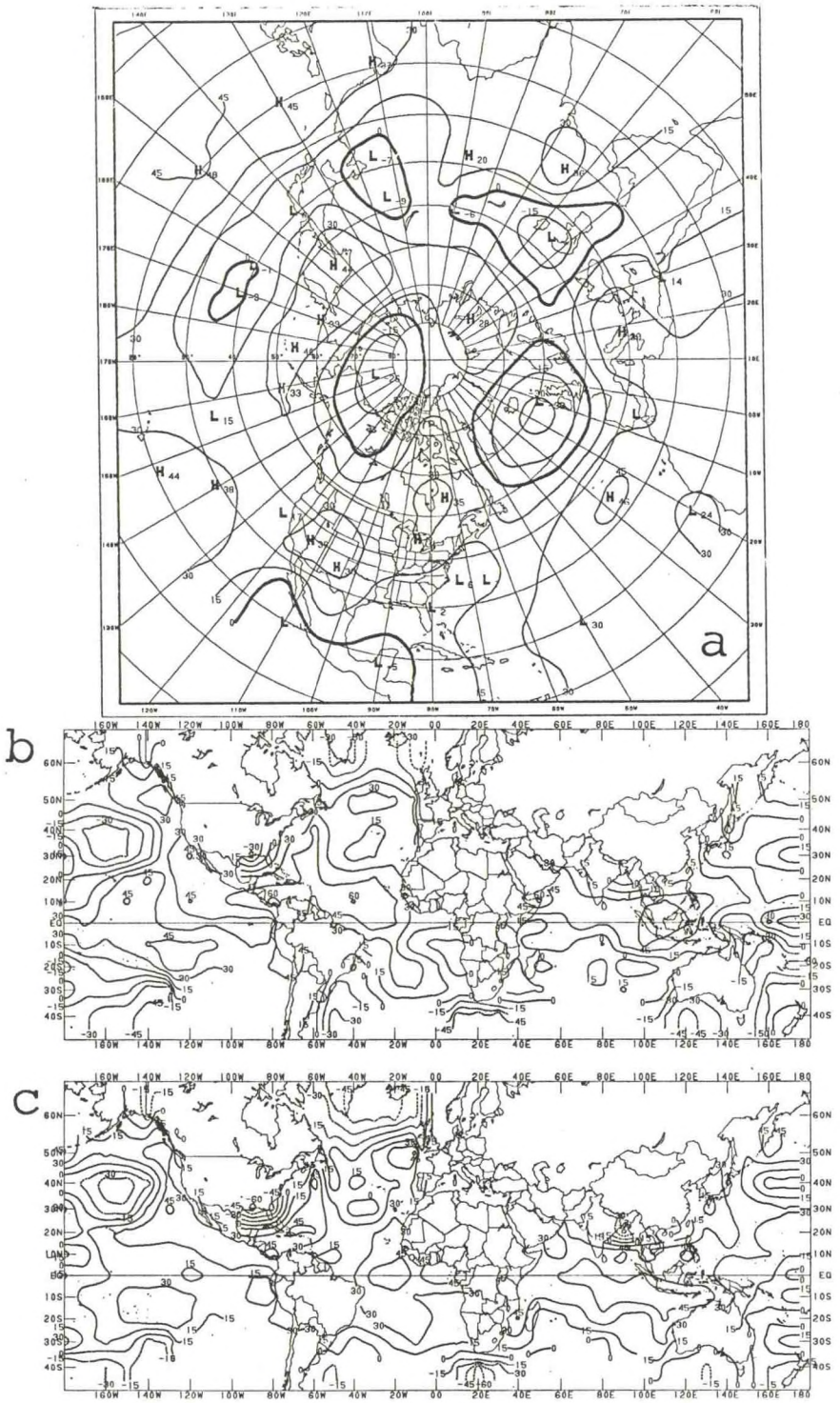

48. Part (a): The principal predictand loading pattern for mode 2 for the prediction of Jul-Aug-Sep 700 mb height in the Northern Hemisphere at 1 month lead. Parts (b and c): SST predictor loadings for mode 2 for the first (Jun-Jul-Aug) predictor period and for the fourth (Mar-Apr-May) period. Parts (d) and (e): As in parts (b) and (c) except for 700 mb predictor loadings for first and fourth periods.

d
e

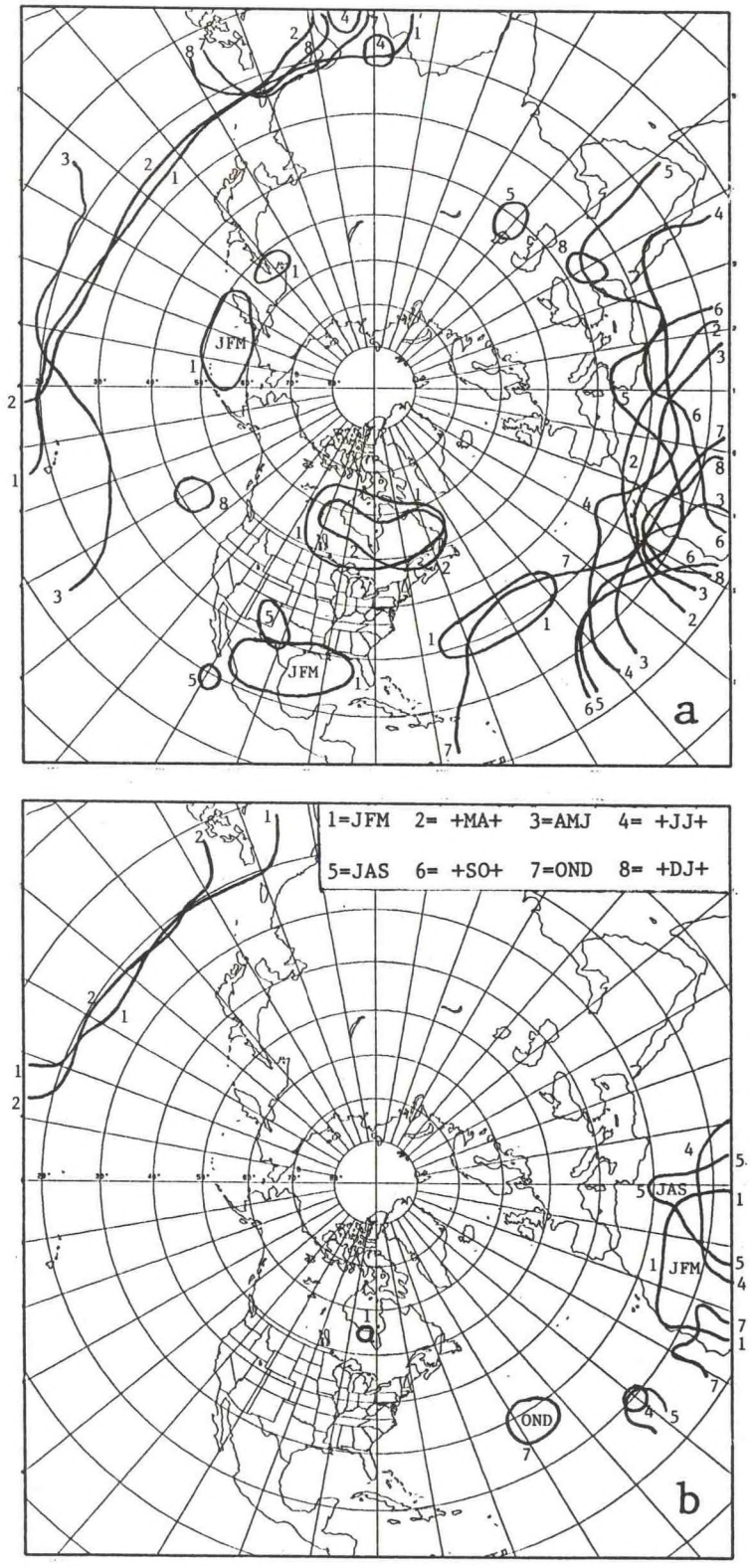

49. Summary of seasonality of highest cross-validated predictive skill for Northern Hemisphere 700 mb height. Areas of skill of 0.45 or greater are contoured in part (a), and 0.60 or greater in part (b). The eight overlapping 3 month seasons are identified by numbers as defined in the inset of part (b).

45-50°N, and in North America both near Hudson's Bay and in the western Gulf of Mexico and southern U.S. In the summer, with the extratropics mostly exempt from ENSO effects, the highest predictability resides largely at subtropical latitudes in North Africa and southern and central Asia.

Table 5 summarizes the predictor and predictand scenarios for 8 overlapping three month seasons for all modes giving rise to local cross-validated skill peaks of 0.4 or higher. In addition to the cold and warm season relationships highlighted above, a previously undocumented scenario leading to an NAO pattern in late fall (OND) is indicated in Table 5. Apparently, an NAO pattern shifted slightly to the south (with zero anomaly line at 40N instead of the prototypical 50N) tends to occur the fall following a spring and summer onset of an ENSO event with the tropical Pacific SST anomaly limited to the eastern half of the Pacific Basin. The sequence of events includes a partial but strong summer SZ pattern with subtropical Atlantic and North African anomalies of sign like that of the eastern tropical Pacific SST, followed by the late fall NAO-like predictand 700 mb pattern with the lower latitude sign the same as that of the subtropical SZ anomaly.

Table 5. Summary of CCA predictor and predictand scenarios, described by loading patterns, for skill-producing 1 month lead forecasts of 700 mb height anomalies in the Northern Hemisphere for eight overlapping three month seasons. The four predictor periods are listed in leftmost column beneath the predictand season and areal (hemispheric) mean cross-validated skill. "Winter" refers to DJF, "late winter" to +FM+, etc. Polarities (i.e. signs) of centers of loading patterns are defined relative to one another rather than in an absolute sense, as a collective reversal of signs would be equally representative. "ENSO signature" in SST loadings refers to an anomaly in the eastern half or the east-central portion of the tropical Pacific Ocean. Indian Ocean anomalies of same sign may also appear. New or unexpected major non-summer and non-winter results are underscored.

Season/ Areal average skill/ The four predictor seasons	Predictor and Predictand Loading Patterns	Regions with Cross-Validated Skill of 0.4 or Greater; [ ] Indicates Mode of Origin
JFM 0.19 winter spring summer fall	MODE 1: SST: Strong ENSO signature develops in summer and fall with opposite anomaly sign around Indonesia in fall. 700mb: PNA pattern, with western North American anom. of sign like trop. Pacific SST and without southeast U.S. center, develops in fall. Predictand: Anom. of same sign as trop. Pacific SST in (1) subtrop. central and western Pacific, (2) south-central Canada, and (3) western North Africa. Opposite sign of anom. (1) from western Atlantic (near 30N) through southeast U.S., Gulf of Mexico and northeast Mexico, and (2) outer Aleutians through Kamchatka to north of northeastern China. MODE 2: SST: ENSO signature previous winter, locating just off South American coast in spring and summer, dissipating in fall. 700mb: SZ pattern with low latitude anom. sign like trop. Pacific SST in fall, strongest over	Subtrop. central [1 and 2] and western [1] Pacific non-western Canada [1] Southeast U.S., Gulf of Mexico, northeast Mexico [1] second center in western Atlantic (30N,40-60W) [1] Northern Japan, Kamchatka, outer Aleutians [1] North Africa [1]

		Pacific. Predictand: Weak PNA-like pattern with northwest U.S. anom. sign like trop. Pacific SST, and opposite sign centered at 50N,170W.	
		MODE 1: SST: ENSO signature develops in late spring and becomes strong in late summer and late fall; Indian Ocean also assumes same anom. sign in late fall. Opposite anom. sign in Indonesia in late summer and late fall. 700mb: Anom. of opposite sign as trop. Pacific SST appears in subtrop. Pacific late winter, migrating to 35N in late spring and 40N in late summer and late fall; in late fall the oppositely signed anom. appears in subtrop. Pacific as part of a combined PNA/TNH pattern. Predictand: Anom. of same sign as trop. Pacific SST in (1) subtrop. central and western Pacific, (2) southern Canada, and (3) western North Africa. Opposite sign of anom. (1) from central Atlantic (near 30N) through southeast U.S., Gulf of Mexico and Mexico, and (2) outer Aleutians through Kamchatka to southeastern Siberia.	Subtrop. central [1 and 2] and western [1] Pacific North Africa [1] South-central and southeastern Canada [1 and 2] Gulf states of U.S. (except Florida) and Gulf of Mexico, northeast Mexico; central Atlantic at 30-35N [1 and 2]
+MA+ 0.18 late winter late spring late summer late fall			
		MODE 2: SST: Moderate ENSO signature only adjacent to South American coast in late winter, late spring and late summer, dissipating in late fall; opposite sign anom. in Indonesia behaving in parallel. 700mb: Incomplete SZ pattern with same anom. sign as trop. Pacific SST at subtrop. latitudes in late summer and late fall. Predictand: Full PNA/TNH-like pattern (centers at 20N,170W; 45N,155W; 65N,95W; 30N,90W); this reinforces several skill areas associated with mode 1.	South of Aleutians to Kamchatka [2 and 1]

	MODE 1: SST: Anom. centered at 20N, 140W, gradually waning from spring through following winter; anom. of same sign in east Indian Ocean in winter; anom. of opposite sign in East China Sea in fall. 700mb: Largely noisy fields, some strong small centers.	Subtrop. Pacific (160E-140W) [2 and some 1] Subtrop. east Atlantic to North Africa [some 3, some 1, some 2]
AMJ 0.12 spring summer fall winter	Predictand: Anom. of same sign as trop. Pacific SST in subtrop. latitudes (SZ pattern) from eastern Atlantic through North Africa and Asia. Distorted PNA structure with anom. of same sign as trop. Pacific over western North America.	Cambodian Peninsula [some 1, some 3, some 2]
	MODE 2: SST: ENSO signature in spring, summer, fall and winter, strongest in spring and summer; Indian Ocean assumes same anom. sign in summer, fall and winter, while Indonesia has opposite sign in summer and fall. 700mb: SZ pattern with same anom. sign as trop. Pacific SST in summer, fall and winter; TNH pattern with compatible polarity (Canadian center with same sign as trop. Pacific SST) in winter. Predictand: Weak SZ pattern with same anom. sign as trop. Pacific SST; Imperfect PNA/TNH pattern with compatible polarity.	
	MODE 3: SST: Focused anom. in central trop. Pacific in spring; same sign of anom. in trop. Atlantic in spring, summer and winter; in trop. Indian Ocean in summer and fall; and in western trop. Pacific in spring, summer and fall. 700mb: Anom. of opposite sign of trop. Atlantic SST in subtrop. at various longitudes at various periods, except anom. of same sign as SST over subtropical east Atlantic in winter. Predictand: Anom. of opposite	

	sign of trop. Atlantic SST in subtrop. Atlantic and central and western Pacific (i.e., partial SZ pattern).	
	MODE 1: SST: Anom. in Atlantic off South American coast at 20S in late spring, late summer and late fall; same anom. sign in Indian Ocean in late summer. 700mb: Anom. of opposite sign of trop. Atlantic SST over southern U.S. in late spring, late summer and late fall; over east subtrop. Atlantic in late spring, over North Africa in late spring, late summer and late winter. Anom. of same sign as trop. Atlantic SST over subtrop. Pacific late summer, late fall and late winter. Predictand: Anom. of opposite sign of trop. Atlantic SST in North Africa, subtrop. Asia, northern Mexico, Greenland and Alaska; anom. of same sign as trop. Atlantic SST in Pacific at 30N,160W.	Subtr. East Atlantic through North Africa [1 and some 2] Cambodian Peninsula [some 1 and some 3] Southeast U.S., centered 30N,80W [some 1, some 3, some 2]
+JJ+ 0.13 late spring late summer late fall late winter		
	MODE 2: SST: Anom. just off South American west coast in late spring and late summer, and same sign anom. in Atlantic at 30N,60W in late winter. Same sign anom. in North Atlantic at 40N,60W in late fall, and in east Indian Ocean in late spring. Opposite anom. sign in Indonesia and at 40S,160W in late spring and late summer. 700mb: SZ pattern with anom. of same sign as Atlantic SST in subtrop. Pacific, Atlantic, and North Africa in late spring, late summer and late fall; includes southern U.S. in late summer and somewhat in late fall and late winter. Predictand: Anom. of same sign as Atlantic SST in Pacific near 150W, and more weakly in North Africa. Anom. of this same sign near Novaya Zemlya and southern Kamchatka.	

	MODE 3: SST: Anom. in northern trop. Atlantic (10-20N) in late spring, late summer, late fall and more weakly in late winter; same sign of anom. in southern Indian Ocean all four of these seasons; same sign of anom. in far western trop. Pacific in late spring, late summer and late winter. 700mb: Anom. of same sign as trop. Atlantic SST in west-central U.S. in late spring, late summer and late fall; same anom. sign. in western Canada in late winter. Predictand: Weak anom. of same sign as trop. Atlantic SST in south-central Canada and in East China Sea/southern Japan.		
---	---	---	---
	MODE 1: SST: Moderate ENSO signature in summer; anom. of same sign in northern trop. Atlantic in summer, fall and winter and in Indian Ocean in fall and winter. Anom. of opposite sign in east China Sea in fall and winter. 700mb: Anom. of same sign as trop. Atlantic SST, in subtrop. Pacific in fall, winter and spring; opposite sign anom. at variable locations in extratrop., including east U.S. in fall and winter, other U.S. in winter and spring. Predictand: Anom. of same sign as trop. Atlantic SST from Korea to north of Hawaii (30N), in Atlantic at 40N,50W, and over Greenland; opposite anom. sign across Asia, in the Gulf region of U.S., and in Alaska.	Subtrop. east Atlantic, North Africa and Red Sea [some 2, some 1] Near Aral Sea (40N,60E) [1] Western south U.S. (Texas, New Mexico) [some 2, some 1]	
JAS 0.18 summer fall winter spring	MODE 2: SST: Anom. in trop. Pacific at 10-20S,130W all four predictor seasons (weaker in spring); same sign of anom. in trop. Atlantic in summer and fall and more weakly in winter and spring. Anom. of same sign in North Atlantic at 40N,60W in all four predictor seasons, and near Indonesia in all four seasons (weaker in winter). Opposite sign		

	anom. at 40S,0-40E in fall and winter, in northern Gulf of Mexico weakly in fall and more strongly in winter and spring, and east of India in spring. 700mb: SZ pattern with same sign of anom. in subtrop. as trop. Pacific SST in summer, fall, winter and spring (more weakly in winter). Predictand: SZ pattern with same sign of anom. in subtrop. as trop. Pacific SST. This includes low latitude Atlantic, Pacific (most strongly), Asia and Africa, with a northerly protrusion into the western region and Rockies of U.S. Scattered oppositely signed anom. at mid-latitudes (e.g. west of England and north of Alaska).	
---	---	---
	MODE 1: SST: ENSO signature far east trop. Pacific, south of equator, in all four predictor periods; strongest in late winter. Same anom. sign in North Atlantic (center at 40N, 60W) in late fall, late winter and late spring; same sign also in trop. Indian Ocean late winter and late spring. Opposite anom. sign in eastern Indian/western Pacific oceans late summer and more weakly in the following late spring. 700mb: Anom. of same sign as trop. Pacific SST at subtropical latitudes (SZ pattern) in all four predictor periods. TNH/PNA pattern in late winter with Canadian center of same sign as trop. Pacific SST. Predictand: Subtropical anom. of same sign as trop. Pacific SST (SZ 700mb pattern). Included are the Atlantic, Gulf of Mexico, North Africa and the Pacific.	Subtrop. eastern Atlantic and North Africa, 40W-20E [1]
+SO+ 0.08 late summer late fall late winter late spring		

	MODE 1: SST: ENSO event develops in spring and summer east of Date Line. Anom. of opposite sign had been in trop. Atlantic in winter, as well as anom. of same sign as Pacific SST in North Atlantic (40N, 60W). Anom of opposite sign in west Indian Ocean and west trop. Pacific Ocean in summer. 700mb: TNH pattern with Canadian center of same anom. sign as trop. Pacific SST in spring. Partial SZ pattern with subtrop. latitude of same sign as trop. Pacific SST in Atlantic, Africa and western Asia in summer. Predictand: Strong NAO-like pattern with same sign as trop. Pacific SST at 25-30N,35-45W; opposite sign centered at 55N,35W.	Subtrop. Atlantic, adjacent to North Africa [1] Phillipines [1]
OND 0.11 fall winter spring summer		
---	---	---
	MODE 1: SST: ENSO signature develops in late fall and lasts through late winter, late spring and late summer. Anom. of same sign as trop. Pacific SST in Indian Ocean and northern trop. Atlantic Ocean late spring and late summer. Opposite sign anom. at 20S at Date Line tucked south of the major anomaly band. 700mb: PNA pattern without SE U.S. center in late fall, with western North American center of same sign as trop. Pacific SST. Combined TNH/NAO pattern in late winter, with matching polarity to PNA pattern preceding it. SZ pattern in late spring (mostly in Atlantic and southeast Asia) with subtrop. anom. of same sign as trop. Pacific SST. More longitudinally global SZ pattern of same polarity in late summer. Predictand: TNH/PNA pattern with Canadian center of sign like trop. Pacific SST, and subtrop. anom. of same sign in western Asia and North Africa contributing to SZ-like pattern.	Phillipines [2 and some 1] Western North Africa [2 and 1] Eastern Pacific (40N, 140W) [some 1 and some 2] South of Black Sea [1] Hudson Bay [1 and some 2]
+DJ+ 0.16 late fall late winter late spring late summer		

MODE 2:

SST: Anom. centered in trop. Atlantic late fall and late winter. Same sign anom. at 40S,70-120E in late winter and late spring, at Date Line at 20N late winter and at 30S in late spring. Same sign anom. also in western trop. Pacific in late winter, late spring and late summer, and south of Japan in late spring and late summer. Weak anom. of opposite sign over wide area of trop. Pacific in late summer.

700mb: Weak PNA pattern with western North American center of sign like trop. Atlantic SST, in late fall. NAO pattern with low latitude (35-40N) band of same sign as trop. Atlantic SST, in late summer.

Predictand: Anom. of same sign as most of the SST features over Britain, off northwest U.S. coast, and in northwestern China. Opposite sign anom. east of Phillipines, west of North Africa, in Novaya Zemlya and (more weakly) over Hudson Bay.

e. Prediction of European Surface Temperature

Because there is a moderately strong relationship in many locations at certain times of the year between surface temperature and the mid-tropospheric geopotential height field for averaging periods of 5 days or greater (Klein 1983, Klein and Yang 1986, Klein et al. 1989), low predictive skill might be expected in Europe during most of the year on the basis of the predictability of the 3 month mean 700 mb height in the NH (Fig. 44). To verify this, CCA was applied to 1 and 3 month mean forecasts for the network of 59 European stations shown in Fig. 50. Twelve periods are used as forecast targets, as only regular monthly mean data were available. The predictor set found to produce the most skill in the U.S. temperature experiments was retained here (700 mb height, SST weighted double, and European surface temperature itself). A plot of the annual march of cross-validated CCA skill for 3 month periods is shown in Fig. 51a. The expectation of modest skill is generally confirmed. A weak tendency for skill appears during the winter season for leads of 1, 4 and 7 months, and a slightly stronger skill tendency is suggested in fall (both for Aug-Sep-Oct and Sep-Oct-Nov) for forecasts made 1, 4, 7 or 10 months in advance. The cross-validated skill for persistence forecasts is shown in Fig. 51b; skills here are low, as they are in the U.S. (Fig. 4b).

The forecasts for Sep-Oct-Nov made at the end of August contain higher skill (0.19) than any of the other 1 month lead forecasts. The geographical distribution of this skill is shown in Fig. 52a. The primary predictable area is in south-central Europe, including the western Mediterranean Sea (Corsica and Sardinia), southern France, northeastern Spain and northwestern Italy. A weaker skill region (not shown, as skills peak in the 0.20's) is found along eastern Scandinavia. The geographical distribution of persistence skill for the same forecasts (Fig. 52b) indicates a partly congruent but weaker (0.11 mean) pattern.

The mode 1 CCA loading patterns are found to be more organized and internally consistent than those of the higher order modes, with eigenvalue nearly twice that of mode 2. The principal predictand loading pattern for mode 1 is presented in Fig. 53, in which both the main southern Europe and weaker northern extension skill areas are well represented. We also note that both skill areas (in fact, 55 of the 59 stations) carry the same loading sign, implying that European temperature generally tends to vary in monopole fashion in response to the mode 1 predictor patterns.

The predictor loading patterns for the final two predictor periods (Feb-Mar-Apr in part [a] and May-Jun-Jul in part [b]) are shown for SST and 700 mb height in Figs. 54 and 55, respectively. The early spring and early summer SST patterns reveal like-signed anomalies in all three tropical oceans, in somewhat similar fashion to the predictors of U.S. summer temperature discussed in section 4a(1[b], 2, and 3) above. The first two predictor peri-

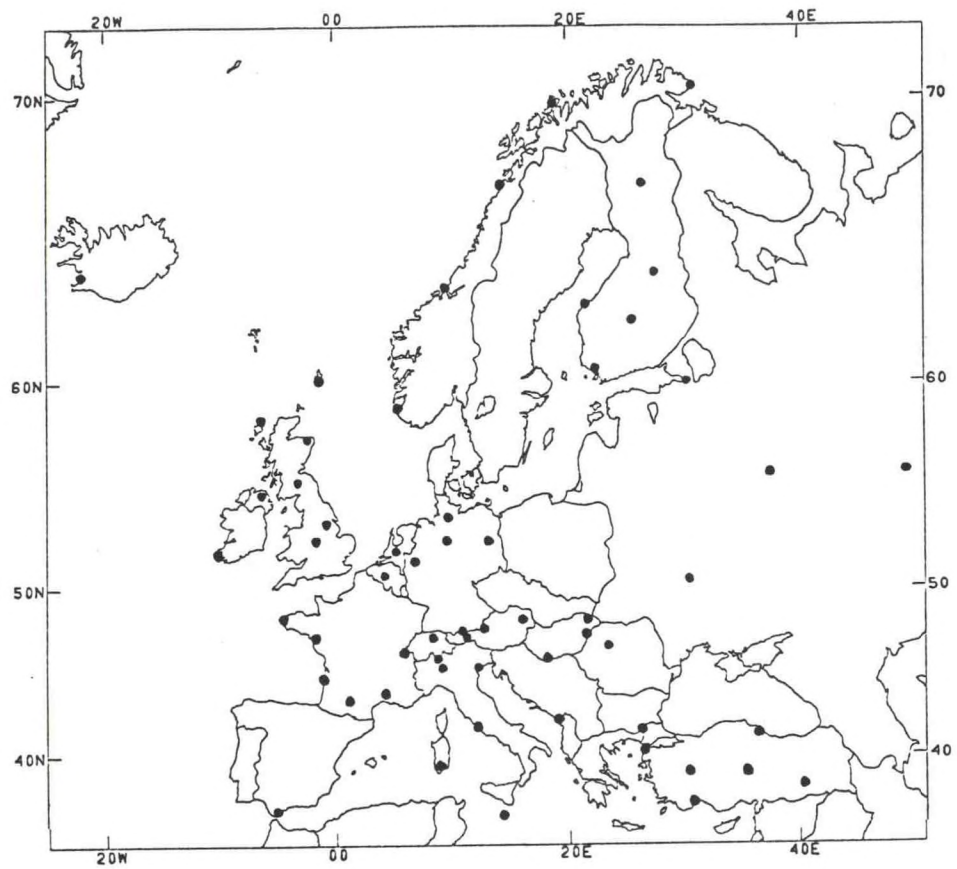

50. The network of 59 European stations used for CCA based temperature prediction experiments.

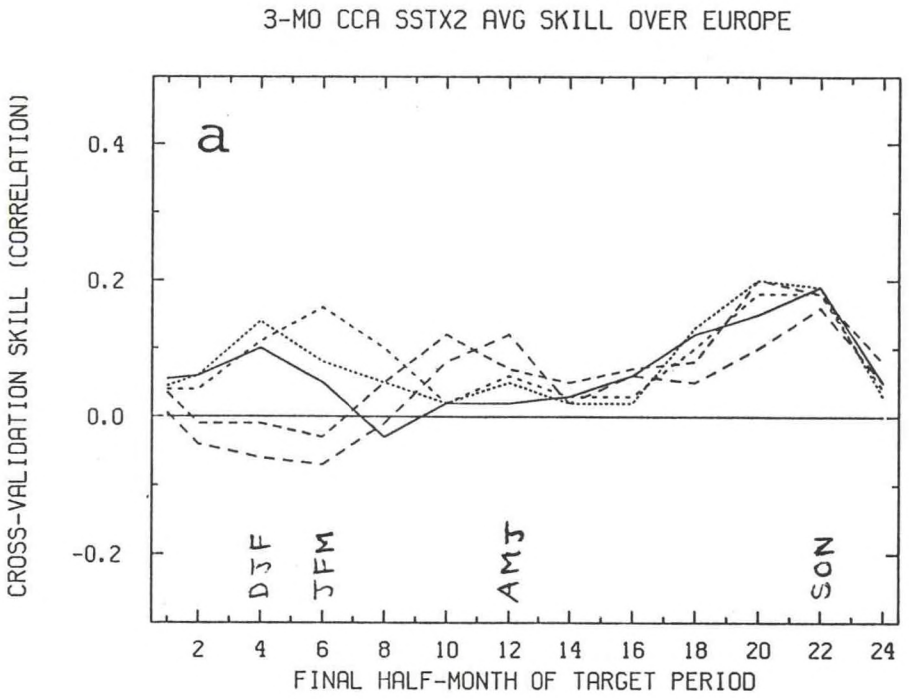

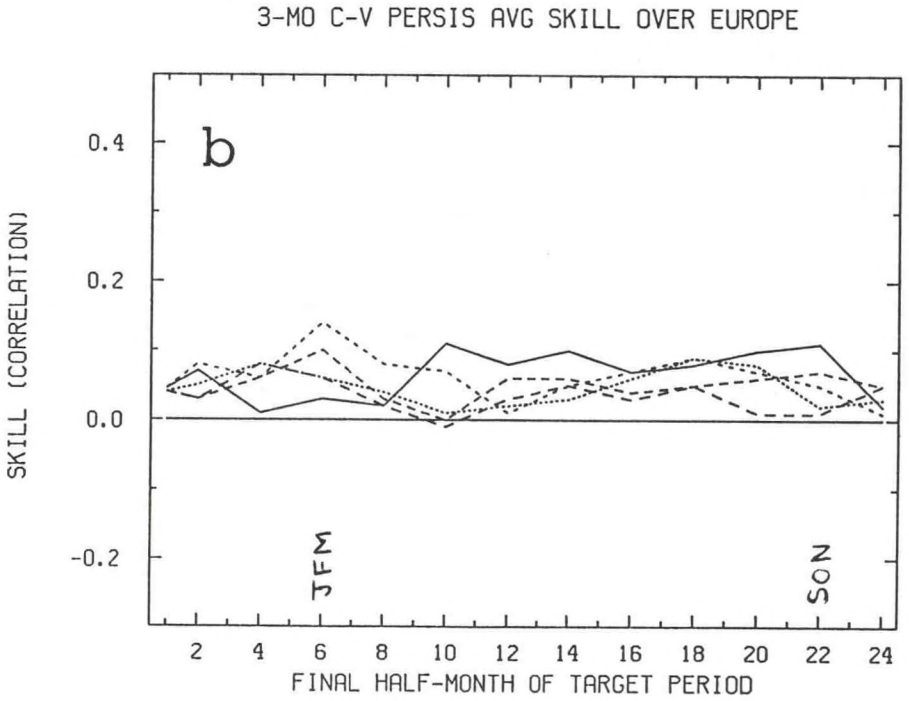

51. Part (a): CCA forecast skill averaged over Europe for 3 month mean temperature for each of 5 lead times, with the SST field weighted double. Each of the four predictor periods is three months in duration. Results for 12 seasons are represented. Part (b): As in part (a) except for persistence forecasts.

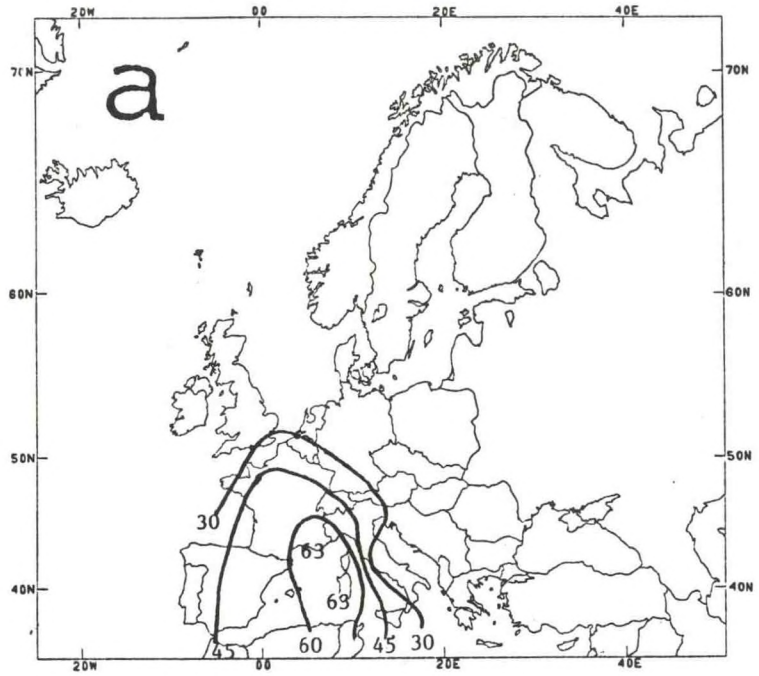

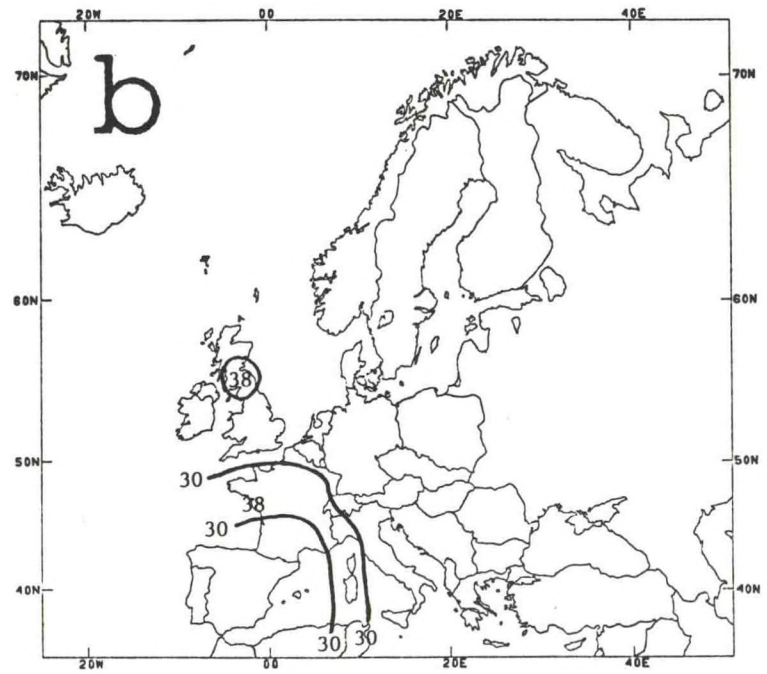

52. Part (a): Geographical distribution of CCA skill in forecasting 3-month mean European surface temperature at 1-month lead with double-weighted SST predictors for Sep-Oct-Nov. Part (b): As in part (a) except for persistence forecasts.

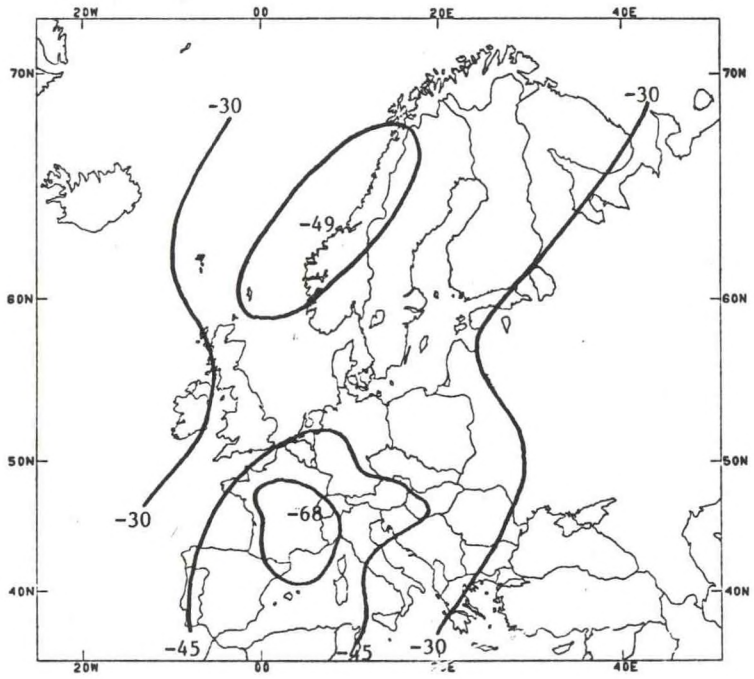

53. **The principal predictand loading pattern for mode 1 for the prediction of Sep-Oct-Nov European surface temperature at 1 month lead.**

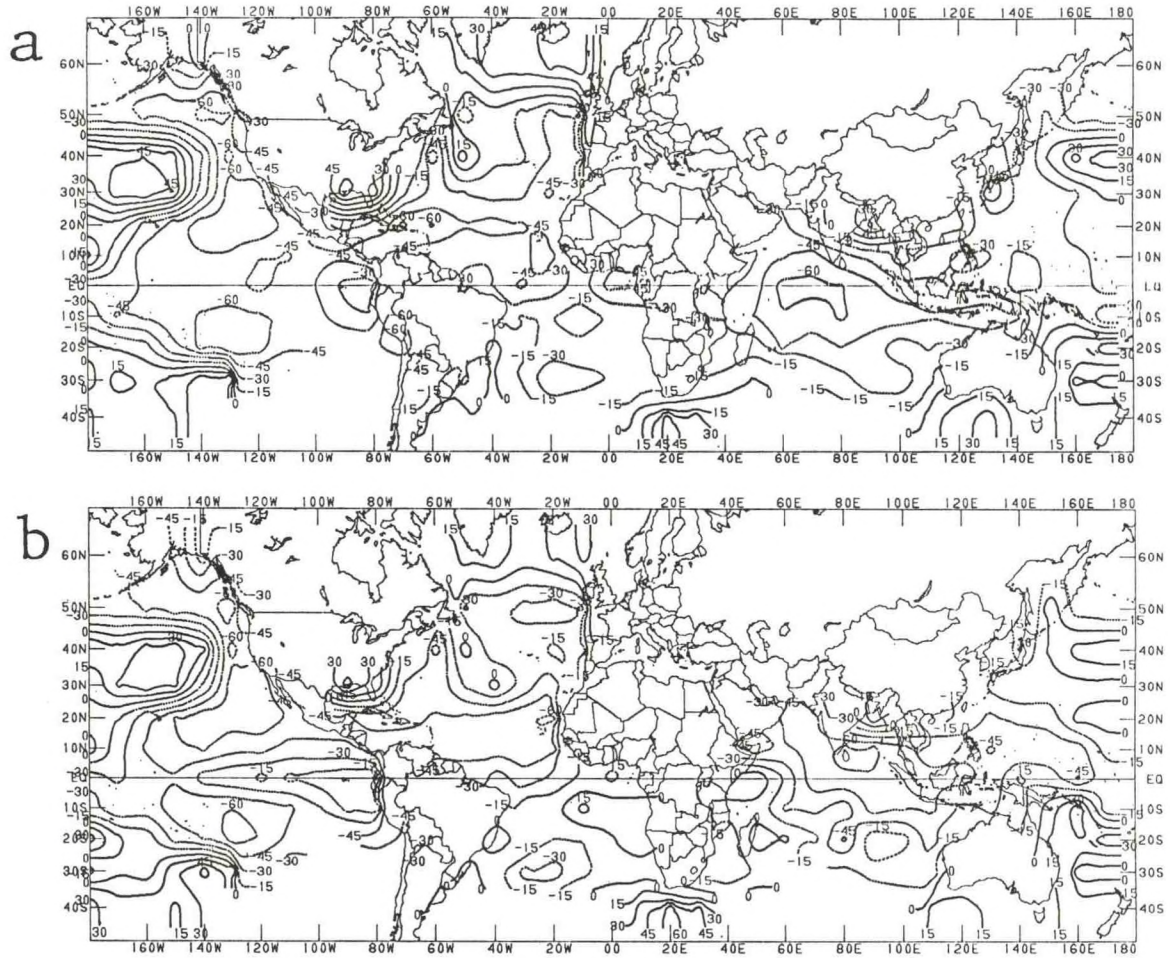

54. SST predictor CCA loadings for mode 1 for prediction of Sep-Oct-Nov European surface temperature at 1 month lead. Parts (a) and (b) show loadings for the third (Feb-Mar-Apr) and fourth (May-Jun-Jul) predictor periods, respectively.

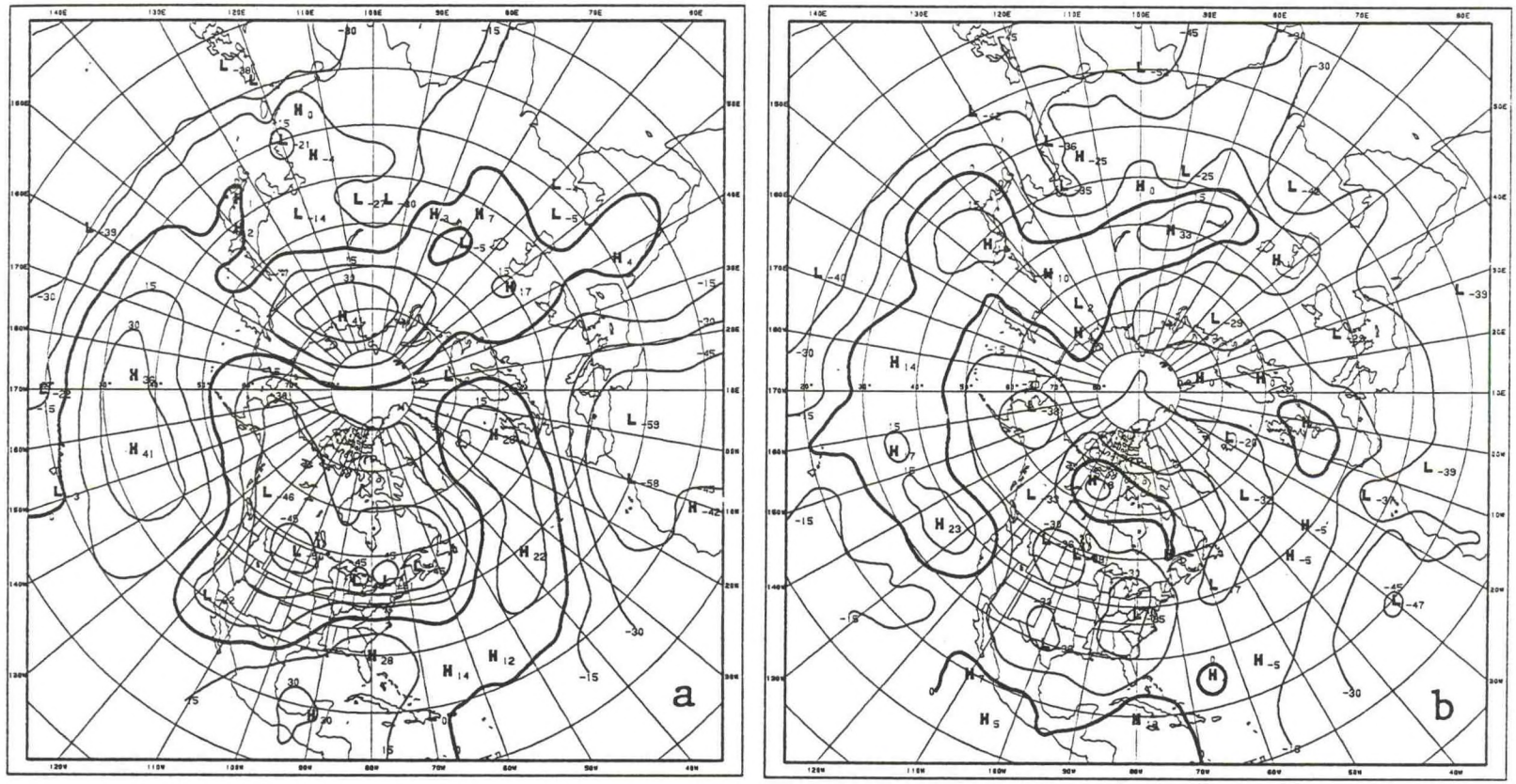

55. As in Fig. 54, except for 700 mb predictor loadings for the third and fourth periods for forecasts of Sep-Oct-Nov European surface temperature.

ods (not shown) have similar patterns, but loadings in the Pacific and Indian oceans are slightly stronger than those in the Atlantic. The 700 mb height pattern in early spring (Fig. 55a) reveals a PNA/TNH combination that might be expected in association with the dissipating cold (warm) ENSO SST pattern (Fig. 54a), and also low latitude negative (positive) anomalies in northwest Africa and much of the Pacific. While the PNA/TNH pattern is expectedly not present in the early summer loading pattern shown in Fig. 55b (they are not warm season patterns), the low latitude anomalies remain, being distributed fairly uniformly about the globe. Apparently the same relationship between like-signed worldwide tropical ocean anomalies and subtropical NH 700 mb height that was shown to associate with the overall summer temperature anomaly in the U.S. (section 4a(1[b], 2 and 3) also affects portions of Europe's autumn temperature anomalies. In fact, the canonical component time series for mode 1 (not shown) is moderately correlated (negatively, due to the arbitrarily opposing polarities) with that shown in Fig. 22 for prediction of mid-Jun to mid-Sep U.S. temperature, including the interdecadal component of the variation. While the preceding winter's cold (warm) ENSO events play a role in fall European and summer U.S. temperature effects, of vital importance also is the accompanying or closely following cold (warm) anomalies in the tropics of the other two major oceans. In both the U.S. and Europe, the subsequent surface temperature anomalies tend to assume the same sign as the tropical SST and subtropical 700 mb height anomalies. This scenario in Europe is found not only for fall (Sep-Oct-Nov) but to a lesser extent also for Jun-Jul-Aug, Jul-Aug-Sep, Aug-Sep-Oct and Oct-Nov-Dec. The effect on fall temperature in mainly southern Europe is not well indicated in the Oct-Nov-Dec forecast experiments for the entire NH 700 mb height field (section 4d, Fig. 44g), in which high predictability in North Africa does not extend northward into Europe. This finding is reminiscent of a similar outcome for predicting late summer climate in the U.S., in which the relationship for surface temperature was not of similar nature to that for 700 mb height. This suggests that the physical connection between antecedent worldwide tropical SST anomalies (with the accompanying low latitude 700 mb height anomalies) and southern European surface temperature in fall may be similar to that between these same antecedent factors and overall U.S. surface temperature in late summer (see result in section 4a(1[b]) versus that in 4c).

While the above fall predictive scenarios may not have been previously documented, predictive patterns have been identified in Europe at other times of the year. In particular, Halpert and Ropelewski (1992) found a cold Feb-Mar-Apr-May pattern over North Africa and southwestern Europe (especially Spain) following the winter of a cold ENSO event. While the CCA skill shown for Feb-Mar-Apr in Fig. 51a for 1 month lead is near zero, relatively high skill (0.37) centered in southern Spain is found to be linked to an ENSO SST signature as CCA mode 1, with anomaly signs as stated in Halpert and Ropelewski. (The latter work linked the pattern to cold ENSO events only, whereas here it is detected using data for all years.)

Another European relationship is documented in Fraedrich and Muller (1992), in which ENSO events are associated with a Dec-Jan-Feb temperature anomaly in Scandinavia of sign opposite that of the tropical Pacific SST. Although Fig. 51a shows 0.10 CCA skill averaged over Europe for that period, an area with somewhat higher skill is found over Scandinavia and the northern United Kingdom, with 0.28 peak skill at Trondheim, Norway. This pattern is linked weakly as mode 2 to ENSO in the manner stated by Fraedrich and Muller. It should be noted, however, that during both recent warm ENSO events 1991-92 and 1992-93 (not included in the present analyses) this relationship was strongly opposed and may no longer appear in updated analyses.

The annual march of skill for European surface temperature forecasts of 1 month periods is shown in Fig. 56a, revealing a profile of similar skill levels to, but somewhat different shape from, that for 3 month periods. Skills of the corresponding cross-validated persistence forecasts are shown in Fig. 56b. The 0.5 and 1.5 month lead CCA forecasts for July appear to have the highest skill of any leads or seasons (means of 0.24 and 0.25, respectively). Examination of the CCA diagnostics for these forecasts (not shown) shows highest skill (0.40 to 0.51) to be in the western Mediterranean Sea (centered at Sardinia), southeastern France, Italy and Northern Yugoslavia, as well as another area from northern United Kingdom to the Netherlands, northwestern Germany and southern Denmark. The geographical distribution of persistence skill (not shown) is quite weak (with mean of 0.10) and is focused in Italy/Sardinia and also just south of Finland in northwestern European Russia. The dominant CCA mode's principal predictand pattern is a double-peaked monopole (with some weaker oppositely signed loadings in Turkey) quite similar in shape to the CCA skill pattern, emphasizing the area in northwestern Europe. The associated mode 1 predictor loading patterns are mainly uninteresting. However, the fourth period (mid-May to mid-June) does show SST anomalies of the same sign as found over Europe in the eastern Indian Ocean and an SZ pattern in 700 mb height with like-signed low latitude loadings, especially over North Africa and southeast Asia/west Pacific. Another feature in all four SST predictor loading fields is sharply focused like-signed loading centers in the Atlantic at 40^{o}N, 60^{o}W (south of Nova Scotia) and 50^{o}N, 10^{o}W (just south of Ireland). These locations have been found in other analyses to be related to meanderings of the Gulf Stream (Chester Ropelewski, personal communication). It may thus be speculated that the course of the Gulf Stream can affect European temperature in July--perhaps in particular its course just south of Ireland, not far from the northwestern European July high skill region.

5. Discussion and Conclusions

This study systematically explores the strengths and sources of statistical predictive short-term climate skill at various lead times for the NH for both surface climate and 700 mb geopotential height. The focus is both on large areas within the hemisphere and on smaller regions such as the surface climate in

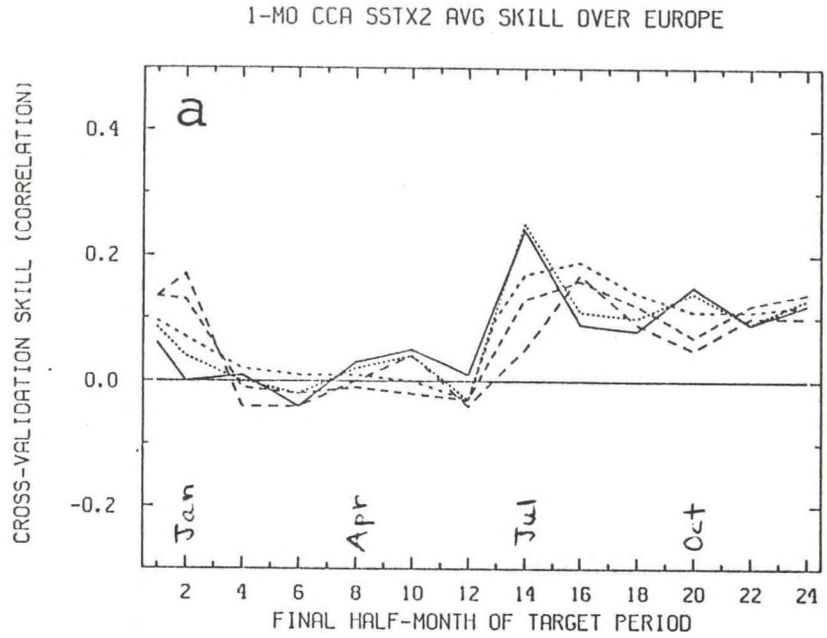

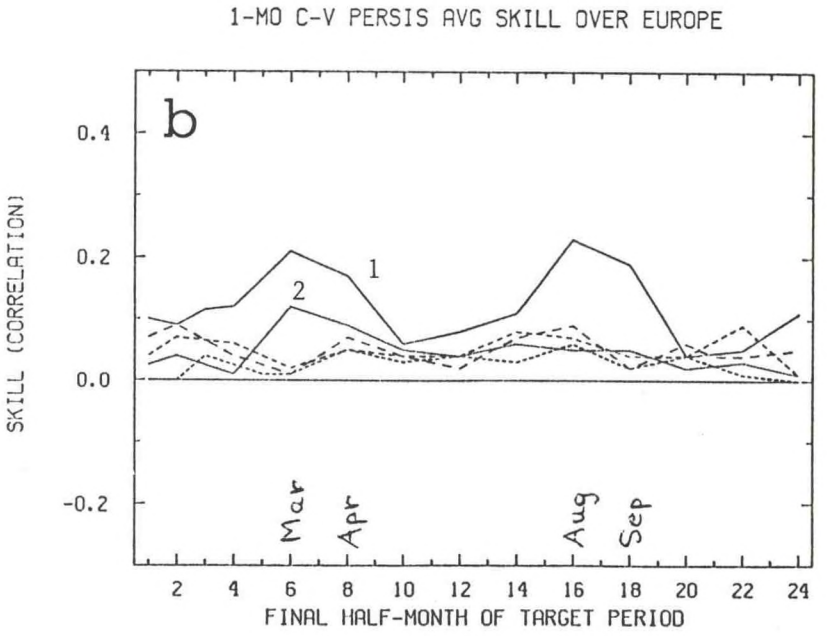

56. Part (a): CCA forecast skill averaged over Europe for 1 month mean temperature for each of 5 lead times, with the SST field weighted double. Each of the four predictor periods is one month in duration. Results for 12 seasons are represented. Part (b): As in part (a) except for persistence forecasts.

the United States or Europe. The purpose of the study is to identify relatively reliable predictive relationships, both from the standpoint of obtaining clues to possible physical mechanisms, and for empirical predictive guidance for long-range forecasts which often do not yet benefit substantially from the output of dynamical models.

The chosen methodology for the study is canonical correlation analysis (CCA) with separate predictor and predictand EOF analyses as preliminary filters. CCA is a multivariate linear regression technique that uses eigenanalysis to relate predictors to predictands as patterns in both time and space. It has the capability to approximately represent numerous complicated interactive linear and nonlinear phenomena as several linear summary scenarios. Like any linear model, it fails to fully utilize nonlinear relationships. As a linear statistical modelling technique, CCA is among a select group of advanced methods (two others being singular value decomposition [SVD] and principal oscillation pattern [POP] analysis) that identifies systematic predictor-predictand pattern linkages within data sets characterized largely by random variability. It not only derives prediction models for the forecasting of patterns, but also generates useful diagnostics, including the predictor patterns that are found to give rise to predictive skill in specified regions.

Predictand averaging periods of 1 and 3 months are used, with 4 consecutive predictor periods of the same duration to detect evolutionary developments leading to specific predictand outcomes. A lead time separating the predictor and predictand times is varied from a half month to roughly a year. Predictor fields are NH 700 mb height, quasi-global SST and prior values of the predictand field itself. Cross-validation is used to obtain skill estimates that are usually not inflated by artificial skill. Persistence is used as a reference competitor, but is useful only at the shorter lead times.

In general, results reveal modest statistical predictive skill, with less than 20 percent of the predictand variance explained by the best predictor sets in most situations. However, there are certain fields, locations and times of the year when predictability is far above chance expectation--in fact, good enough to be economically useful. Skill for forecasts of 3 month mean climate is generally superior to that for 1 month means, because the signal-to-noise ratio is more favorable in the former. The global SST field is the more important of the three predictor fields in producing the instances of relatively high skill. This could be the case either because (1) SST represents the lower boundary condition, which is more important on the time scale of months than the atmosphere's internal dynamics, or (2) SST is the only field in this study that directly provides tropical information, which turns out to be a major skill source in both cold and warm seasons. The skill level is relatively insensitive to the forecast lead time, such that inserting 3 (or sometimes considerably more) months between the predictor and predictand periods does not cause more than a slight skill decrease.

This result has favorable implications for long-lead forecasting, which is presently not done on an official basis in the U.S. government.

Much of the higher skill occurs in association with fluctuations of ENSO and is found in mid-winter through spring in the Pacific and North American regions. Specifically, a warm (cold) ENSO episode is found to create positive (negative) 700 mb height anomalies in south-central Canada as well as the central and western subtropical Pacific, and negative (positive) anomalies along the 50-55^{o}N latitude band from Japan to the Gulf of Alaska as well as along the 25-30^{o}N latitude band from western Mexico to the central Atlantic. Like-signed surface temperature anomalies accompany the height features, positioned roughly congruently with zonally elongated height anomalies but to the west of the more circular height anomalies. For example, in a warm ENSO event the largest positive temperature anomalies occur in southwestern Canada rather than between Minnesota and Hudson Bay where the non-elongated height anomaly is found.

Even with the cross-validation technique, forecast skill (expressed as a temporal correlation between CCA forecasts and observations over a 37 year period) in the centers of the best predictable regions is near or in excess of 0.6 for both height and temperature. Precipitation anomalies are also found in accordance with expected anomalies in mean flow and storm tracks that associate with the height anomalies; e.g. in a warm ENSO event it is wetter in all except the western flank of the negative height anomaly band across the southern U.S. Predictive skill for precipitation is at a considerably lower maximum level of 0.4.

Warm season predictive skill, while lower than that of winter-spring, forms a secondary seasonal maximum whose skill sources reveal ocean-atmosphere relationships not clearly documented in previous work. The major finding is in the prediction of generalized positive (negative) U.S. surface temperature anomalies in middle to late summer (and in fall in southern Europe), and like-signed 700 mb height anomalies at lower latitudes throughout much of the NH (i.e. 20-40^{o} but with some farther northerly continental protrusions). This set of anomalies is found to occur during and shortly following long-lived episodes of positive (negative) SST anomalies in the tropical oceans throughout the world. The occurrence of a mature ENSO event in the prior winter often contributes to such a condition. The most conducive SST state is that in which the Pacific, Atlantic and Indian oceans have the same anomaly sign in the leading spring season. It is found that mature Pacific ENSO events the preceding winter are often accompanied by a like-signed but somewhat weaker SST anomaly in the Indian Ocean which endures for several months after the dissipation of the tropical Pacific anomaly in spring. Furthermore, the winter Pacific SST anomaly may be followed by a like-signed anomaly in the tropical Atlantic (especially at 0-20^{o}N) that persists from March through at least the early summer--i.e. peaking slightly later than the Indian Ocean anomaly. The overall scenario may then be summarized:

Warm (cold) anomalies in the world's tropical oceans in spring and/or early summer appear to lead to general anomalous warmth (coolness) from mid-July through August in much of the U.S. and in southern Europe in autumn (but more weakly detectable beginning in summer). Like-signed worldwide tropical SST anomalies also give rise to the warm season Subtropical/Zonal (SZ) low-frequency atmospheric variability pattern at 700 mb, with the low latitude band assuming the same anomaly sign as that of the SST.

A physical explanation for the development of a spring SST anomaly in the Atlantic following the peak of an ENSO related like-signed Pacific anomaly is not apparent. Advection of warm Pacific water is not possible. One possible response to ENSO heating is a zonally symmetric temperature perturbation in much of the overlying tropical troposphere. Over time, this could increase the temperature in all tropical oceans. Effects from altered cloud cover and radiation related to the Pacific aspects of ENSO are also conceivable. More definitive answers to this requires careful study using coupled models. The actual anomaly magnitudes in the Atlantic are less than those in the Pacific; however, the standardization that is done in the present CCA removes this disparity in the modelling of the predictive relations.

The fact that linear statistical predictability using advanced techniques is in general modest may mean that linear models cannot adequately represent the dynamics of the atmosphere, part of which is nonlinear even for long time means, and that simple or complex physical models potentially could do better. More pessimistically, the skill realized here may nearly represent an upper bound for predictive skill using any approach, given that the unpredictable part is largely related to the internal atmospheric dynamics, most of which acts over a shorter time scale and has a short (about two weeks) inherent limit of predictability. Which of these two possibilities is closer to the truth may be revealed by future advances in dynamical modelling. Hopefully, the skill of models using explicit physics will eventually surpass that of the best linear or nonlinear statistical models, without requiring long historical data sets.

In conclusion, the present study has revealed two major sources of statistical predictability. The primary source, ENSO fluctuations, has already been well recognized. While its effects on NH climate are demonstrated here and elsewhere, its prediction is still a major challenge (e.g. Cane et al. 1986, Cane and Zebiak 1987, Barnett et al. 1988, Inoue and O'Brien 1984). A related but different source, the overall worldwide tropical SST anomaly, has not heretofore been known to affect the low and sometimes middle latitude NH geopotential height and temperature, such as late summer temperature in much of the U.S. or fall temperature in southern Europe. We look to physical modelling studies to provide concrete explanations for these associations and identify still others.

Acknowledgments

I wish to thank Drs. Edward Epstein, Robert Livezey and Huug van den Dool for their careful reviews of this report.

References

Anderson, C.W., 1984: An Introduction to Multivariate Statistical Analysis, 2nd ed., Wiley and Sons, 675 pp.
prediction of short-term climate fluctuations using a climate state vector. J. Atmos. Sci., 35, 1771-1787.

Barnett, T.P., 1981: Statistical prediction of North American air temperature from Pacific predictors. Mon. Wea. Rev., 109, 1021-1041.

Barnett, T.P. and Preisendorfer, R., 1987: Origins and levels of monthly and seasonal forecast skill for United States surface air temperatures determined by canonical correlation analysis. Mon. Wea. Rev., 115, 1825-1850.

Barnett, T.P., K. Brennecke, J. Limm, and A.M. Tubbs, 1984: Construction of a near-global sea level pressure field. SIO Ref. Ser., 84-7. Scripps Institute of Oceanography, 33 pp.

Barnett, T., N. Graham, M. Cane, S. Zebiak, S. Dolan, J. O'Brien, and D. Legler, 1988: Prediction of the El Nino of 1986-1987. Science, 241, 192-196.

Barnston, A.G., 1994: Linear statistical short-term climate predictive skill in the Northern Hemisphere. J. Climate, 7, accepted.

Barnston, A.G. and R.E. Livezey, 1987: Classification, seasonality and persistence of low-frequency atmospheric circulation patterns. Mon. Wea. Rev., 115, 1083-1126.

Barnston, A.G. and R.E. Livezey, 1989: An operational multifield analog predictive system for United States seasonal temperatures. Part II: Spring, summer, fall and intermediate three-month period experiments.

Barnston, A.G. and R.E. Livezey, 1991: Statistical prediction of January-February mean Northern Hemisphere lower tropospheric climate from the 11-year solar cycle and the Southern Oscilation for west and east QBO phases. J. Climate, 2, 249-262.

Barnston, A.G., and C.F. Ropelewski, 1992: Prediction of ENSO episodes using canonical correlation analysis. J. Climate, 5, 1316-1345.

Barnston, A.G., and H.M. van den Dool, 1993: A degeneracy in estimated skill in forecasts using regression-based cross-validation designs. J. Climate, 6, accepted.

Barnston, A.G., R.E. Livezey and M.S. Halpert, 1991: Modulation of Southern Oscillation-Northern Hemisphere mid-winter climate relationships by the QBO. J. Climate, 4, 203-217.

Blackmon, M.L., J.E. Geisler, and E. J. Pitcher, 1983: A general circulation model study of January climate anomaly patterns associated with interannual variation of equatorial Pacific sea surface temperature. J. Atmos. Sci., 40, 1410-1425.

Brankovic, C., T.N. Palmer, F. Molteni, S. Tibaldi and U. Cubasch, 1990: Extended-range predictions with ECMWF models: Time-lagged ensemble forecasting. Q. J. R. Meteorol. Soc., 116, 867-912.

Bretherton, C.S., C. Smith and J.M. Wallace, 1992: An intercomparison of methods for finding coupled patterns in climate data. J. Climate, 5, 541-560.

Cane, M.A., and S.E. Zebiak, 1987: Prediction of El Niño events using a physical model. In Atmospheric and Oceanic Variability, edited by H. Cattle, Royal Meteorological Society, 153-181, James Glaisher House, Bracknell, England.

Cane, M.A., S.E. Zebiak and S.C. Dolan, 1986: Experimental forecasts of El Nino. Nature, 321, 827-832.

Chen, W.Y., 1989: Estimate of dynamical predictability from NMC DERF experiments. Mon. Wea. Rev., 117, 1227-1236.

Chervin, R., 1986: Interannual variability and seasonal climate predictability. J. Atmos. Sci., 43, 233-251.

Dixon, K.W., and R.P Harnack, 1986: The effect of intraseasonal circulation variability on winter temperature forecast skill. Mon. Wea. Rev., 114, 208-214.

Douglas, A.V., 1989: The severe drought of 1988: Possible response to persistent El Nino conditions. Proceedings of the Thirteenth Annual Climate Diagnostics Workshop, Cambridge, Massachusetts, October 31-November 4, 1988, 12-18.

Douglas, A.V. and P.J. Englehart, 1981: On a statistical relationship between autumn rainfall in the central equatorial Pacific and subsequent winter precipitation in Florida. Mon. Wea. Rev., 109, 2377-2382.

Epstein, E.S., 1992: ENSO's precipitation signature in the U.S. Are wet days wetter or more frequent? Proceedings of the Sixteenth Annual Climate Diagnostics Workshop, Los Angeles, California, October 28-November 1, 1991, 22-28.

Erickson, C.O., 1983: Hemispheric anomalies of 700 mb height and sea level pressure related to mean summer temperatures over the United States. Mon. Wea. Rev., 111, 545-561.

Esbensen, S.K., 1984: A comparison of intermonthly and interannual teleconnections in the 700 mb geopotential height field during the Northern Hemisphere winter. Mon. Wea. Rev., 112, 2016-2032.

Fraedrich, K. and K. Muller, 1992: Climate anomalies in Europe associated with ENSO extremes. Int. J. Climatol., 12, 25-31.

Glahn, H., 1963: Canonical correlation and its relationship to discriminant analysis and multiple regression. J. Atmos. Sci., 25, 23-31.

Graham, N.E., J. Michaelsen, and T.P. Barnett, 1987a: An investigation of the El Nino-Southern Oscillation cycle with statistical models. 1. Predictor field characteristics. J. Geophys. Res., 92, 14251-14270.

Graham, N.E., J. Michaelsen, and T.P. Barnett, 1987b: An investigation of the El Nino Southern Oscillation cycle with statistical models. 2. Model results. J. Geophys. Res., 92, 14271-14289.

Halpert, M.S., and C.F. Ropelewski, 1989: Atlas of Tropical Sea Surface Temperature and Surface Winds. NOAA ATLAS No. 8, 13 pp + 150 figures. U. S. Government Printing Office 1989-242-312/04048 (Available from Climate Analysis Center, W/NMC52, Washington, DC 20233).

Halpert, M.S., and C.F. Ropelewski, 1992: Surface temperature patterns associated with the Southern Oscillation. J. Climate, 5, 577-593.

Harnack, R.P., 1979: A further assessment of winter temperature predictions using objective methods. Mon. Wea. Rev., 107, 250-267.

Harnack, R.P., 1982: Objective winter temperature forecasts: An update and extension to the western United States. Mon. Wea. Rev., 110, 287-295.

Harnack, R.P., and J.R. Lanzante, 1984: Specification of seasonal mean 700 mb height over North America by North Pacific and North Atlantic sea surface temperature. Mon. Wea. Rev., 112, 1626-1633.

Harnack, R., M. Cammarata, K. Dixon, J. Lanzante and J. Harnack, 1985: Summary of U.S. seasonal temperature forecast experiments. Proc. of the Ninth Conf. on Probability and Statistics in Atmospheric Sciences. Virginia Beach, VA 175-179.

Hasselmann, K., 1988: PIPs and POPs: The reduction of complex dynamical systems using principal interaction and oscillation patterns. J. Geophys. Res., 93, 11,015-11,021.

Horel, J.D., 1981: A rotated principal component analysis of the interannual variability of the Northern Hemisphere 500 mb height field. Mon. Wea. Rev., 109, 2080-2092.

Hoskins, B.J., and D.J. Karoly 1981: The steady linear response of a spherical atmosphere to thermal and orographic forcing. J. Atmos. Sci., 38, 1179-1196.

Hotelling, H., 1936: Relations between two sets of variates. Biometrika, 28, 321- 377.

Huang, J. and H.M. van den Dool, 1993: Monthly precipitation-temperature relations and temperature prediction over the U.S. J. Climate, 6, in press.

Inoue, M. and J.J. O'Brien, 1984: A forecasting model for the onset of a major El Nino. Mon. Wea. Rev., 112, 2326-2337.

Iwaska, N., K. Hanawa, and Y. Toba, 1987: Analysis of SST anomalies in the North Pacific and their relation to 500 mb height anomalies over the Northern Hemisphere during 1969-1979. J. Meteor. Soc. Japan, 65, 103-113.

Jones, P.D., T. Wigley and P. Kelly, 1982: Variations in surface air temperatures. Part I: Northern Hemisphere, 1881-1980. Mon. Wea. Rev., 110, 1970-1996.

Kalnay, E. and R. Jenne, 1991: Summary of the NMC/NCAR Reanalysis Workshop of April 1991. Bull. Am. Meteor. Soc., 72, 1897-1904.

Kiladis, G.N. and H.F. Diaz, 1989: Global climatic anomalies associated with extremes in the Southern Oscillation. J. Climate, 2, 1069-1090.

Kinter, J.L. and J. Shukla, 1989: Reanalysis for TOGA (Tropical Oceans Global Atmosphere). 1-3 February 1989 meeting at the Center for Ocean-Land-Atmosphere Interactions. Bull. Am. Meteor. Soc., 70, 1422-1427.

Klein, W.H., 1983: Objective specification of monthly mean surface temperature from mean 700-mb height in winter. Mon. Wea. Rev., 111, 674-691.

Klein, W.H., and J.E. Walsh, 1983: A comparison of point-wise screening and empirical orthogonal functions in specifying monthly surface temperature from 700 mb data. Mon. Wea. Rev., 111, 669-673.

Klein, W.H. and R. Yang, 1986: Specifications of monthly mean surface temperature anomalies in Europe and Asia from concurrent 700 mb monthly mean height anomalies over the Northern Hemisphere. J. Climatol, 6, 463-474.

Klein, W.H., A. Shabbar and R. Yang, 1989: Specifying monthly mean surface temperatures in Canada and Alaska from the 500 mb height field. J. Climate, 2, 631-638.

Kushnir, Y. and J.M. Wallace, 1989: Low-frequency variability in the Northern Hemisphere winter: Geographical distribution, structure and time dependence. J. Atmos. Sci., 46, 3122-3142.

Lanzante, J.R., 1984: A rotated eigenanalysis of the correlation between 700 mb heights and sea-surface temperatures in the Pacific and Atlantic. Mon. Wea. Rev., 112, 2270-2280.

Lau, N.C., 1985: Modeling the seasonal dependence of the atmospheric response to observed El Ninos in 1962-76. Mon. Wea. Rev., 13, 1970-1996.

Livezey, R.E., 1990: Variability of skill of long-range forecasts and implications for their use and value. Bull. Amer. Meteor. Soc., 71, 300-309.

Livezey, R.E. and K.C. Mo, 1987: Tropical-extratropical teleconnections during the Northern Hemisphere winter. Part II: Relationships between monthly mean Northern Hemisphere circulation patterns and proxies for tropical convection. Mon. Wea. Rev., 115, 3115-3132.

Livezey, R.E., and A.G. Barnston, 1988: An operational multifield analog prediction system of United States seasonal temperatures. Part I: System design and winter experiments. J. Geophys. Res., 93, 10953-10974.

Livezey, R.E., Barnston, A.G. and B.K. Neumeister, 1990: Mixed analog/persistence prediction of United States seasonal mean temperatures. Int. J. Climatology, 10, 329-340.

Horel, J.D. and J.M. Wallace, 1981: Planetary-scale atmospheric phenomena associated with the Southern Oscillation. Mon. Wea. Rev., 109, 813-829.

Lorenz, E.N., 1982: Atmospheric predictability experiments with a large numerical model. Tellus, 34, 505-513.

Madden, R.A., 1976: Estimates of the natural variability of time average sea level pressure. Mon. Wea. Rev., 104, 942-952.

Madden, R.A. and P.R. Julian, 1971: Detection of a 40-50 day oscillation in the zonal wind in the tropical Pacific. J. Atmos. Sci., 28, 702-708.

Madden, R.A., and D. Shea, 1978: Estimates of the natural variability of time averaged temperatures over the United States. Mon. Wea. Rev., 106, 1695-1703.

Michaelsen, J., 1987: Cross-validation in statistical climate forecast models. J. Climate Appl. Meteor., 26, 1589-1600.

Milton, S.F., 1990: Practical extended-range forecasting using dynamical models. Meteorol. Mag., 119, 221-233.

Mo, K.C., and R.E. Livezey, 1986: Tropical-exptratropical geopotential height teleconnections during the Northern Hemisphere winter. Mon. Wea. Rev., 114, 2488-2515.

Murphree, T. and H. van den Dool, 1988: Calculating tropical winds from time mean sea level pressure fields. J. Atmos. Sci., 45, 3269-3282.

Namias, J., 1981: Teleconnections of 700 mb height anomalies for the Northern Hemisphere. Calcofi Atlas No. 29.

Namias, J., 1982: Anatomy of Great Plains protracted heat wave (especially the 1980 U.S. summer drought). Mon. Wea. Rev., 110, 824-838.

Nicholls, N., 1987: The use of canonical correlation to study teleconnections. Mon. Wea. Rev., 115, 393-399.

NOAA 1983: Statewide Average Climate History. Historical Climatology Series 6-1, National Climate Data Center, Asheville, NC, 184 pp.

Opsteegh, J.D. and H.M. van den Dool, 1980: Seasonal differences in the stationary response of a linearized primitive equation model: Prospects for long range weather forecasting? J. Atmos. Sci., 37, 2169-2185.

Penland, C., 1989: Random forcing and forecasting using principal oscillation pattern analysis. Mon. Wea. Rev., 117, 2165-2185.

Preisendorfer, R.W., 1988: Principal components analysis in meteorology and oceanography. In Developments in Atmospheric Sciences, edited by Curtis Mobley, 17, Elsevier, New York, New York, 425pp.

Reynolds, R.W., 1988: A real-time global sea surface temperature analysis. J. Climate, 1, 75-86.

Ropelewski, C.F. and M. S. Halpert, 1986: North American precipitation and temperature patterns associated with the El Nino/Southern Oscillation (ENSO). Mon. Wea. Rev., 114, 2352-2362.

Ropelewski, C.F., and M.S. Halpert, 1987: Global and regional scale precipitation patterns associated with the El Nino/Southern Oscillation. Mon. Wea. Rev, 115, 1606-1626.

Ropelewski, C.F., and P.D. Jones, 1987: An extension of the Tahiti-Darwin Southern Oscillation Index. Mon. Wea. Rev., 115, 2161-2165.

Ropelewski, C.F., and M.S. Halpert, 1989: Precipitation patterns associated with the high index phase of the Southern Oscillation. J. Climate, 2, 268-284.

Shea, D.J. and R.A. Madden, 1990: Potential for long-range prediction of monthly mean surface temperatures over North America. J. Climate, 3, 1444-1451.

Shukla, J., 1985: Predictability. In Advances in Geophysics, 28B, Academic Press, Inc., 87-123.

Shukla, J., and J.N. Wallace, 1983: Numerical simulation of the atmospheric response to equatorial sea surface temperature anomalies. J. Atmos. Sci., 40, 1613-1630.

Slutz, R., S.J. Lubler, J.D. Hiscox, S.D. Woodruff, R.J. Jenne, D.H. Joseph, P.M. Steurer, and J.D. Elius, 1985: Comprehensive Ocean Atmosphere Data Set, National Oceanic and Atmospheric Administratration, Boulder, CO. (Available from Climate Research Program, ERL, R/E/AR6, 325 Broadway, Boulder, CO 80303.)

Toth, Z. 1989: Long-range weather forecasting using an analog approach. J. Climate, 2, 594-607.

Trenberth, K.E., 1984: Some effects of finite sample size and persistence on meteorological statistics. Part II: Potential predictability. Mon. Wea. Rev., 112, 2369-2378.

Van den Dool, H.M., 1984: Long-lived air temperature anomalies in the mid-latitudes forced by the surface. Mon. Wea. Rev., 112, 555-562.

Van den Dool, H.M., 1987: A bias in skill in forecasts based on analogues and antilogues. J. Clim. Appl. Meteor., 26, 1278-1281.

Van den Dool, H.M. and J.L. Nap, 1985: Short and long range air temperature forecasts near an ocean. Mon. Wea. Rev., 113, 878-886.

Van den Dool, H.M. and S. Saha, 1990: Frequency dependence in forecast skill. Mon. Wea. Rev., 118, 128-137.

Van den Dool, H.M., W.H. Klein and J.E. Walsh, 1986: The geographical distribution and seasonality of persistence in monthly mean air temperatures over the United States. Mon. Wea. Rev., 114, 546-560.

Van Loon, H. and R.A. Madden, 1981: The Southern Oscillation. Part I: Global associations with pressure and temperature in northern winter. Mon. Wea. Rev., 109, 1150-1162.

Von Storch, H.,T. Bruns, I. Fischer-Bruns and K. Hasselmann, 1988: Principal oscillation pattern analysis of the 30- to 60-day oscillation in general circulation model equatorial troposphere. J. Geophys. Res., 93, 11,022-11,036.

Wallace, J.M., and D.S. Gutzler, 1981: Teleconnections in the geopotential height field during the Northern Hemisphere winter. Mon. Wea. Rev., 109, 784-812.

Wallace, J.M., C. Smith, and C.S. Bretherton, 1992: Singular value decomposition of wintertime sea surface temperature and 500 mb height anomalies. J. Climate, 5, 561-576.

Xu, J.-S. and H. von Storch, 1990: Principal oscillation pattern: Prediction of the state of ENSO. J. Climate, 3, 1316-1329.

*U.S. GOVERNMENT PRINTING OFFICE: 1993-341-926-92625